# Selenium Speciation and Localization in Sediment and Benthic Invertebrates from Lakes Receiving Treated Metal Mine Effluent

**A Thesis Submitted to the College of**

**Graduate Studies and Research**

**in Partial Fulfillment of the Requirements**

**for the Degree of Master of Science**

**in the Department of Geological Sciences**

**University of Saskatchewan**

**Saskatoon**

**by**

**Justin John Tse**

## Permission To Use

In presenting this thesis/dissertation in partial fulfillment of the requirements for a Postgraduate degree from the University of Saskatchewan, I agree that the Libraries of this University may make it freely available for inspection. I further agree that permission for copying of this thesis/dissertation in any manner, in whole or in part, for scholarly purposes may be granted by the professor or professors who supervised my thesis/dissertation work or, in their absence, by the Head of the Department or the Dean of the College in which my thesis work was done. It is understood that any copying or publication or use of this thesis/dissertation or parts thereof for financial gain shall not be allowed without my written permission. It is also understood that due recognition shall be given to me and to the University of Saskatchewan in any scholarly use which may be made of any material in my thesis/dissertation.

Requests for permission to copy or to make other uses of materials in this thesis/dissertation in whole or part should be addressed to:

Head of the Department of Geological Sciences

University of Saskatchewan

114 Science Place

Saskatoon, Saskatchewan, S7N 5E2

Canada

## Abstract

The objective of this research project was to establish a better understanding of the mechanism(s) and route(s) by which selenium (Se) may enter an aquatic ecosystem that has been receiving treated metal mine effluent from an upstream uranium milling operation. Synchrotron based X-ray absorption spectroscopy (XAS) and X-ray fluorescence (XRF) imaging, which require little sample pre-treatment, were employed to study the speciation and distribution of Se in complex sediment and benthic invertebrates samples collected from the field. Laboratory based inductively coupled plasma mass spectrometry (ICP-MS) provided quantitative Se concentrations. Samples were taken from Fox Lake and Unknown Lakes, downstream of the mill, and Yeoung Lake as a control. The variation in Se speciation as a function of depth in intact sediment cores may provide insight into the species of Se available to the sediment dwelling benthic invertebrate communities. Therefore, a custom sample holder was designed to facilitate analysis of intact sediment cores at cryogenic temperatures. Additionally, laboratory reared chironomids were water-exposed to various Se species, to compare their Se speciation and localization to chironomids collected in the field.

The successful demonstration of the custom sample holder and viable use of synchrotron XAS and XRF in studying sediment and chironomid samples have revealed that biologically relevant Se forms were present in sediment at depths accessible by the benthic invertebrate community. These Se forms included selenomethionine-like and selenite species, and to a lesser degree elemental Se; an increased proportion of reduced Se species was observed as depth increased. Other elements measured concurrently with Se included As, Zn, Cu, Ni, Fe, and Mn, providing an estimation of the redox boundary found both in Fox and Unknown Lake, as well as suggesting the presence of iron species that

could aid in the reduction of Se. Field and laboratory reared chironomids showed similar Se species, and XRF imaging revealed the localization of Se in 4 distinct regions: head capsule, brain, salivary glands, and gut lining. Overall, the project has provided important insights into the interactions of Se with this aquatic ecosystem, which may have future applications in cold water systems with elevated Se concentrations

## Acknowledgements

I would like to thank my supervisor Dr. Ingrid Pickering for her invaluable guidance, advice, and patience for teaching to ensure I would understand concepts. I would also like to thank my committee members, Drs. Graham George, Karsten Liber, Kevin Ansdell, and Jim Merriam, whose suggestions, advice, and constructive discussions aided my research. Much gratitude is given to Stanford Synchrotron Radiation Lightsource (SSRL) staff scientists Sam Webb, Matthew Latimer and Eric Nelson for ensuring enjoyable beamtime. SSRL is operated for the U.S. Department of Energy (DoE) Office of Science by Stanford University. The SSRL Structural Molecular Biology Program is supported by the DoE Office of Biological and Environmental Research, and by the National Institutes of Health, National Center for Research Resources, Biomedical Technology Program (P41RR001209).

I gratefully acknowledge support from, Natural Sciences and Engineering Research Council of Canada, Cameco Corporation Collaborative Research and Development Grant (David Janz) and a CIHR-THRUST Fellowship.

Without the help and critique of my family, friends, and colleagues, I would never have accomplished what I have done. I thank the wonderful Pickering and George group members: Ruwandi Andrahennadi, Juxia Fu, Meki Gallegos, Gosia Korbas, Jake Pushie, Tracy MacDonald, Satya Singh, Cheryl Wiramanaden, and Soo In Yang. Liber and Janz group members are gratefully acknowledged for their continual support in the field and laboratory: Elise Bird, Eric Franz, Meghan Goertzen, Dominique Hauck, Mike Kautzman, and Jamie Phibbs. I am most grateful for my family Eileen, John, Timothy, and John Waylon in their never-ending support and encouragement.

## Table of Contents

## List of Tables

## List of Figures

## List of Abbreviations

3D: Three-Dimensional

*C. dilutus*: *Chironomus dilutus*

CLS: Canadian Light Source

CysSeSeCys: Selenocystine

*D. melanogaster*: *Drosophila melanogaster*

DMSeO: Dimethyl Selenoxide

EtOH: Ethanol

EXAFS: Extended X-ray Absorption Fine Structure

FeSe: Iron Selenide

GPX: Glutathionine Peroxidase

ICP-MS: Inductively Coupled Plasma Mass Spectrometry

KBD: Kashin-Beck Disease

KSD: Keshan Disease

LINAC: Linear Accelerator

$NaSeO_3$: Sodium Selenite

$Na_2SeO_4$: Sodium Selenate

NSS: Without Soller Slits

NSS-WC: Worst Case Scenario Without Soller Slits

$P_H$: Projected Horizontal Length

PoF: Point of Fluorescence

R-SeO-R: Selenoxide

$Se_0$: Elemental Selenium

Se-H: Selenol

SeMet: Selenomethionine

SPS2: Selenophosphate Synthetase 2

SS: With Soller Slits

SSRL: Stanford Synchrotron Radiation Lightsource

TrxR: Thioredoxin Reductase

UHMWPE: Ultra High Molecular Weight Polyethylene

XAS: X-ray Absorption Spectroscopy

XRF: X-ray Fluorescence

# CHAPTER 1

# INTRODUCTION

# Chapter 1 - Introduction

## 1.1. Objective

A lake system in Northern Saskatchewan has been receiving treated metal mine effluent from an upstream uranium milling operation. It has been noted that the selenium (Se) concentrations in the affected lake system are elevated with respect to surrounding lake systems. Synchrotron X-ray absorption spectroscopy and X-ray fluorescence imaging may provide insight into the possible effects of Se on this aquatic ecosystem, by examining the forms and routes by which Se interacts with lower trophic levels. Future endeavors may include a method for the sequestration and removal of Se to return this aquatic environment to unmodified times, ie. bioremediation.

## 1.2. Selenium

### 1.2.1. General

The first noted discovery of selenium (Se) was as early as the 13th century by the famous Italian adventurer, Marco Polo (Reilly, 1996). He dictated in his novel, *Il Milione,* that as he traveled through "a mountainous area on the far border of Cathay (China)" he was warned by various merchants of poisonous plants along the mountain that caused the hooves of animals to drop off (Pisa and Polo, 1300). It was not until Jöns Jakob Berzelius, in 1817, that Se was isolated from reddish deposits left after sulfuric acid production. Initially, tellurium was thought to be the culprit based on its smell; however, closer inspection from Berzelius revealed that it was not tellurium but had very similar properties. Therefore, when Berzelius finally isolated the mysterious substance and because of its similarities to tellurium (after the Greek word for Earth, *tellus*), he called it selenium (after the Greek word for moon, *selene*) (Berzelius, 1818; and Reilly, 1996). In nature Se is ubiquitous and can be found at trace levels in almost all types of soils and water. Selenium can be found in several forms including selenate, selenite, elemental selenium selenides and organic

forms such as selenomethionine; elemental Se also has 3 allotropic forms: red, grey, and black Se.

Selenium is used in many manufactured products: photovoltaic cells, rectifiers, pigments, metallurgy, glass, and other applications (STDA, 2010). Despite wide use in society, Se cannot be mined as a primary product and is mainly obtained as a by-product of many industrial processes such as copper and sulfuric acid production. In both copper and sulfuric acid production, Se is found in the system because of its association with the raw materials, copper ore and pyrite, respectively. Some waste products are refined to extract the Se. In addition to Se's use in industrial products, it is required as a micronutrient for healthy living in humans and animals; however, concentrations outside of Se's beneficial range may induce effects of Se deficiency or toxicity.

### 1.2.2. Benefits

In humans, Se is a component of the essential amino acid selenocysteine, which is present in glutathionine peroxidase (GPx), thioredoxin reductase (TrxR), and many other essential selenoproteins. GPx has an important role in reducing hazardous hydrogen peroxide ($H_2O_2$) into water. Normally $H_2O_2$ is utilized for destruction of bacteria and viruses (Rotruck *et al.*, 1972). TrxR is essential in the reduction of thioredoxin, which is responsible for cell growth, inhibition of apoptosis, DNA synthesis, gene transcription, and production of antioxidants (Reilly, 1996; Arnér and Holmgren, 2000; and Mustacich *et al*., 2000). Selenium has a very narrow beneficial range, and levels of Se above and below this range could result in Se toxicity or deficiency, respectively. Studies in fish have shown that dietary concentrations > 3 µg $g^{-1}$ can lead to growth inhibition, tissue damage, reproductive impairment and death (Hodson and Hilton, 1983; Lemly, 1993; and May *et al*., 2008).

### 1.2.3. Selenium Deficiency

Selenium deficiency indirectly causes the body to be more susceptible to foreign invaders, *ie*. bacteria and viruses. It is hypothesized that Se deficiency causes the immune system to work at sub-optimal conditions, providing less effective protection (Combs, 2000; and Zimmerman and Kohrle, 2002). The most notable cases of Se deficiencies occurred in Keshan Country of the Heilongjiang province, China (Li *et al*., 1985) and through areas stretching from the Far East, from Eastern Siberia to Central China (Wapnir, 1990). These two areas of Se deficiencies led to the classification of the Keshan Disease (KSD) and Kashin-Beck Disease (KBD), respectively. Although both diseases have an overlap of affected areas and are caused by Se deficiency, the symptoms of each differ from one another. KSD is characterized by multifocal necrosis and replacement fibrosis of the myocardium, which may result in cardiomyopathy (heart failure). KBD is characterized by osteoarthropathy, a disease affecting the bones, joint and growth plate cartilages (Moreno-Reyes, 2009).

### 1.2.4. Selenium Toxicity

On the opposite side of the spectrum, Se toxicity, or selenosis, can also be very problematic. Selenium is found to be toxic in chronic “high” doses of ≥ 400µg $day^{-1}$ for humans (Institute of Medicine, Food and Nutrition Board, 2000) and ≥ 10µg $L^{-1}$ for fish (Schultz and Hermanutz, 1990; and Lemly, 1996). In some cases, Se has been shown to cause larval deformations oviparous animals . In addition to the concentration, the chemical form of Se is also important; for example, low concentrations of dimethyl selenide are extremely toxic while elemental Se, even in high concentrations, is relatively non-toxic (Parizek *et al*., 1980; and Cummins and Kimura, 1971). The exact mechanism by which Se toxicity occurs is not known. In some cases, it is thought that Se is taken up through the same mechanisms as sulfur due to their chemical similarity (Brown *et al*., 1981). However, the suggestion that the accidental substitution of Se in place of sulfur can lead to different tertiary and quarternary structures and

therefore different protein function (Lemly, 2002; and Brown *et al*., 1981) is unlikely. Macromolecular crystallography routinely substitutes selenomethionine for methionine to aid in structure solution and the enzyme activity is not compromised by this substitution (Yuan *et al.*, 1998). Another prevailing theory includes the reaction of Se with thiols to produce superoxides, or free radicals ($O_2^-$) (Spallholz and Hoffman, 2002). Overall the cause of Se toxicity is dependent on the chemical form, very complex, and not fully understood.

### 1.2.5. Selenium in the Environment

Shamberger (1981) has presented a simplified geochemical cycle of Se (Fig. 1.1). Selenium's widespread occurrence at low levels in natural environments arises from the early stages of magma production in which Se separates from the parent magma. When the magma begins to crystallize, volatile components such as Se and sulfur separate, remain mobile, and are able to spread further distances leading to the association of Se with many sulfide ores (Shamberger, 1981). During weathering, the Se separates from the sulfides ores through oxidation into elemental Se or selenite, $SeO_3^{2-}$, where it may then associate with, for example, ferric hydroxide surfaces (Howard, 1977). Weathering of Se-bearing rocks distributes Se into the soil and subsequently into plants and other organisms.

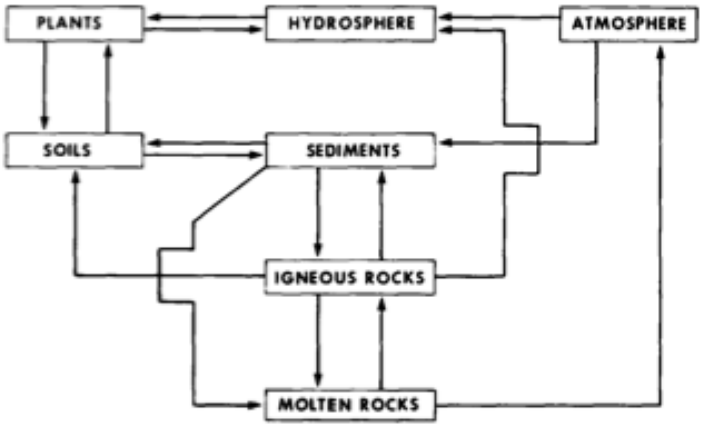


**Fig. 1.1**. Geochemical cycle of Se (Shamberger, 1981).

There is a greater chance of Se uptake and bioaccumulation the more mobile and biologically available the Se species. The mobility and uptake of Se is dependent on many factors and thus very complex (Fig. 1.2): it is influenced by pH, species, oxidation state, redox potential, microbial community, etc (Hartikainen, 2005; and Masscheleyn, *et al.,* 1990). Investigations have included the effects of Se adsorption to carrying clay content and Se's absorption into plants based on the present pH (Gissel-Nielsen, 1971). There has also been research on observing the effects of Se when pH and redox potential is varied (Masscheleyn, *et al.*, 1990). Thus, analyzing the effects of Se within a closed or even open system that takes into account all the various factors can be extremely difficult.

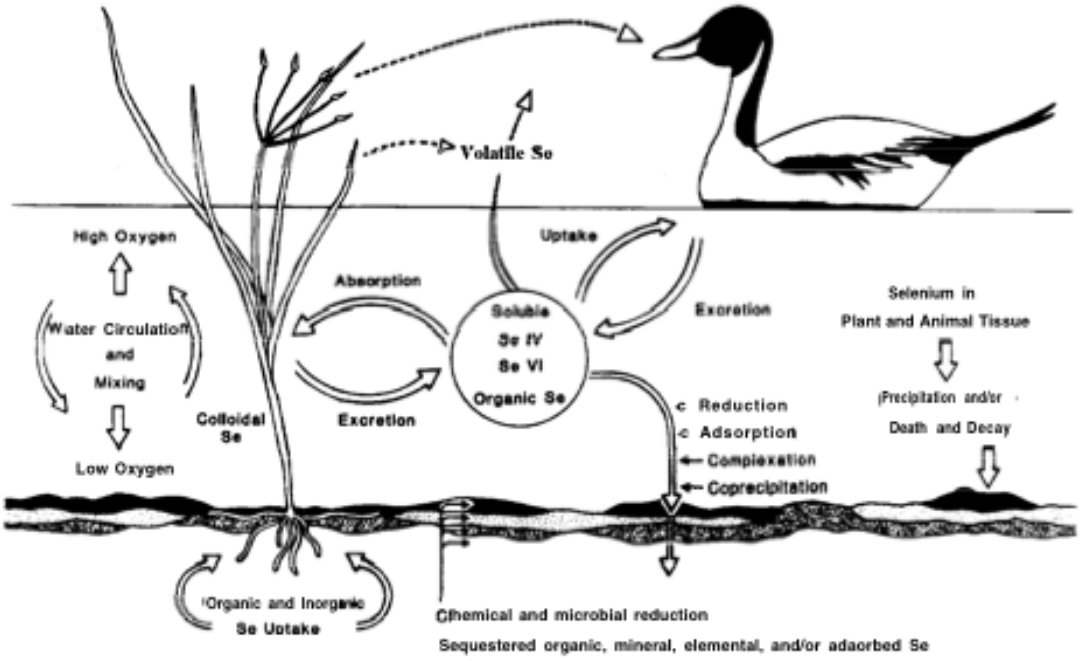


**Fig 1.2.** Simplified figure of the environmental cycling of Se (Lemly, 1999).

Uptake of Se from the soil into plants can occur via several Se species, selenate, selenite, or organic selenium (Shamberger, 1981). Some plants, such as *Astralagus bisulcatus*, have been shown to accumulate high levels of Se as Se-methylselenocysteine with no detrimental effects (Trelease *et al.,* 1960,

Terry *et al.,* 2000, Sors *et al*., 2005). Sediment dwelling bacteria have been shown to convert inorganic and organic Se into two main volatile Se species: dimethyl selenide and dimethyl diselenide (Chau *et al.,* 1976; and McCarty *et al.,* 1993). Under certain conditions, elemental selenium can be produced by bacteria (Garbisu *et al.,* 1996; and Oremland *et al.,* 1989). A variety of insects fed an elevated Se diet exhibited a selenomethionine-like species as the major organic Se species (Andrahennadi *et al*., 2007; and Vickerman *et al*., 2004).

Previously, one of the most comprehensive attempts to understand the transfer of Se through an aquatic ecosystem was performed in the mid 1980s, investigating the Kesterson National Wildlife Refuge in California, United States. This refuge was once an evaporation pond for agricultural waters, and over time the Se concentration was raised to a concentration in which the surrounding wildlife may be affected (Presser and Barnes, 1984). Extensive research has been performed on trophic levels ranging from the sediments to birds (Clark, 1987; Clark *et al.,* 1989; Ohlendorf *et al.,* 1986; Ohlendorf and Hothem, 1987; Weres *et al*., 1989) and the biogeochemical cycling of Se throughout the aquatic ecosystem (Presser and Ohlendorf, 2005). Since the late 1990s methods have been proposed to stimulate bioremediation of this aquatic ecosystem (Losi and Frankenberger, 1997; and Frankenberger and Arshad, 2001).

In *A. bisculcatus*, the pre-dominant organic species of Se found was Thus, Se-methylselenocysteine may be the Se form that is bioaccumulated, and grazers feeding on these plants may exhibit Se toxicity. This certain instance occurred in South Dakota, US, in the 1930s where large quantities of livestock exhibited symptoms of “blind staggers”; after ingesting Se hyper-accumulating plants they became blind, walked in a staggered fashion, and eventually died (Rosenfield and Beath, 1964). It has been suggested that the cause may be ingestion of

excess sulfur rather than Se (Beke and Hironaka, 1991); however, the exact mechanism has yet to be determined.

## 1.3. History and Background of the Site

Our research is focused on the Key Lake operation, located in Northern Saskatchewan (Canada) approximately 700 km north of Saskatoon (Fig. 1.3). Uranium (U) ore mined from McArthur River is transported 80 km to Cameco's Key Lake site, the world's largest high-grade U milling operation. The treated metal mine effluent from the milling process is released into the David Creek drainage system (Fig. 1.3) resulting in elevated Se in the aquatic ecosystem.

In addition to U's use in nuclear power and munitions it plays a major role in today's society, since the current theory suggests that Earth's molten core and tectonic plates are in part due to the decay of U (Bercovici *et al*., 1989, and Herndon, 1996). Some other uses of U include medical isotopes or dating the age of old samples. Uranium is widely distributed at low levles in rocks and seawater, the cost to benefit ratio in its extraction is very high (Tsezos *et al.*, 1984).

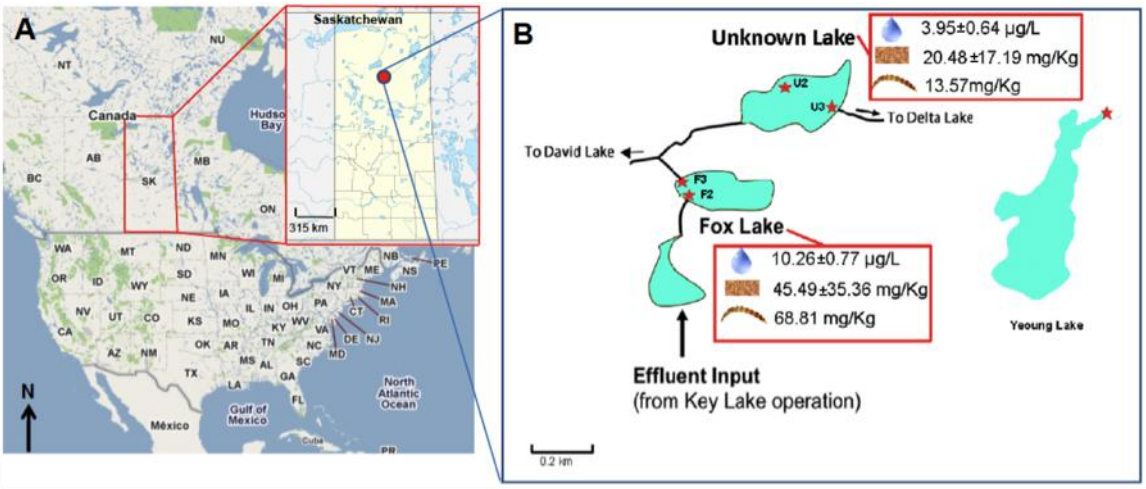


**Fig. 1.3. A)** Map of Saskatchewan, Canada, showing the study area as a red dot. **B)** A schematic map depicting the locations chosen for sediment and chironomid sampling. Yeoung Lake is located 8.2 km SE of Fox and Unknown Lake, and was chosen as the reference lake. Mean concentrations of water, sediment, and benthic invertebrates for Fox and Unknown Lake are presented (Wiramanaden *et al.*, 2010b).

There has been an increase in U mining operations around the world due to the increasing demand of nuclear power. Kazakhstan (~27%), Canada (~20%), and Australia (~16%) U mining operations constitute ~ 63% of the world's U (WNA, 2010). Uranium is typically milled and processed until it becomes $U_3O_8$, or yellowcake, its most stable form. This allows for safe transportation in between processing plants and nuclear power plants all over the world. Once arrived at the power plant, the yellowcake is further processed into $UO_2$, the most common form used in nuclear power plants. Uranium can be further sub divided into the most readily used isotope, $^{235}U$, for nuclear power.

## 1.4. Source of Selenium from Uranium Processing

The by-products associated with mining and processing of raw materials are a major concern. One concern is Se as the by-product of U processing. During the alkaline leaching of U ore, Se is leached and tends to accumulate and get re-circulated in the leachate (red arrow, Fig. 1.4) (Gupta and Singh, 2003; and Committee on Accessory Elements, 1979). This is controlled by siphoning part of the leachate away each cycle (Fig. 1.4) (Committee on Accessory Elements, 1979). In more mainstream and commercial processes, Se is found in the remnants of copper purification and sulfuric acid production (Reilly, 2006).

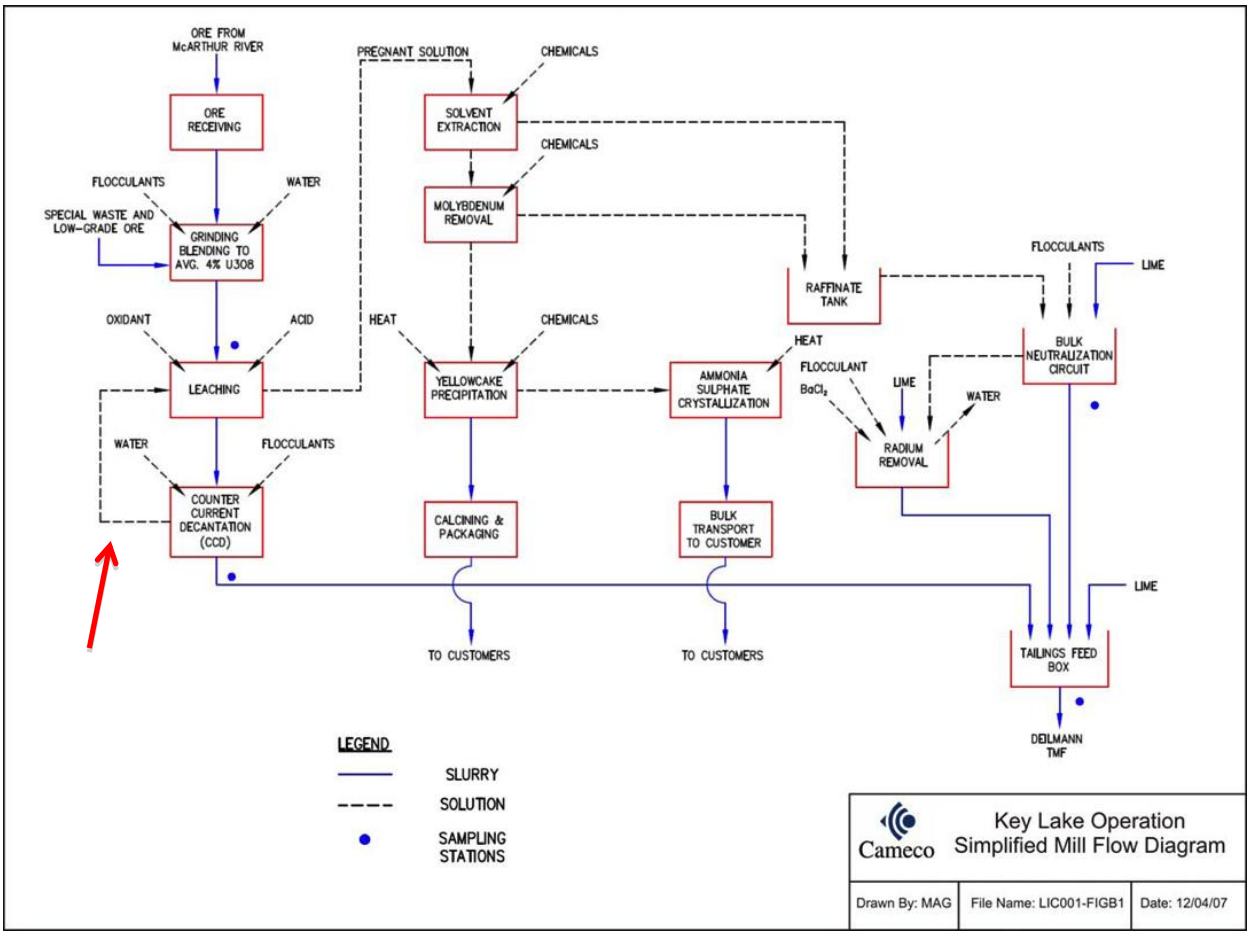


**Fig. 1.4.** Simplified Mill Flow Diagram at Key Lake (Cameco. Key Lake Extension Project: Project Description. Safety, Health, Environment & Quality. March, 2010). Red arrow denotes the step in the U enriching process where Se is accumulated in the leachate.

The treated mine effluent from U ore processing is released into a nearby lake system, resulting in elevated concentrations of Se relative to surrounding unconnected/unaffected lakes, potentially causing disturbances to the lakes' aquatic ecosystem (Fig. 1.3). The next section briefly addresses the characteristics of this site.

## 1.5. Site Description – Key Lake

### 1.5.1. General

Our research revolves around the Key Lake operation, located in Northern Saskatchewan (Canada) approximately 700 km north of Saskatoon (N 57º13'14.91", W 105º37'59.29") (Wiramanaden *et al*., 2010a; and Wiramanaden *et al*., 2010b) (Fig. 1.1). Located in the Boreal Shield ecozone (Cameco, 2010) the lake system has been receiving treated metal mine effluent from an upstream U ore processing mill, causing elevated Se levels in the aquatic ecosystem. The lakes have relatively shallow depths (< 20m) with a few deep areas (> 20m) and are mainly comprised of sand substrates (Cameco, 2010). Lakes in Northern Saskatchewan are typically nutrient poor, and have pH ranging from alkaline to slightly acidic, depending on surrounding bogs and muskeg (Cameco, 2010). Conductivity measurements demonstrate that the dispersion of treated effluent mixes fully within Wolf, Fox and Unknown Lake (Cameco, 2010). Yeoung Lake (N 57º 10'39.3", W 105º 35'00.1"), located ~8.2 km SE of Fox and Unknown Lake, was chosen as the reference site, due to its proximity, similar aquatic geochemistry, and disconnect from the affected lake system (Fig. 1.3).

Knowledge of the surrounding wildlife is essential in understanding organisms that may be affected by elevated levels of Se. Selenium can be readily taken up and then bioaccumulated through a food chain, suggesting that any vegetation or wildlife nearby may be affected by increased concentrations of

Se. Spruce, balsam fir and Jack pine are the major forest cover (Cameco, 2010). Susceptible wildlife includes caribou, great grey owl, bald eagles, osprey, aquatic furbearers, and moose (Cameco, 2010).

Past laboratory studies have shown that elevated levels of Se in northern pike eggs collected from the study site receiving environment have been linked to an increase in larval deformities in a laboratory study(Muscatello et al., 2006). These teratogenic effects included craniofacial deformities, skeletal deformities, and edema (Muscatello *et al*., 2006). To study the effects of the elevated levels of Se, synchrotron based X-ray absorption spectroscopy (XAS) and X-ray fluorescence (XRF) imaging was employed. The use of synchrotron characterization techniques allows the analysis of very complex samples with little to no pre-treatment and it also provides the ability to look at an element and its respective chemical forms.

## 1.6. Synchrotron

### 1.6.1. What is it?

A synchrotron is a facility for the generation of a wide spectrum of intense and nearly coherent electromagnetic radiation. It consists of several basic components (Fig. 1.5A) a) electron gun; b) linear accelerator (LINAC); c) booster ring; d) and storage ring. Assembled, these pieces have the capabilities to accelerate electrons or protons/lead ions to relativistic speeds. The electron gun is responsible for the production of electrons by heating up a cathode till electrons are released; for the Canadian Light Source (CLS), this cathode is a tungsten-oxide disk (CLS, 2009). These electrons then enter the LINAC where they are accelerated to a given energy by passing through multiple oscillating electric potentials. From here, the accelerated electrons enter the booster ring where they are further accelerated, via radio frequency (RF) amplifiers, to speeds nearing that of light and the energy of the storage ring (Winick, 1994). In the storage ring electrons are constantly losing energy in

the form of radiation, emitted tangentially to the electrons' orbit, as their direction changes due to magnetic fields (Ezquerra *et al.*, 2009). The energy lost is recovered by constant "boosts" from RF cavities spaced evenly across the storage ring.

Though the resulting accelerated electrons are referred to an electron "beam", they actually are discrete bunches of electrons. As a result of the discrete bunches the RF cavities must be synched to provide a "boost" at the exact instant bunches of electrons are to pass (Willmot, 2011). These synchronizations of RF cavity boosts give rise to the name synchrotron.

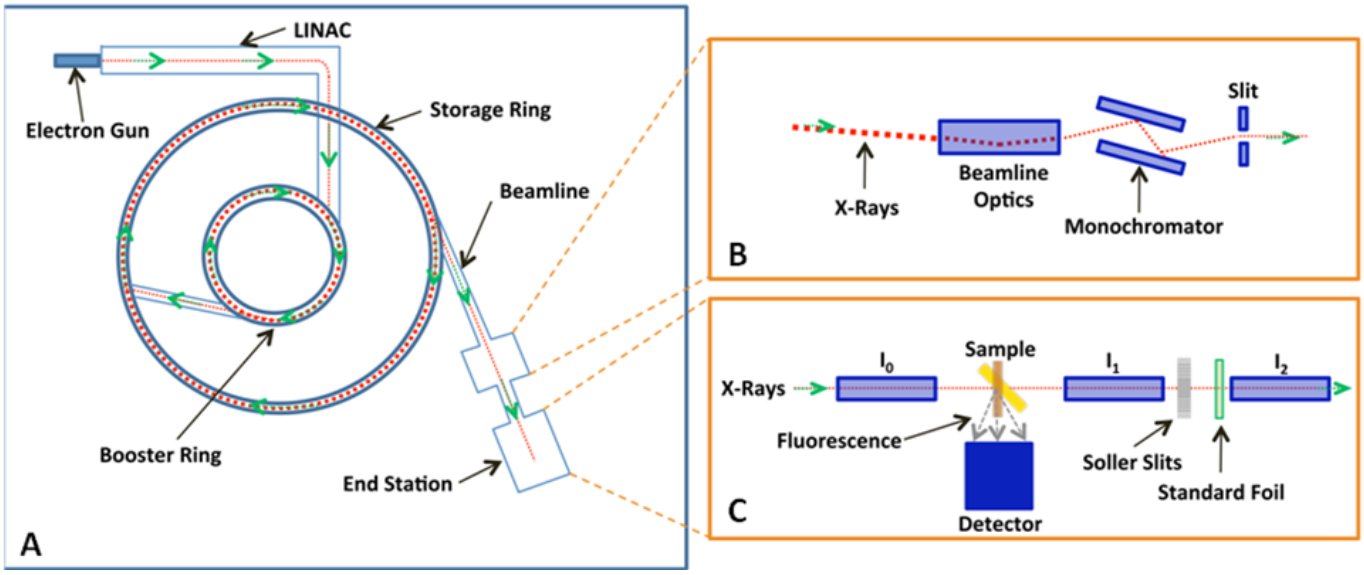


**Fig. 1.5.** (**A**) General overview of a synchrotron. (**B**) General description of a primary optical enclosure (POE) for a spectroscopy beamline. (**C**) General outline of a spectroscopy beamline's end station.

#### *1.6.1.1. Beamlines*

To harness the high energy X-rays, beamlines are constructed tangentially to the storage ring. Characterization of samples is achieved by bombardment of X-rays or other electromagnetic radiation. Beamlines receive these X-rays

either from a bend magnet, part of the storage ring, or an insertion device, such as a wiggler or undulator, which enhances the intensity of the X-rays. While the electrons travel along the storage ring they are constantly emitting X-rays with an angular distribution of $\Delta\theta$ both vertically and horizontally tangent to their path (Winick, 1994). By inducing an oscillatory path for the electron beam, an insertion device increases the intensity of the x-ray beam to be utilized by beamlines. These oscillations, or changes in direction, cause coherent interference resulting in a more intense beam (Hulbert and Williams, 1998).

The resulting X-rays, or white beam, are collected and passed through a monochromator crystal to select for a specific X-ray energy (Saisho and Gohshi, 1996). The ability to select single energies is essential for the study of specific elements using techniques such as XAS or XRF. Adjusting the angle at which X-rays hit the monochromator crystals provides specific wavelengths, $\lambda$ (Eq. 1.1), and the beam spot size is adjusted via slits (Fig. 1.5B).

$$n\lambda = 2d\sin\theta$$

**Eq. 1.1**. Bragg diffraction equation.

The *sin* of an angle, sin $\theta$, multiplied twice the lattice plane separation, 2*d*, will equal multiples, *n*, of a wavelength, $\lambda$. The angle $\theta$ is used in selection of particular wavelengths, $\lambda$ (Eq. 1.1); however, as $\theta$ changes so will the position of the diffracted X-ray beam. Therefore, in a double monochromator system, the second crystal is parallel to the first crystal, which allows the diffracted beam to remain parallel to the incident beam.

### 1.6.2. X-ray Absorption Spectroscopy (XAS)

#### *1.6.2.1. Background*

X-ray absorption spectroscopy (XAS) involves analyzing the interaction of X-rays with matter as a function of incident X-ray energy. An absorption edge

occurs for every element, produced when the incident X-ray energy is sufficient to eject a core electron from its respective shell (Gautreau and Savin, 1999). These “edges” are specific to every element; analyzing the shape and position of these edges by scanning a narrow energy range surrounding the edge gives species details about the element of interest. K-edges are produced when inner core electrons (1s electrons) absorb the energy from the beam and have the energy to overcome the binding forces and are ejected from the core as a photoelectron, also known as the photoelectric effect (Fig. 1.6A). Fig. 1.6B demonstrates that every element has a unique energy at which its absorption edge occurs. In addition to each element having a different absorption edge energy, different chemical types of each element will also produce a different spectral shape (Fig. 1.7). For example, species of different oxidation states appear at different energies; increases in oxidation state require more energy to remove an electron, and shift spectra to higher energies. In the case of an unknown sample, such as Se in sediment, the resulting spectrum can then be fit using a linear combination approach to deduce the relative contributions of standards to the spectrum of the unknown.

Extending the energy range further past the absorption edge, and before another element’s absorption edge, can give information about an atom’s local environment, also known as extended X-ray absorption fine structure (EXAFS) spectroscopy (George and Pickering, 2007). A typical spectroscopy beamline setup used to analyze near-edges and EXAFS of samples is demonstrated in Fig. 1.5C.

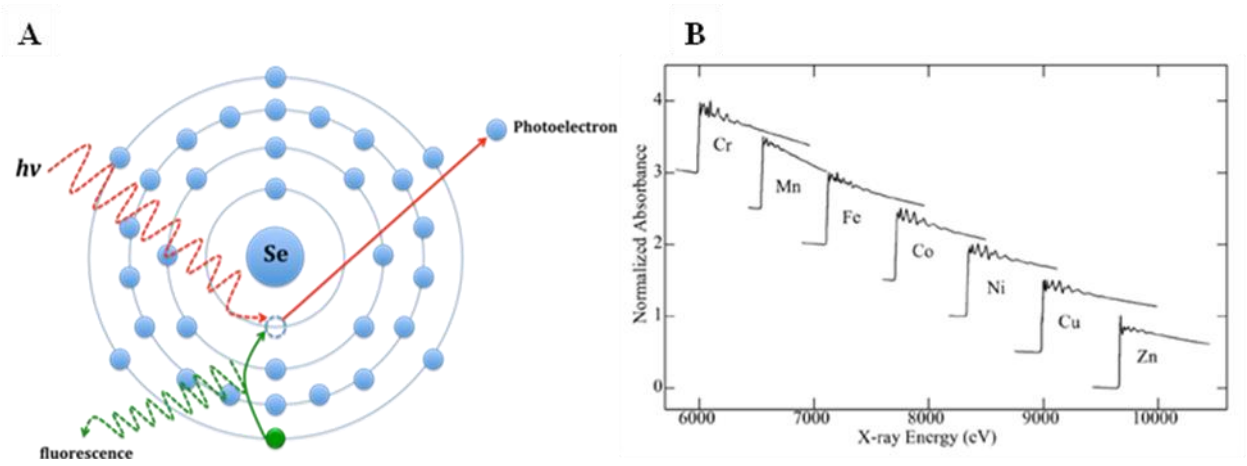


**Fig. 1.6**. (**A**) Diagram of photoelectric effect and fluorescence production. (**B**) K-edges of multiple elements. Pickering, I., and George, G. *Lecture 4: X-ray Absorption – Interaction of X-rays with Atoms and Molecules.* Geology 898 Class. University of Saskatchewan, Saskatoon, SK. 22 January 2009. Reproduced with permission.

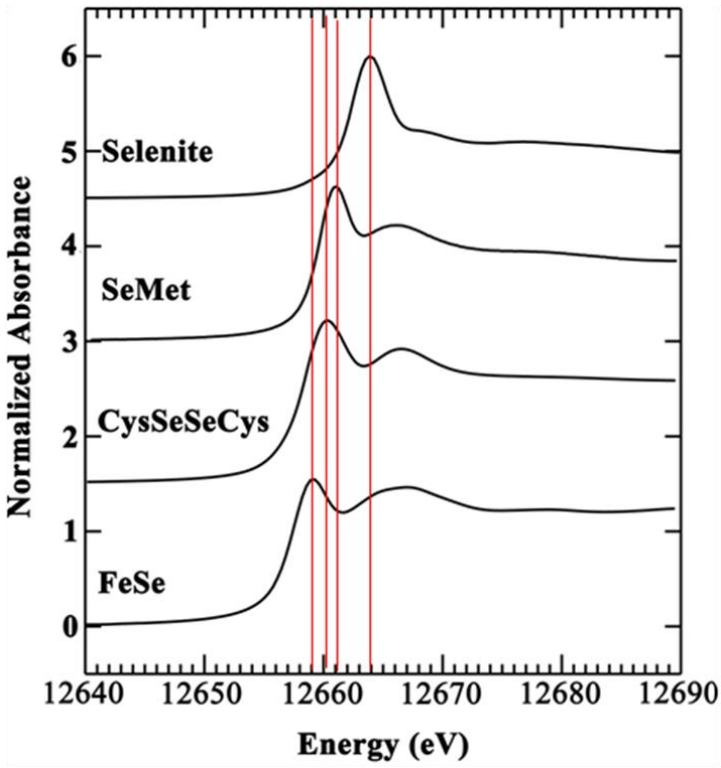


**Fig. 1.7.** Stack plot of four Se standards: iron selenide (FeSe), selenocystine (CysSeSeCys), selenomethionine (SeMet) and selenite. Red lines pass through the white line of each standard and help emphasize that each standard produces a slightly different spectra at a different energy.

### 1.6.3. Transmission and X-ray Absorption Spectroscopy (XAS)

#### *1.6.3.1. Background*

XAS can be recorded using transmission or fluorescence and these are both a direct result of the absorption process. Transmission analysis can be used to analyze strong or concentrated samples, while fluorescence is generally used for weaker samples. Transmission, T, involves analyzing the change in an X-ray beam; therefore, the log of the ratio between readings of ion chambers placed after and before the sample ($I_0/I_1$), respectively (Mandelkow and Bazin, 1988) (Eq. 1.2). The ion chamber readings represent the beam's intensity. Thus, as the beam passes through a sample with sufficient energy to eject an inner core electron, the X-ray beam's intensity will decrease.

$$T = \log\left(\frac{I_0}{I_1}\right)$$

**Eq. 1.2.** Equation for transmission.

Using a wide energy range can reveal the presence of multiple absorption edges of various elements. Fluorescence is produced as a result of the X-ray absorption process. X-rays with sufficient energy can remove an electron from its orbital creating a vacancy. An electron from a higher energy orbital will lose energy to fill the vacancy; the energy lost can be released in a form of a fluorescent photon (Fig. 1.6A) or an Auger electron. For sensitivity to the lowest concentration samples, an energy-dispersive detector is used to allow differentiation between incoming X-ray photons of varying energies, including separation of fluorescence from the element of interest from scattered photons or fluorescence from other elements.

#### *1.6.3.2. X-ray Fluorescence (XRF) Imaging*

Fluorescence that arises from the absorption of sufficiently high energy X-rays can be collected and utilized to provide distribution maps of elements and

species of interest. X-ray fluorescence imaging (XRF) employs fluorescence to map a sample (Kudo, 2000). Since all elements with an absorption edge below the incident energy will fluoresce, maps of localization and distribution of elements of interest can be obtained by selecting an incident energy above all of their absorption edges. By setting specific “windows” on the detector, one can look at multiple elements at once. These windows cause the resulting element’s image to only display the fluorescence collected within a specific energy range.

XRF is effective in providing detailed maps of the location/presence of elements of interest in a sample. Combining XRF with XAS allows one to select points of interest from the fluorescence map and collect near-edge spectra, which will give information on chemical forms at those points of interest. XAS's sensitivity to chemical form allows tuning of the XRF incident energy to different features in the near-edge, which can provide maps of different chemical forms of specific elements in the sample (Pickering *et al*., 2000).

## 1.7. Overview of Thesis

Selenium’s very narrow beneficial range has made it an element of much interest to scientists. Through the collaboration with various principal investigators at the Toxicology Centre (University of Saskatchewan) a holistic approach has been taken to study the effects of Se on the Key Lake system. Various trophic levels have been studied, both in the field and through laboratory experiments, in order to provide a better understand of the Se species present and their effects on the following outlined specimens. In this thesis, the investigation of the speciation and localization of Se found in sediment and benthic invertebrates from affected lakes may shed light on the route(s) by which Se bioaccumulates and is biotransformed through lower trophic levels of the aquatic ecosystem. Synchrotron XAS and XRF imaging

techniques are employed to provide a better understanding of the speciation and localization of Se in sediment and benthic invertebrate samples.

This thesis is centered on the use of synchrotron radiation to investigate speciation and localization of Se in sediments and organisms, and involves in part some development of the techniques. Chapter 2 describes the design, construction, and testing of a Soller slit apparatus to solve the problem of a distortion present in the spectra of samples run in transmission. This distortion is caused by fluorescence from the foil entering the ion chamber downstream of the sample ($I_1$).

The study of sediments is discussed in Chapters 3 and 4. Chapter 3 explains additional technique developments, specifically two devices that were created to aid in studying intact sediment cores at cryogenic temperatures. These devices include a guide rail system to help cut sediment cores, and a sediment holder to allow fluorescence and transmission analysis of intact sediments cores under cryogenic temperatures (~10 K). XAS analysis of sediments using this holder can provide information on Se species as a function of depth. Chapter 4 presents the results obtained from both devices as well as the data collected on Se, and other elements, in a sediment core as a function of depth.

Chapter 5 describes a comparative study of benthic invertebrates, chironomids, collected from the field with *Chironomus dilutus* grown in the laboratory and exposed to various Se spiked water conditions to mimic conditions found in the field. Distributions of Se and other elements are compared using synchrotron XRF measurements of both field and laboratory reared chironomids. The study includes XRF imaging of preserved chironomids, bulk XAS analysis, and inductively coupled plasma mass spectrometry (ICP-MS) measurements for

total Se concentration. The combination of XAS and XRF to examine chironomids will allow the determination of Se species present in the whole chironomid, and localization of Se in the chironomid, respectively.

This thesis concludes with Chapter 6, which presents an overall summary and discussion. Proposed future work on sediments and chironomids is also found in this chapter, to provide an idea of what may be required to further solidify results presented in this thesis.

The thesis is written in paper format with the result that certain materials, such as materials and methods, appear in more than one chapter.

# CHAPTER 2

# SOLLER SLITS

# [1]Chapter 2 – Soller Slits

## 2.1. Abstract

The measurement of X-ray absorption spectroscopy (XAS) in transmission is the method of choice for strong or concentrated samples. In a typical XAS experiment above 5 keV the sample is placed between the first ($I_0$) and second ($I_1$) ion chambers, with a standard foil placed between the second ($I_1$) and third ($I_2$) ion chambers for simultaneous calibration of energy during sample analysis. However, some fluorescence from the foil may be registered in $I_1$ that may cause anomalies in the transmission signal of the sample, especially when the sample edge jump is relatively small. To remedy this, Soller slits were constructed and placed between the foil and $I_1$ to minimize the back fluorescence from the standard foil. A comparison of a blank and standard sample, measured with and without Soller slits or under a worst case scenario, where the standard foil is against $I_1$, displayed a significant improvement in the resulting transmission spectra when Soller slits were implemented. These results demonstrate the advantages of Soller slits when analyzing weak signal samples via transmission XAS.

## 2.2 Introduction

Since their creation in 1924 (Soller, 1924), Soller slits have been used in a variety of experimental configurations to help collimate the beam of interest, whether it is parallel, converging or diverging. In general, Soller slits with closely spaced blades have shorter blades lengths, and the inverse is applicable. Housed in a casing and angled as the X-rays of interest, the blades are composed of a material that will strongly absorb any scattered beams and not fluoresce in the energy range of interest. In fluorescent XAS, Soller slits

[1] This chapter is based on the Communication published as Tse, J.J, George, G.N., and Pickering, I.J. Use of Soller slits to remove reference foil fluorescence from transmission spectra. Journal of Synchrotron Radiation. 2011, v.18, pp 527-529. Reproduced with permission from the International Union of Crystallography (IUCr).

increase the signal to noise ratio by eliminating scatter, that arises from sample, prior to the detector (Lytle *et al*., 1975; and Samant *et al*., 1987).

Transmission XAS is utilized in place of fluorescence XAS when the sample is sufficiently concentrated that the fluorescence may cause anomalies in the detection. A typical transmission XAS measurement (Fig. 2.1) involves a sample between $I_0$ and $I_1$ with a standard foil downstream between $I_1$ and $I_2$, for internal energy calibration. Back-fluorescence from the foil into $I_1$ (Fig. 2.1) appears as an inverted edge superimposed on the transmission data of the sample *(T,* Eq. 2.1*)*.

$$T = \log\left(\frac{I_0}{I_1}\right) \qquad \textbf{Eq. 2.1}$$

This effect becomes more pronounced when the foil is closer to $I_1$ or the signal from the sample is weak (Fig. 2.2). In the present study, the elemental Se foil has a lower excitation energy than the selenate sample, leading to a trough in the spectrum. To minimize this effect, Soller slits, to be placed between the foil and $I_1$, were constructed (Fig. 2.3).

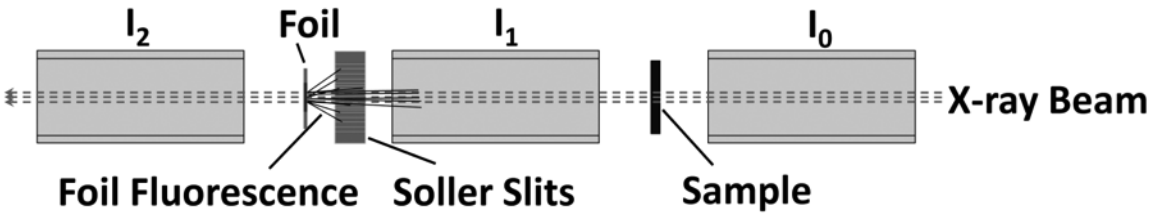


**Fig. 2.1.** Plan view of a typical transmission XAS setup.

## 2.3. Materials and Methods

The Soller slit assembly consists of an Al case with slots that accommodate up to 21 vertical blades (Fig. 2.3). The assembly was fabricated by Vantec Design & Manufacturing LTD (Saskatoon, SK, Canada). The case assembled with 4 separate Al pieces held together by 8 M2 x 8 head cap Allen screws. The width of the Soller slits (Fig. 2.3) is identical to that of the ion chamber for easy alignment. If properly aligned, the beam will travel through 13 “inner blades” spaced 2.0 mm apart in the middle of the Soller slit, while 8 “outer blades” are spaced 4.0 mm apart; the closer spaced blades provide less back-fluorescence. Ideally a set of horizontal slits would also be present; however, the openings in the ion chamber are much larger in the horizontal direction.

Silver (Ag) was chosen for the blade material due to its high Z, long-term stability, machinability, and availability. Sheets of 0.25 mm thick Ag (Surepure Chemetals, Florham Park, NJ, USA) were cut with an X-Acto No. 2 knife into blades measuring 30 mm (vertical height) × 25 mm (length along the beam). All edges of the blades were sanded with 3M™ diamond lapping film to remove any burrs acquired during the cutting process. A thickness of 0.25 mm allowed for 0% transmission at energies below 15 keV and up to 2.2% transmission at 21 keV (McMaster, *et al*., 1969). To demonstrate the effectiveness of the Soller slit, a Se-free blank and 4.3 mM $Na_2SeO_4$ standard were measured under 3 conditions described below. The blank consisted of an aqueous solution of a standard biochemical buffer, 100 mM MOPS (pH 7), with 30% v/v glycerol added to reduce ice crystal formation upon freezing. The 4.3 mM $Na_2SeO_4$ solution was created by a 1:5 dilution of a 21.4 mM solution of $Na_2SeO_4$ in 100 mM MOPS (pH 7) and 30% glycerol. Samples were measured on beamline 7-3 at the Stanford Synchrotron Radiation Lightsource (SSRL) in custom 2 mm path length Vero White polymer cuvettes, 90º to the incident beam, at 10K (Oxford Instrument Liquid Helium cryostat). The energy was selected with a Si(220) double crystal monochromator, a 15 keV cutoff achieved by adjusting the angle

of the upstream Rh-coated vertically collimating mirror, nofocusing optics and a 1.0 x 8.0 mm (height x width) beam defined using slits upstream of $I_0$.

Measurements of the blank and dilute selenium sample were made under three conditions. (1) With Soller slits (SS) between the standard foil and $I_1$ with ~ 3 mm on either side. (2) Without the Soller slits (NSS). (3) In a worst-case scenario with no Soller slits (NSS-WC), $I_1$ was moved downstream so that it was flush with the foil, maximizing the foil fluorescence entering $I_1$.

## 2.4. Results and Discussion

The effects of foil fluorescence entering $I_1$ are shown in Fig. 2.2. In NSS-WC and even NSS, the blank spectra (Fig. 2.2A) showed a significant negative feature, which also appeared as a trough in the pre-edge region of the 4.3 mM $Na_2SeO_4$ spectrum (Fig. 2.2B). Substantial reduction of back-fluorescence from the foil into $I_1$ was observed (Fig. 2.2B) with the use of of the Soller slits. Though residual back-fluorescence is observed in SS, the contribution is negligible compared to NSS and NSS-WC. Estimated from the height of the foil white line above background, the ratio of back-fluorescence intensities in the three cases NSS-WC:NSS:SS is 2.45:1:0.09

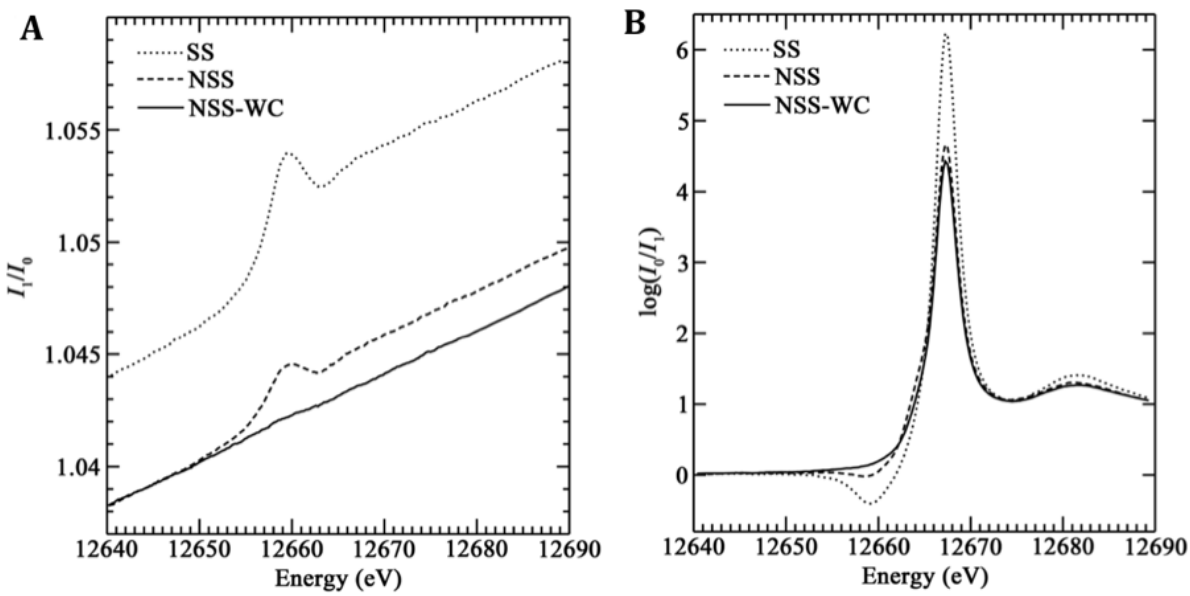


**Fig. 2.2. (A)** Spectra from the blank under the 3 conditions, plotted as $I_1/I_0$ to emphasize the back-fluorescence signal. **(B)** Background subtracted and normalized transmission spectra from 4.3 mM $Na_2SeO_4$ run under the 3 conditions. The 12663 eV shoulder is a small fraction of selenite produced by selenate photoreduction in the X-ray beam even at 10K.

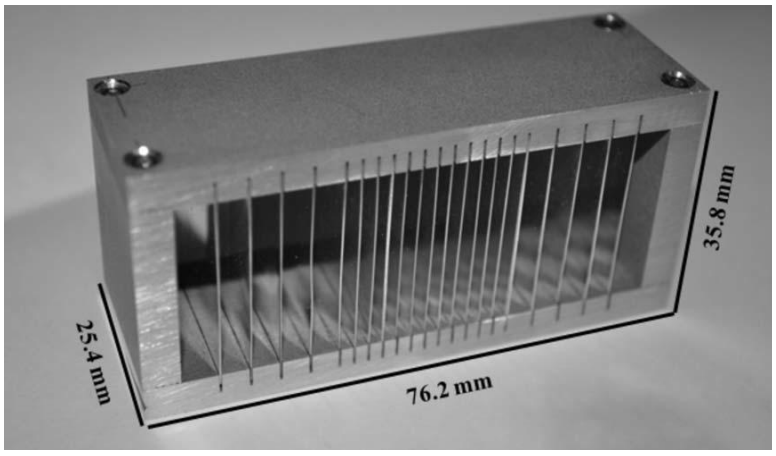


**Fig. 2.3.** Image of Soller slits.

The Soller slit assembly's effectiveness in the horizontal dimension was predicted from a general single point of fluorescence (PoF) between two blades (Fig. 2.4). The current configuration predicted a projected horizontal length ($P_H$) of 2.21 mm (Eq. 2.2), equivalent to an angle of 71 mrad. Regardless of the PoF position on a line normal to the blades, $P_H$ remained the same. In the absence of Soller slits, the angle calculated from the width of ion chamber opening (approximately 64 mm) at a distance $D_I$(Fig. 2.4) was 1.60 rad. Thus, the calculated intensity ratio NSS:SS is about 1:0.04, slightly better than the observed ratio of 1:0.09, the difference is possibly due to uncertainties in measuring the very small SS back-fluorescence (Fig. 2.2A). Quantifying foil fluorescence into $I_1$ for NSS-WC was difficult due to the acute angles occurring with the foil so close to $I_1$; however, more back-fluorescence is expected for NSS-WC compared with SS and NSS due to the foil's proximity.

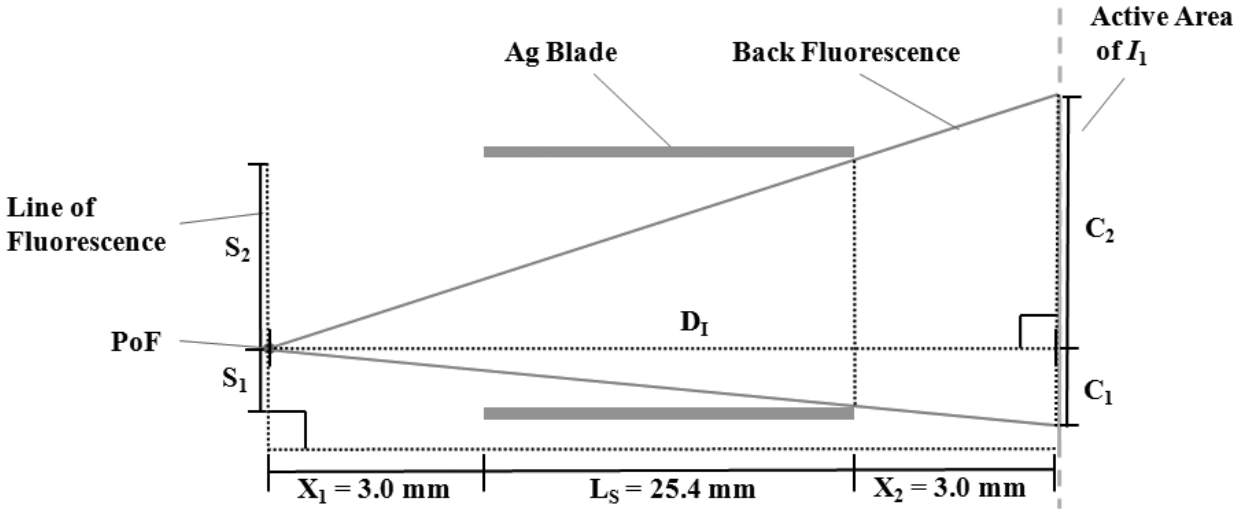


$$\therefore P_H = \frac{D_I D_S}{D_I - X_2} \qquad \textbf{Eq. 2.2}$$

**Fig. 2.4.** Schematic demonstrating the amount of foil fluorescence entering $I_1$ in the horizontal plane from any point of fluorescence (PoF) along the line of fluorescence. $\mathbf{L_s}$= length of Soller slit blades. $\mathbf{D_s}$ = distance between Soller slit blades ($S_1$ + $S_2$). $\mathbf{D_I}$ = distance from foil to $I_1$ ($L_s$ + $X_1$ + $X_2$). $\mathbf{X_1}$ = distance from foil to Soller slit. $\mathbf{X_2}$ = distance from the Soller slit to $I_1$. $\mathbf{P_H}$= horizontal projection onto $I_1$. Since $P_H=C_1+C_2$, and $C_1/S_1 = C_2/S_2 = D_I/(D_I-X_1)$, therefore $P_H=D_ID_S/(D_I-X_2)$.

In summary, the use of Soller slits to remove foil fluorescence is advantageous when collecting transmission XAS of weak/dilute signal samples. Foil back-fluorescence anomalies are essentially removed by the Soller slits, allowing for more accurate spectra. The simplicity of the Soller slit design and the relatively low cost of materials allow easy creation of custom Soller slits for any XAS beamline.

# CHAPTER 3

# SEDIMENT SAMPLE HOLDER

## Chapter 3 - Sediment Sample Holder

### 3.1. Abstract

A versatile sample holder is described for analysis of intact sections of heterogeneous sediment cores using synchrotron XAS at approximately 10 K in a liquid helium flow cryostat. Cryogenic temperatures are essential in determining accurate chemical speciation as a function of depth in intact sediment cores. Control samples were measured to test possible shadowing effects in fluorescence measurements. The successful demonstration of the stability and minimal shadowing of the sample holder at ~10 K suggests its viability for studying sediment samples. In addition, the sample holder houses inner sample cells, fabricated by 3D printing, which can be customized for a wide range of applications and samples.

### 3.2. Introduction

We designed, constructed and demonstrated the effectiveness of a custom holder used in synchrotron XAS analysis of spatially heterogeneous samples in a liquid helium flow cryostat. Spatially heterogeneous samples include sediment cores for which speciation and abundance of elements may vary with depth. Under room temperature analysis, extensive chemical modification and spatial migrations are expected. Although preservation methods such as resin infusion or embedding (Lamoureux, 1994) would allow for intact sediment cores to be sectioned and analysed, these chemical procedures may cause speciation changes. Use of liquid helium (~10 K) rather than liquid nitrogen (~77 K) to maintain sample temperature minimizes any photo-induced changes of the sample due to the intense X-ray beam. By maintaining the sediment core frozen throughout preparation and analysis, its depth profile and speciation of elements remain intact. The sample holder facilitates analysis of sediment core sections at approximately 10 K with minimal pre-treatment or preparation of the cores.

Cryogenic XAS of bulk sediment can involve grinding a frozen sediment sample until homogeneous (Wiramanaden *et al*., 2010a), thus losing any depth profiles that the sediment may have exhibited. Analysis also can be achieved by homogenizing short sections (e.g. 1 cm depth) of whole cores (Martin *et al*., 2011); however, variations may occur at a finer scale especially near the sediment-water interface. A commercially available alternative to analyzing frozen whole sediment cores is a Displex® (Advanced Research Systems); however, this system can cost in excess of $30,000, requires special and expensive shipping procedures, and necessitates long downtime between samples due to warming and cooling cycles.

To facilitate analysis of intact cores at 10K, a custom sediment sample holder was designed for the Oxford Instruments CF1208 liquid helium flow cryostat, which is currently employed for bulk XAS at the Stanford Synchrotron Radiation Lightsource (SSRL), Canadian Light Source (CLS) and several other synchrotron facilities worldwide. The sample holder was designed to analyze speciation variations as a function of depth for intact frozen sediment core segments. Using vertical cryostat translation, spectra at spatial increments of 100 µm are achievable. In addition, a guide rail system was developed in order to accurately cut segments of frozen sediment cores to fit inside the sample holder and cryostat.

## 3.3. Guide Rail System

The sample cell was designed to utilize the maximum amount of viewable area given by the cryostat. Sediment cores were larger than the sample cell; therefore, samples required some cutting to fit within the sample cell. To help maintain constant proportions with the Zephyr ring saw (Gryphon Corp.) (Fig. 3.1A) a guide system (Fig. 3.1B) was designed and built. The guide system had a knob for easy adjustments and the work area was large enough to accommodate sizable samples.

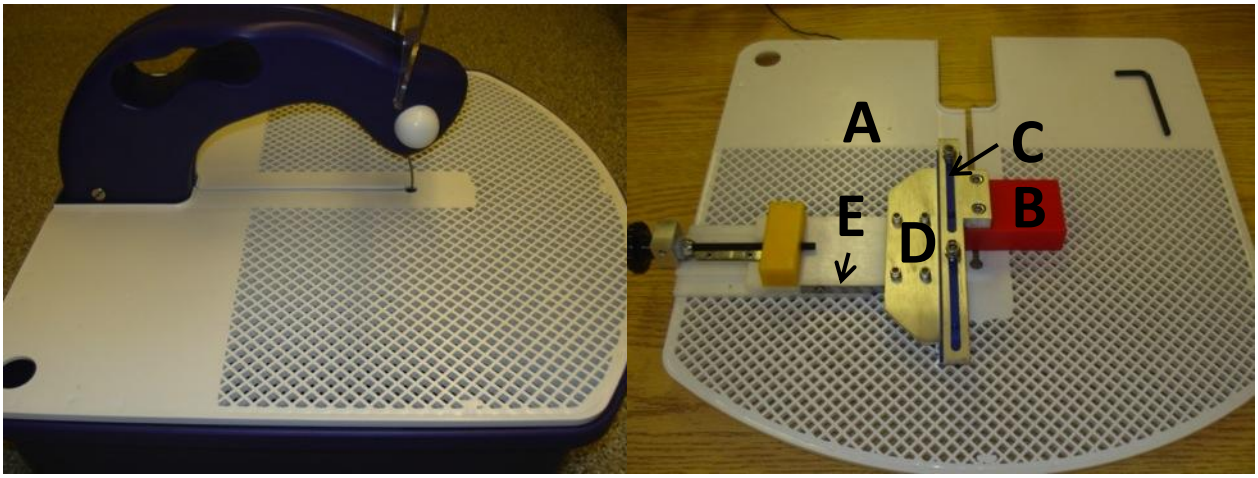


**Fig. 3.1**. **(A)** Zephyr ring saw. **(B-E)** Guide rail system designed for the work surface of the Zephyr ring saw.

The Zephyr ring saw was chosen due to its portability, diamond blade, and ability to subsection sediment cores into acceptable sizes for the sample holder. The steel core circular blade is coated with diamond flecks/fragments which will eliminate metal transfer onto the sample, making the Zephyr saw ideal for omni-directional cutting and preparing samples for synchrotron trace element analysis. Initially, the plan was to bring the Zephyr saw to the beamline and cut cores on-site; however, shipping various cores frozen was more costly and risky than shipping sub samples of the cores.

To minimize the effects of human error in cutting sediment samples, a guide rail system was required. The design for the guide rail system had to be one that could conform to the pre-existing Zephyr work surface (Fig. 3.1A). Sediment cores will come in contact with the guide rail system; therefore, the contact surfaces must be comprised of a material that is non-metallic, to reduce any metal transfer to the sample. Vantec Design & Manufacturing Ltd was responsible for the construction of the guide rail system. The material chosen was ultra-high-molecular-weight polyethylene (UHMWPE). Due to its availability

and low price, UHMWPE was used for most of the guide rail system (Fig. 3.1B and C). A ruler (Products Engineering) (Fig. 3.1E) screwed into one of the UHMWPE to allow for accurate (± 0.25 mm) adjustments of the distance between piece C and the circular ring blade (Fig. 3.1C). Some steel pieces were used for support (Fig. 3.1D).

One restriction provided by the Zephyr saw is the constant need for water to cool down the blade, which generates a lot of heat through friction from cutting a sample. The Zephyr saw utilizes a built-in water reservoir to maintain blade cooling during cutting. Prior to any sample cutting, this reservoir is emptied and the saw run until no dripping water is observed over the sample cutting area. This heating of the blade could be detrimental to the sample, as heat could melt the sample, change Se speciation, and lose the sediment depth profiles. Therefore, prior to any cutting, samples were frozen in liquid nitrogen to keep sediment profiles intact and aid in cooling down the blade during cutting.

## 3.4. Sediment Holder

The sample holder comprised two main pieces: the outer sample holder and the sample cell. The outer sample holder was mainly comprised of Al, machined by Vantec Design & Manufacturing Ltd from a stock Al cylindrical bar by computer numerical control machining and electrical discharge machining (Fig. 3.2B). Additional pieces were custom printed on a 3D printer (Objet Eden500V) in VeroWhite (Objet FullCure®830), shown to have no interference from elements within our energy range of interest (data not shown, 12520 – 12860 eV), and attached by #0-80 nylon screws. The front/back or sides of the sample holder were angled or shortened, respectively, to maximize a cone of fluorescence from the centre of the sample holder at a 45º or 90º sample orientation. In the cryostat, the sample holder had a 0.75 mm clearance on all sides and could accommodate samples of 10 mm × 10 mm × 5 mm (width × height × depth).

Measurement of subsequent segments of the same core allowed analysis of additional depths.

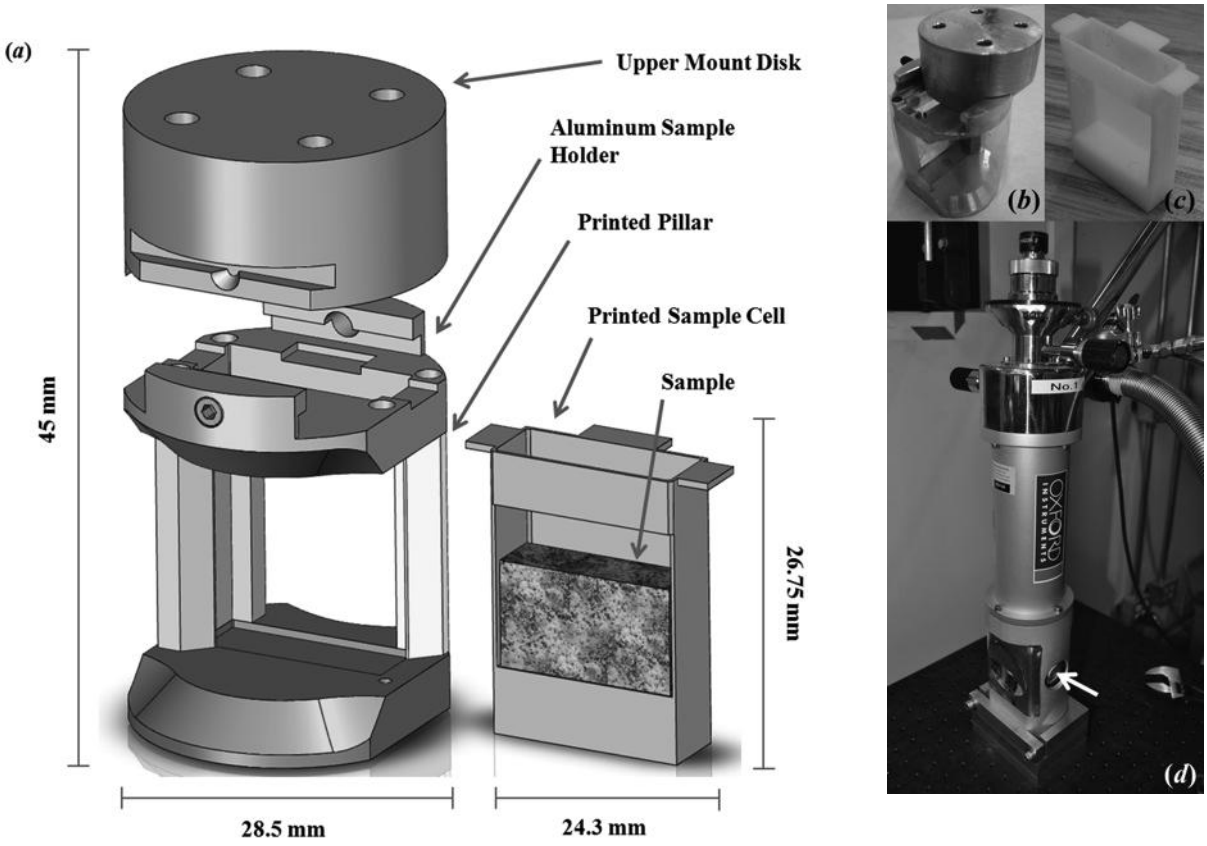


**Fig. 3.2.** Computer-aided design drawing of the sample holder and sample cell **(A)**, with the finished sample holder **(B)** and sample cell **(C)**. The assembly sits inside a CF1208 cryostat denoted by the arrow shown in **(D).**

The pillars were removable, interchangeable, and shaped to allow maximum fluorescence from the sample with the fluorescence detector at 90° to the incident beam. One pillar was constructed of aluminum (Al) to add structural stability to the sample holder at cryogenic temperatures; the other pillar and sample cells, used to contain samples, were printed of VeroWhite to maximize fluorescence from the sample to the detector (Fig. 3.2B and C). Interchangeability of the pillars allowed for maximum fluorescence collection regardless of detector position relative to the cryostat, ie. left or right of the cryostat, with the printed pillar always on the detector's side. The sample cells

had a carved out window to expose the whole sample surface to the incident beam, and fluorescence to the detector. The use of printed sample cells allowed for cheap mass production, minimal absorption, and custom modifications.

A window of kapton film (38µm thick) around the sample holder added a second layer of containment. Since moisture in the air could cause freezing of the sample cell to the inside of the sample holder resulting in extended sample change times and loss of valuable beamtime, a hole in the bottom disk of the sample holder allowed a mid-sized Allen key to push the sample cell out of the sample holder without the removal of the kapton film. After initial trials showed that the upper mounting disk froze to the top disk of the sample holder, both surfaces were finely polished to reduce water nucleation, reducing the duration of sample changes from about 15 to 7 minutes.

To demonstrate the effectiveness of the sample holder a homogeneous Se standard, 10 mg $L^{-1}$ of Se as sodium selenate ($Na_2SeO_4$) dissolved in Barnstead water (18.2 MΩ-cm), was measured to investigate any shadowing effects on the fluorescence signal or interference that may occur from the cryostat or detector position. The sample face was divided into 3 columns, spaced 0.25 mm apart, and each column was divided into 21 vertical points, spaced 0.5 mm apart, giving an average measured area of 10 mm × 10 mm (height × width). At each point in the homogeneous sample, a short Se K-edge spectrum (12520 - 12860 eV) was measured and its edge jump plotted (Fig. 3.3).

Measurements were conducted on beamline 9-3 at SSRL at ~10K. The energy was selected using a Si(220) double crystal monochromator, with a 15 keV cutoff achieved by adjusting the angle of an upstream Rh-coated vertically collimating mirror. A 0.1 mm × 2.12 mm (height × width) beam, defined by

upstream slits, projected to a 0.1 mm × 3.0 mm illuminated area on the sample which was oriented at 45º to the incident beam.

## 3.5. Results

The effectiveness of the sample holder (Fig. 3.2) was demonstrated by fluorescence measurements from standards, which showed that regardless of sample position with respect to the sample cell and detector, the fluorescent edge jump was essentially invariant (0.181 ± 0.012 standard deviation) (Fig. 3.3); therefore, no shadowing effects or obstructions by equipment were observed. The holder has been used to measure Se and other elements in frozen sections of sediment cores (Fig. 3.4). Additional details are presented in Chapter 4 (Sediments). The sample holder has since been used to house a frozen solution of a highly reactive biomolecule (Pushie *et al*., 2011) during XAS data acquisition. Beam induced chemical changes were minimized by combining multiple short measurements from different spatial locations at 10K.

The price of each printed sample cell (approximately $1 each) allows for mass production and customization. The sample holder was designed for the CF1208 cryostat but will also fit inside newer models, such as the Optistat CF and CF-V (Oxford Instruments).

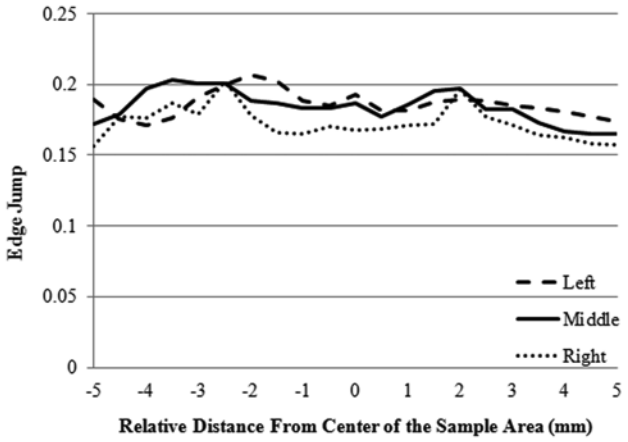


**Fig. 3.3**. Fluorescence intensity as a function of relative vertical position from the center of a homogeneous Se standard.

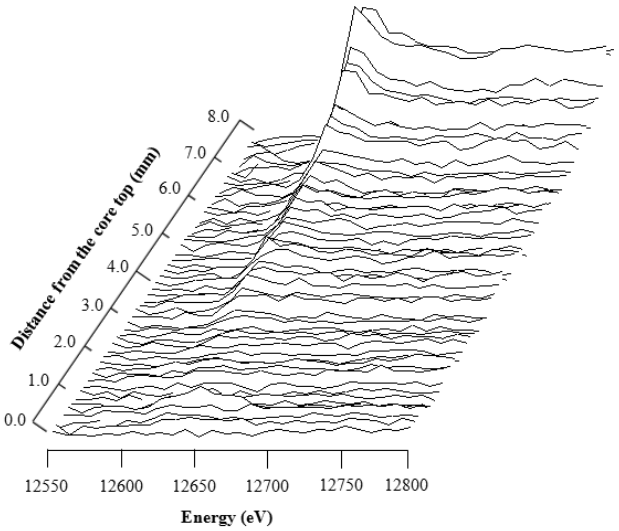


**Fig. 3.4**. Example data set from a sediment core. At 100 µm step sizes, variations in the Se signal can be observed within an 8 mm depth.

# CHAPTER 4

# SEDIMENTS

## Chapter 4 - Sediments

### 4.1. Abstract

A lake system downstream from a U milling operation in northern Saskatchewan has been receiving treated metal mine effluent. This effluent increased the Se water concentrations within this lake with respect to surrounding lake system not receiving effluent. The sediment of the lake system is an important route by which Se may enter the aquatic ecosystem, especially as benthic invertebrate communities inhabit the sediment. By collecting, preserving, sectioning, and analyzing frozen sediment cores and combining synchrotron XAS at high resolution with vertical cryostat movement, it is possible to study changes of Se levels and speciation as a function of depth. These methods demonstrated the presence of biologically available Se species (selenite and selenomethionine-like species) that may be accessible by the benthic invertebrate community.

### 4.2. Introduction

Selenium is a micronutrient, required for the survival for many organisms, and must be regulated to prevent Se deficiency or toxicity. In addition to the required Se intake, the species in which Se is taken up is also very important; in fact, it is the species and not concentration that is the most influential bioavailability factor (Zayed *et al.*, 1998). Selenomethionine and selenocysteine are both Se-containing amino acids commonly found in organisms. Selenocysteine is considered the 21$^{st}$ essential amino acid and is produced and incorporated into proteins very specifically. In humans, selenocysteine is required for the production of glutathionine peroxidase to detoxify hydrogen peroxide ($H_2O_2$) into water, and thioredoxin reductase, used in cell growth, redox signaling, regulation of apoptosis, etc. (Stadtman, 1990; Mustacich, *et al*., 2000; and Arnér and Holmgren, 2000), as well as several other essential enzymes. By contrast, selenomethionine is not an essential amino acid but, when present in abundance, is accidentally substituted for the essential amino

acid methionine in proteins. In nature, Se can exhibit oxidation states ranging from -2 to +6, is found in minute quantities, and is often purified from waste material of other industrial processes, such as copper purification (Thomassen *et al*., 2004), sulfuric acid production (Stewart, 2004), and U ore processing (Gupta and Singh, 2003). In some cases, it may not be profitable to further purify for Se, and the treated waste is disposed.

Selenium has been shown to be toxic to an aquatic ecosystem; in a well-documented case, the Kesterson National Wildlife Refuge located in California, was once used as an evaporation pond for agricultural drain waters. Over extended periods of time Se was at a sufficiently high concentration that decreased wildlife reproduction and increased deaths, especially in waterfowl, were observed (Clark, 1987; and Ohlendorf and Hothem, 1987). There has been extensive research from benthic invertebrates to birds in this particular aquatic ecosystem (Ohlendorf and Hothem, 1987).

In the present case, a lake system in Northern Saskatchewan (Fig. 4.1) has been receiving treated metal mine effluent from an upstream U milling operation. Over time, the treated metal mine effluent has caused the overall Se concentration in a nearby lake system to become elevated with respect to surrounding unaffected lake systems. Previous research has demonstrated that elevated levels of Se can cause larval deformities in northern pike (*Esox lucius*) (Muscatello *et al*., 2006). However, this should not be attributed solely to Se, as the treated effluent is most likely comprised of many compounds, and the exact mechanisms and routes by which Se enters an aquatic ecosystem are not fully understood. To provide additional information in the understanding of how Se many enter an aquatic ecosystem, we propose to study the species of Se in sediment from various sites in the lake system. Sediments may act as one of the initial steps for Se biomagnification through a food chain. Employing

synchrotron XAS combined with the translation of a cryostat will provide valuable data on how Se speciation changes as a function of depth in preserved sediment cores.

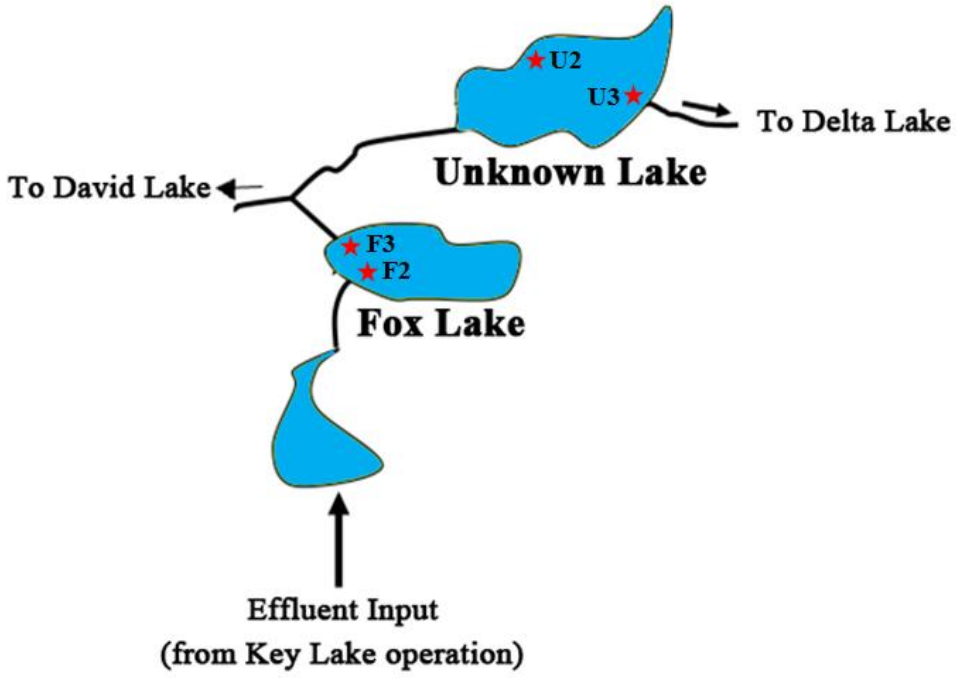


**Fig. 4.1**. Fox and Unknown Lake of the Key Lake system. Sites chosen for study are depicted by red stars.

Previous research on sediments from the same sites has been performed at a coarser resolution (Wiramanaden *et al.*, 2010a). Cores at room temperature were cut into 1cm sections, homogenized in an agate mortar and pestle, frozen, and then Se speciation was measured at 10K using XAS (Wiramanaden *et al*., 2010a). The research of Wiramanaden *et al*. (2010) was essential in understanding the potential Se species that may be present in the sediment; however, as the samples were homogenized, the sediment depth profile was lost and any variations of Se species as a function of depth could not be measured. Building on this previous work, our research focused on analyzing intact, preserved sediment cores with cryogenic (~10 K) temperatures at a finer resolution, especially near the sediment-water interface. In many cases, this is

also the zone inhabited by benthic invertebrates. If samples could be collected, flash frozen and then maintained frozen during transport, preparation, and analysis, any sample degradation should be greatly minimized. Therefore, the ideal method to analyze sediment cores would be at ~10 K, with the added benefit of minimizing any changes of the sample caused by the intense beam of 3$^{rd}$ generation light sources.

## 4.3. Materials and Methods

Sediment cores were collected in both the 2008 and 2009 field season in acrylic core tubes (4.8 cm diameter) with a custom made corer (Wiramanaden *et al.*, 2010a). During the 2009 field season, June 11-16$^{th}$, core samples were taken from Unknown 2 and Fox 3 (Table 4.1). These sites were chosen due to their high Se concentration measured in past years (Wiramanaden *et al.*, 2010b), enabling easier bulk analysis. No cores were taken from Yeoung Lake, the control site for other measurements, as previous bulk measurements showed that the Se concentration was below the detection limit of the beamline. Field season 2008 cores were frozen in a deep freezer; however, large ice crystals were found to form disrupting the sediment depth profile. Therefore to prevent ice crystal formation, the 2009 field season cores were prepared initially by flash freezing in a slurry of liquid nitrogen and iso-pentane, a method known to minimize ice crystal formation by very rapid freezing. Cores were transported back to the Toxicology Center (University of Saskatchewan) by truck in coolers filled with dry ice, and then stored in a ~253 K freezer.

| Lake/Site | Location |
|---|---|
| Fox/2 | N 57º 13’23.8” W 105º 41’04.2” |
| Fox/3 | N 57º 13’27.6” W 105º 41’02.6” |
| Unknown/2 | N 57º 14’02.9” W 105º 40’28.7” |
| Unknown/3 | N 57º 14’00.8” W 105º 40’08.9” |

**Table. 4.1**. Table of GPS coordinates and elevation of the sites of interest.

Cores sub-sampled for synchrotron analysis remained at liquid nitrogen temperatures (~77K) throughout the process. Since XAS is very sensitive to elements that may be present in a sample, especially metal, the prevention of any contamination was crucial. Therefore, to eliminate the possibility of metal contamination a Zephyr (Gryphon Corp.) saw was used to perform cuts on sediment samples used for synchrotron analysis. The Zephyr contains a diamond flake encrusted circular ring saw blade that allows for cutting in any direction without the risk of any metal flakes from the blade falling on the sample. The whole core is too large to be cut by the Zephyr, thus a Ryobi tabletop band saw was used cut the core in half. Once cut in half, the acrylic core is discarded and the remaining core is processed with the Zephyr saw. All pieces after sub sampling are placed in plastic bags, archived, and stored at ~253 K at the Toxicology Center. An overview of the sample preparation is displayed below (Fig. 4. 2)

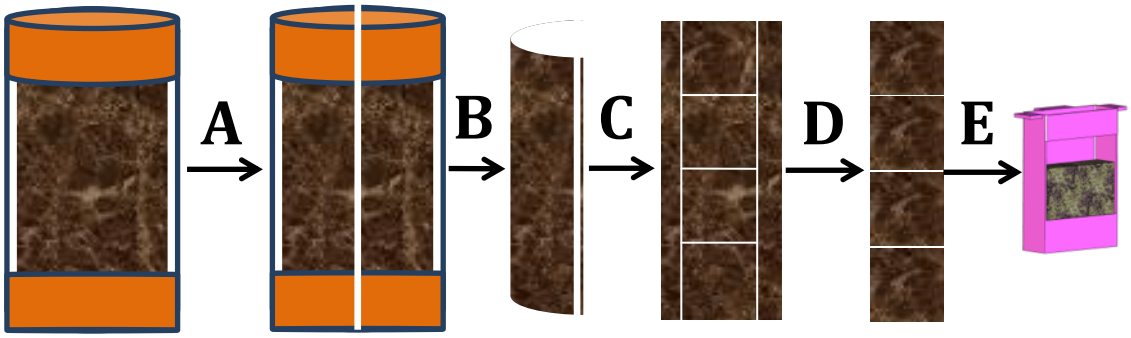


**Fig. 4.2.** Flow diagram of sediment sample preparation. **A** = Whole frozen core (in acrylic casing) is cut in half with a Ryobi band saw. **B** = Casing is discarded and a thin slice is removed with the Zephyr saw, as a precaution in case any metal transferred from the Ryobi blade to the sample. **C** = Using the Zephyr saw, smaller 1 x 1 x 0.5 cm (height x length x width) sections are obtained. **D** = Extra pieces are collected in a Ziploc bag and archived. **E** = Sections are then placed in custom printed cells wrapped in mylar tape.

After cores were sub-sampled, individual samples were placed in 3D printed sample cells wrapped in mylar tape. The sulfur- and metal-free mylar tape acted as a secondary containment of the sample and prevention of contamination of the cryostat. Each sample was then held in place with several frozen drops of glycerol. The printed sample cells were then marked and stored in either a plasmid box or 50 ml Falcon tubes in a -80 °C freezer (Toxicology Center). If the printed cells were stored in Falcon tubes, they were only stored in groups of two separated by several sheets of Kimwipes to avoid any cross-contamination. All samples were then transported to SSRL on dry ice and kept in a -80°C freezer once at the facility.

Samples, inside the custom sediment sample holder (Fig. 3.2) were analyzed at ~ 10 K in a liquid helium cooled cryostat (CF1208, Oxford Instruments) on beamline 9-3 at SSRL. Beamline 9-3 comprises an upstream collimating Rh-coated mirror, a Si(220) double crystal monochromator, and a downstream

focusing mirror, also Rh-coated. A beam size of 0.1 or 0.25 x 2.12 mm (height x width) was achieved using slits upstream of the $I_0$ ion chamber detector, which was filled with nitrogen gas. Sediment cores were oriented at 45° to the incident beam and fluorescence intensities were measured using a multi-element germanium detector. A 3 absorption length As filter placed in front of a Soller slit was utilized to selectively reduce scatter into the detector and causing non-linearities. A near-edge spectrum (12645 to 12855 eV) was collected for each 0.10 or 0.25 mm step across the face of the sediment. Sample spectra were fit using linear combination fitting to deduce the relative contributions of standards to the spectrum of the unknown.

The 9-3 detector setup allowed the analysis of multiple elements using the second set of SCA windows on the detector and this was used to gain additional information about other elements of interest in the sample, namely As, Fe, Ni, Cu, Zn, and Mn. In order to achieve this, after the sediment sample was analyzed for Se, the second set of SCA windows was selected. Additionally the filters, downstream of the sample and before the Soller slits, were changed from As to Ti and to compensate for the higher count rates an upstream 0.25 mm Al filter was also used to attenuate the incident beam. The filters were changed as an As filter would block all the fluorescence from the lower Z elements. Titanium reduces fluorescence from any lower elements such as K, Ca or lower while not significantly attenuating fluorescence from the elements of interest. Using the same step sizes that were performed on the core during Se analysis, depth profiles at 0.10 and 0.25 mm were achieved.

All XAS data collected was processed with the EXAFSPAK suite (George and Pickering, 1993). Processing included background subtraction, normalization and fitting using linear combination fitting (Fig. 4.3). Data fitting was done using linear combination fitting which employs fitting several standard spectra to an

unknown spectrum. Each standard spectra is scaled by a constant coefficient and added to one another until the unknown spectrum can be replicated. The constant coefficients give an idea of the percentage that each standard spectrum makes up an unknown spectrum.

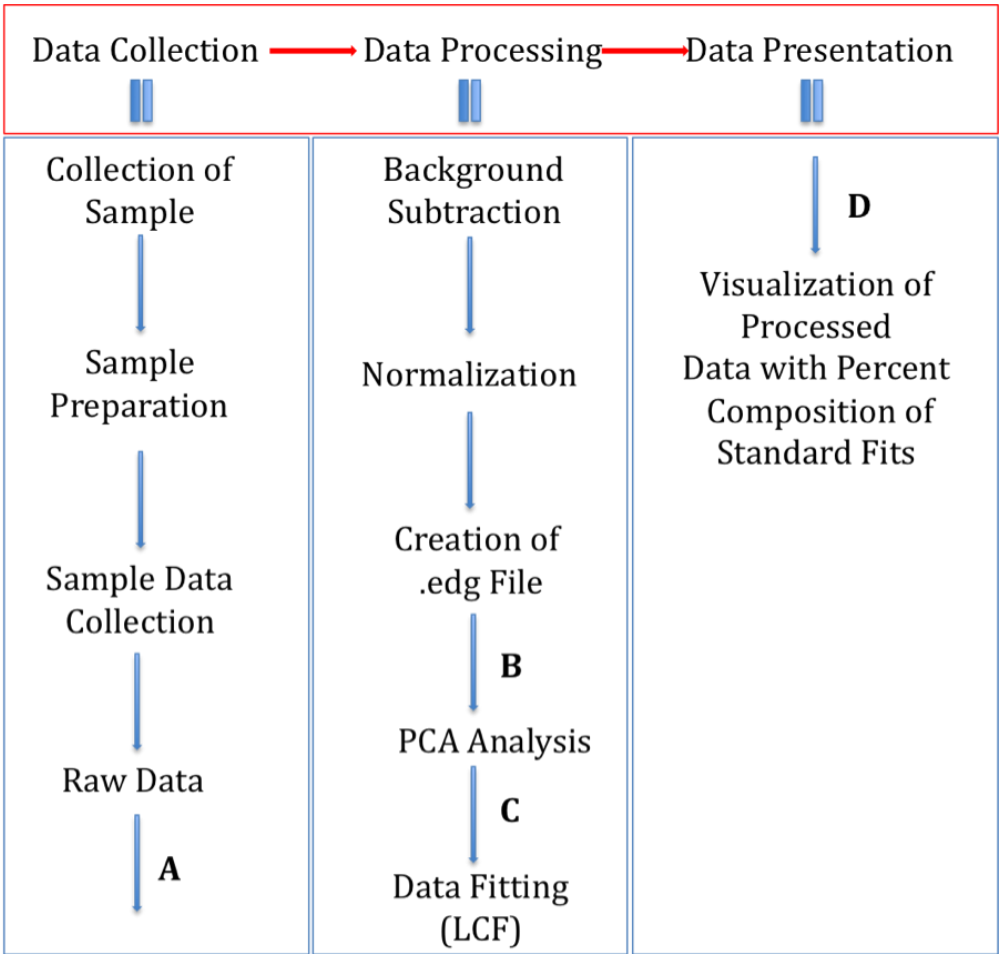


**Fig. 4.3**. Schematic of a samples' life from collection to data presentation. All data analysis was performed in EXAFSPAK (George and Pickering, 1993) using models **A**) *process*, **B**) *pca*, **C**) *datfit*, and **D**) *muldat*

## 4.4. Results

Initial depth profiles of sediment cores from F2 and U3 using the newly designed sediment sample holder demonstrated an increasing trend of total Se signal, as measured by the size of the absorption edge jump measured in fluorescence, as the depth increased within the core samples (Fig. 4.3 and 4.4). It is possible that this increase may be attributed to sediment grain size and/or density; however, the possibility of bacterial contributions cannot be ruled out. The increase in Se may also be representative of the bacterial community as a function of depth, and the presence of bacteria may provide another source of Se for benthic invertebrates. The transmission data, concurrently collected with fluorescence, will also fortify the location of the sediment-water interface (Fig. 4.4B). While a density change is observed across the sediment-water interface, via transmission, fluorescence data shows that the transition of Se over this interface is more gradual (Fig. 4.3 and 4.4A). Previous studies by Wiramanaden *et al*. showed evidence of a correlation between total organic carbon (TOC) and Se concentration (Wiramanaden *et al.*, 2010b); therefore, smaller grain sizes and higher density may provide more surface area and possibly higher Se concentrations. The preliminary results for Fox and Unknown Lake both show a similar Se trend as a function of depth; however, differences are seen in Unknown Lake in that it exhibits an oxidized Se species, selenite, at further depths which are not found in Fox Lake at equivalent depths (Table 4.2).

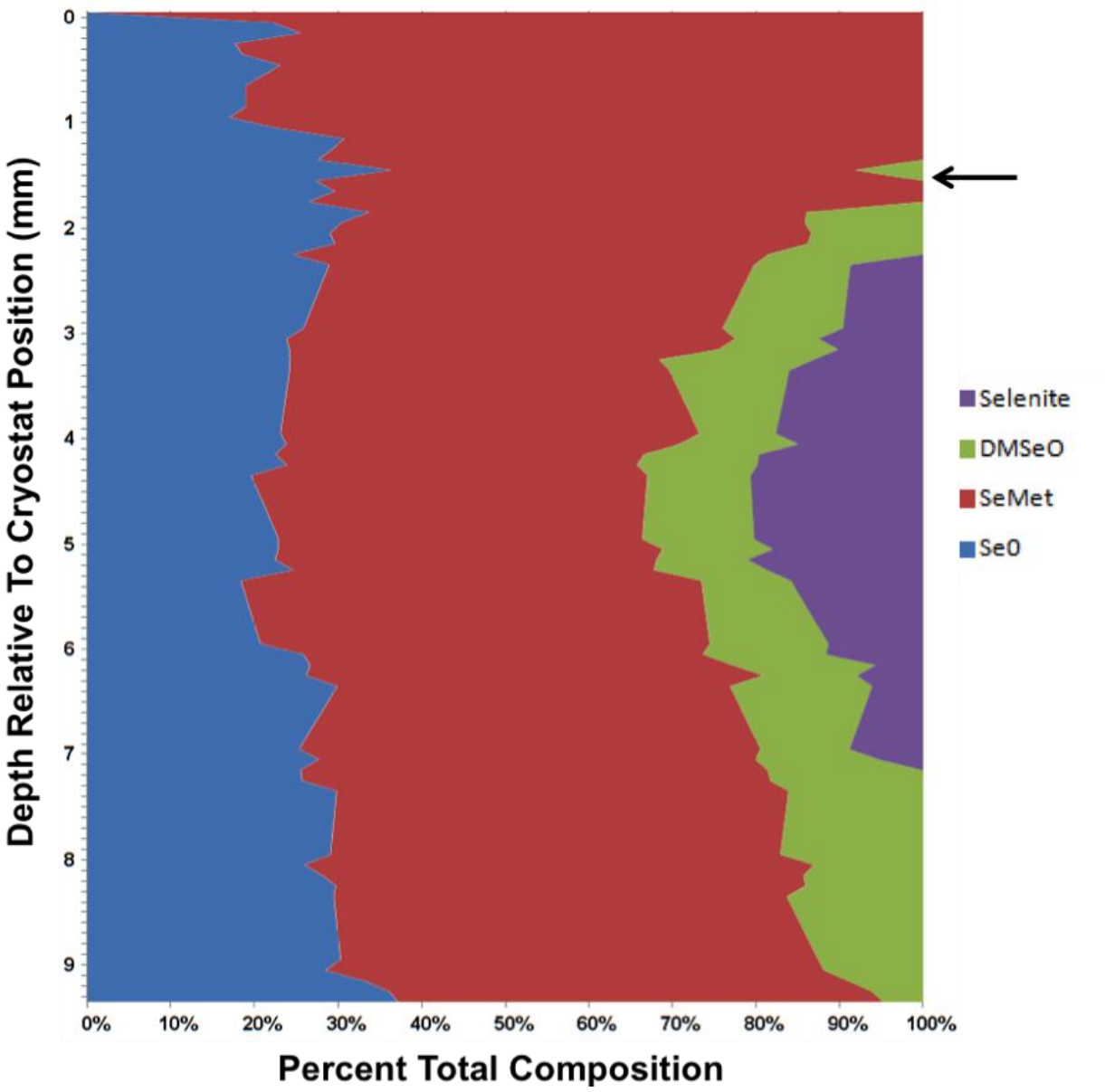


**Fig. 4.4.** Se species as a function of depth in a Fox Lake site 1 sample: elemental Se (Se0), selenomethionine (SeMet), dimethyl selenoxide (DMSeO), and selenite, Black arrow roughly denotes location of the sediment-water interface. Note the change in y-axis increments, from 100 to 250 µm increments once the sediment water interface has been crossed, denoted by the black arrow.

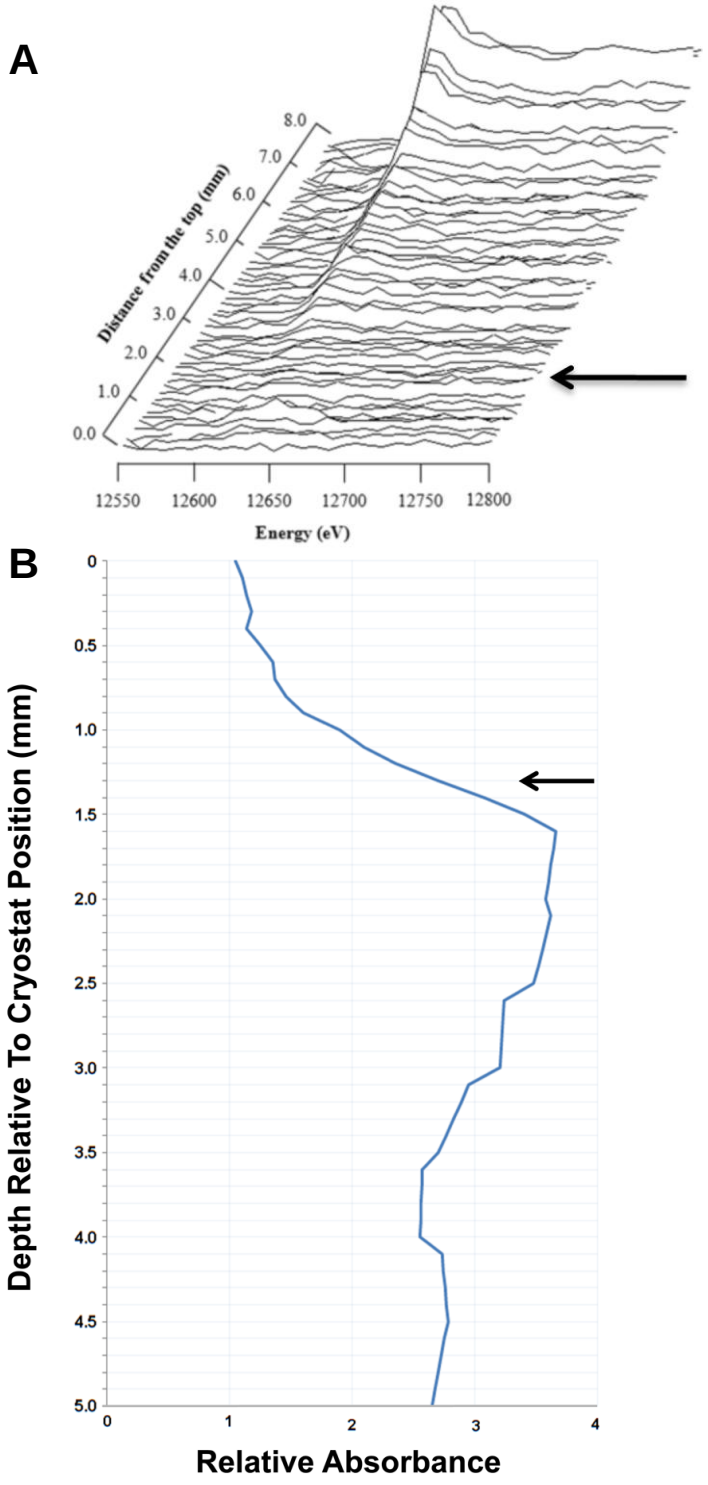


**Fig. 4.5**. **(A)** Selenium depth profile of the 1st cm of a Fox Lake core, graphed to emphasize the increasing trend of Se as a function of depth. **(B)** Graphed absorbance data, at 12680 eV, of another Fox Lake core as a function of depth, more absorption is observed as depth increases. Black arrows roughly denotes the location of the sediment-water interface. Note the change in y-axis increments as once the sediment water interface has been crossed with 100 µm increments, 250 µm step sizes were utilized.

For the 1st cm of a U2 core, 2 replicates were made and the values obtained from fitting were averaged. For sediments where a full sediment depth profile was collected, 1st cm of U2 and the entire F3 core, resulting spectra were grouped in 10 to provide a better signal to noise ratio for fitting. A water leak in the beamline vacuum chamber resulted in the loss of our beamtime on beamline 9-3. Thus, collection of a high-resolution sediment depth profile of U2 was not possible. Therefore, depths exceeding 1 cm for U2 were performed as homogenized 0.5 cm sediment sections on beamline 7-3, similar to the work performed by Wiramanaden *et al.* (Wiramanaden *et al*., 2010a), and values from the fits were averaged.

The majority of Se present in all sediment sections analyzed was selenomethionine or elemental Se species and a small fraction was in the form of selenite (Table 4.2). The presence and bioavailability of a selenomethionine species is most likely due to the presence of organisms or decaying organic matter, and may contribute as a source of Se bioaccumulation. A vast majority of the Se species found originates from the effluent and have been chemically changed via reduction. Reduction of Se can occur biotically or abiotically. It is known that bacteria can reduce Se to an elemental form (Oremland *et al*., 1989); however, it has also been shown that this reduction can occur via iron (II, III) oxide and green rust surfaces (Myneni *et al*., 1997).

| | 1st cm | | 2nd cm | | 3rd cm | | 4th cm |
|---|---|---|---|---|---|---|---|
| | **F3R1** | **U2 (Avg)** | **F3R1** | **U2R3** | **F3R1** | **U2R3** | **U2R3** |
| **Se0** | 27 (1) | 27 (1) | 42 (1) | 50 (1) | 43 (1) | 65 (1) | 52 (1) |
| **SeMet** | 61 (1) | 38 (1) | 58 (1) | 37 (1) | 58 (1) | 24 (2) | 32 (1) |
| **FeSe** | | 36 (2) | | | | | |
| **DMSeO** | 10 (1) | | | | | | |
| **Selenite** | 10 (1) | 6 (1) | | 9 (1) | | 9 (1) | |

**Table 4.2.** The average percentage of composition result of Se species found at various depths in both Unknown and Fox Lake with the bracketed values representing three times the estimated standard deviation.

Selenoxides (R-SeO-R), modeled as dimethyl selenoxide (DMSeO) were only present in sediment samples from Fox Lake. Selenoxides (R-SeO-R) include methionine selenoxide, an oxidation product of selenomethionine. Selenoxides are only observed in the 1$^{st}$ cm of Fox Lake, which is close to the sediment-water interface, where a larger chance for oxidation of selenomethionine can occur.

A metal selenide, modeled as iron selenide, was only found in Unknown Lake sediments. The presence of a metal selenide is not unusual (Wiramanaden *et al.*, 2010a); however, if what is found is truly iron selenide, this may be due to the mineral ferroselite, a $FeSe_2$ mineral. As the presence of a metal selenide was only observed in Unknown Lake, this further emphasizes the heterogeneity of a lake system.

A peak for Fe, As, and Mn was observed in the 1$^{st}$ cm before returning to a background level for the remaining analyzed depths (Fig. 4.5). This increase, represented by increasing edge jumps (Fig. 4.5), is thought to represent the redox boundary present in the sediment depth profile. An increase in sediment

depth results in a more anoxic environment, causing the reduction of compounds. In the case of Fe, Mn, and As, once reduced they can become mobile, and may mobilize upwards towards the surface; once these elements become exposed to oxygen, they will become oxidized and immobile again, thus representing the redox boundary (Boyle, 2001; Cornwell, 1986; Li and MacDonald, 2005; and Peramaki *et al*., 2006). As more sediment is deposited, the previous oxidized layer now becomes anoxic allowing reduction to occur again with mobilization of the elements. Therefore, this continuing cycle causes the redox boundary to be actively moving. This redox boundary is observed primarily in Fox Lake; however, a small peak is observed in Unknown Lake at a similar depth to that found in Fox Lake, possibly suggesting that the redox boundary is located at roughly the same depth in the two lakes. Arsenic is most likely not a naturally occurring element in such high concentrations; therefore, the As found at the redox boundary is most likely attributed to the effluent. This redox boundary also seems to correlate with an increase in Se. The Se depth profile shows an increase to a maximum in the 1$^{st}$ cm, and then decreases and remains at a more constant level, for 3 cm of depth. This overlaps nicely with the other elements as the redox boundary may act as a layer were reduction of Se may occur. Iron (II, III) oxide in addition to green rust has been shown to act as reduction sites for Se (Myneni *et al*., 1997). After Se has interacted with the redox boundary and become reduced, it may accumulate and remain as elemental Se or selenomethionine. This would explain why Se does not decrease in concentration but increases and remains steady, in contrast to the profiles of the other elements. Obtaining X-ray absorption near-edge structure of Fe and Mn would provide more information on the present redox status; however, substantially more beamtime and data processing time would be required. It is important to note that Fig. 4.5 assumes a uniform thickness and matrix composition are present throughout the entirety of the core depth, as we assume that the size of the edge jump equates to the level of the element present.

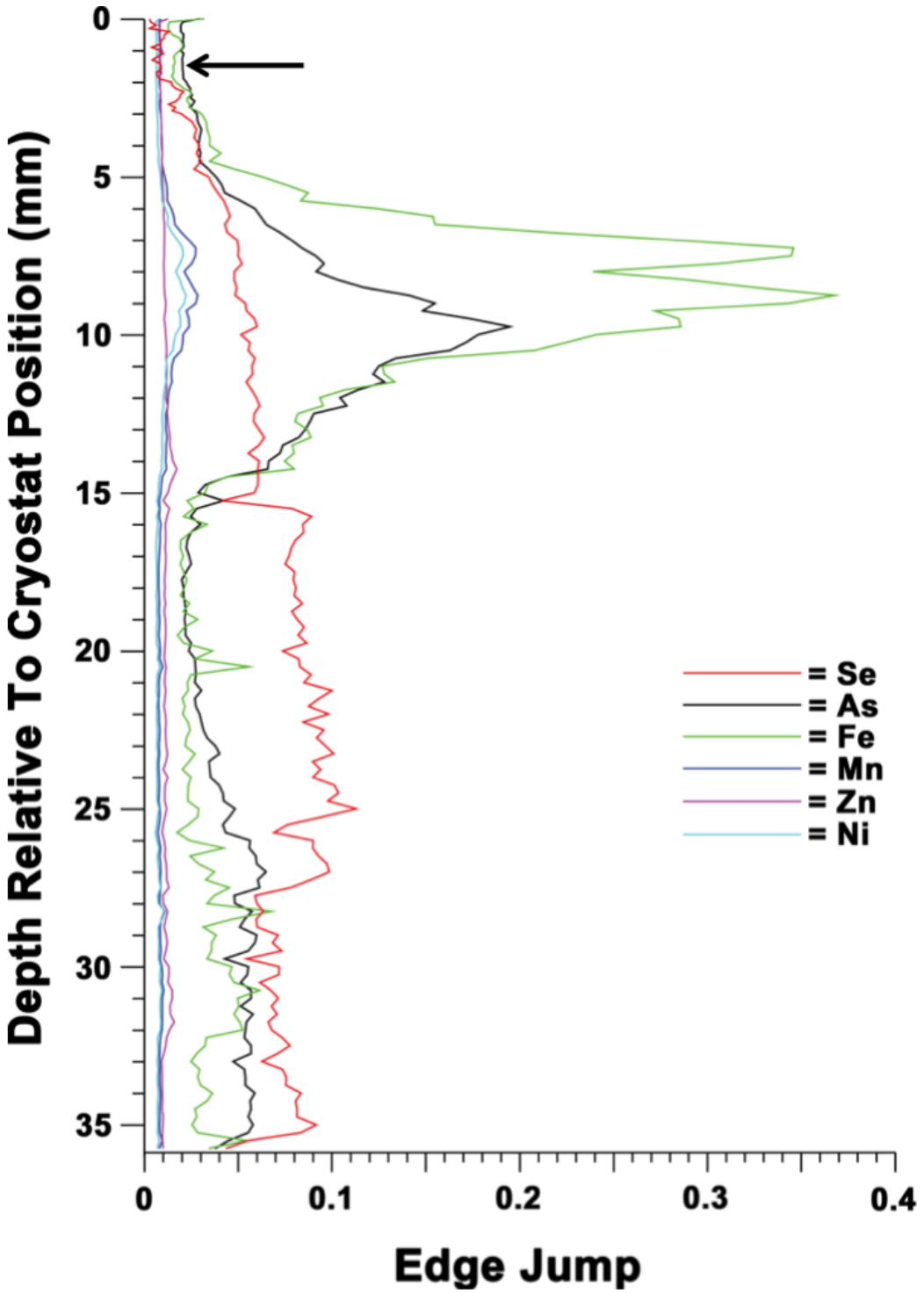


**Fig. 4.6**. Graph depicting the trend of other elements as a function of depth for Fox Lake site 3. The black arrow denotes the rough location of the sediment-water interface.

Thus, throughout the depths of the sampled cores, bioavailable species including selenomethionine species and selenite were present. Elemental Se also may be, to some degree, bioavailable (Gao *et al*., 2000; and Zhang *et al*., 2001). Such species may be taken up by benthic invertebrates and may be bioaccumulated through the food chain. Therefore, understanding the bioavailable species present to lower trophic organisms is important in understanding the bioaccumulation of Se into higher level trophic organisms.

# CHAPTER 5

# CHIRONOMIDS

## Chapter 5 - Chironomids

### 5.1 Abstract

A lake system, downstream of a U milling operation in Northern Saskatchewan, has been receiving treated metal mine effluent which has increased concentrations of selenium (Se) in its aquatic ecosystem. An important step in the transfer of Se through the food chain is the bioaccumulation of Se by chironomids, benthic invertebrates, that serve as a food source for higher trophic level organisms, especially fish. Chironomids have been shown to be excellent health markers for aquatic ecosystems as they are ubiquitous and some species are primary consumers. In this study, chironomids were sampled from various lakes downstream of a U milling operation. For comparison, *Chironomus dilutus* (Chironomidae) were reared in the laboratory and exposed to water spiked with selenate, selenite, or seleno-DL-methionine at the average water concentration of Se found in the respective lakes to mimic field conditions. Synchrotron based XAS and XRF imaging techniques were used to compare laboratory reared chironomids with those collected in the field to give a better understanding by which Se is taken up by this trophic level of the aquatic ecosystem. Field and laboratory reared chironomids showed similar tissue Se speciation and localization. These results suggest that organic Se species R-Se-Se-R and R-Se-R, modeled as selenocystine and selenomethionine respectively, are the major forms of Se in the chironomid tissue. However, water may not be the dominant exposure route, as concentrations found in laboratory reared chironomids were substantially below the concentrations found in field chironomids.

### 5.2. Introduction

Selenium is an important micronutrient required by many organisms. However, above a rather narrow beneficial range Se can be toxic. In nature, Se can be found in oxidation states ranging from - 2 to + 6. The valence and coordination

of Se radically affects its mobility, bioavailability, and toxicity (Geering *et al*., 1968; and Elrashidi *et al*., 1987); therefore, analysis on the chemical form of Se is important. Selenium run-off from disposal areas such as for copper purification (Thomassen *et al*., 2004), sulfuric acid production (Reilly, 1996) or U processing (IAE, 1989) may affect local aquatic systems. Selenium has a tendency to biomagnify through the food chain, such that relatively low levels in surface waters can lead to significantly higher levels for top predators (Hymer and Caruso, 2006). High Se levels in wildlife have known toxic effects including general tissue damage, reproductive failure, and teratogenic effects (Lemly, 1996; Lemly, 1997; Maier and Knight, 1994). Since Se has similar chemistry to that of sulfur, high levels of Se can cause accidental formation and incorporation of the amino acid selenomethionine in place of methionine into proteins. However, Se is required for the essential amino acid selenocysteine, which is necessary for the formation of many enzymes (Stadtman, 1991). Unlike selenomethionine, the production and incorporation of selenocysteine into proteins is highly specific and most likely will not occur accidentally.

The Kesterson National Wildlife Refuge incident is a well-documented example of how an excess amount of Se has been shown to pose health risks. The Kesterson Reservoir was once utilized as an evaporation pond for agricultural drainage waters. The continual drainage over a long period of time increased concentrations of Se, which led to decreased wildlife reproduction and increased deaths, with waterfowl affected more than the sampled mammals and rodents (Clark, 1987; and Ohlendorf and Hothem, 1987).

In the present case, a lake system in Northern Saskatchewan, 57º12’N, 105º41’W (Fig. 5.1), has been receiving treated metal mine effluent from a nearby U milling operation (Wiramanaden *et al*., 2010a; and Wiramanaden *et al*., 2010b). The effluent was found to raise surface water Se levels with respect to surrounding unaffected lakes (Wiramanaden *et al*., 2010a). Previous research has demonstrated that elevated levels of Se can cause larval

deformities in northern pike (Esox lucius) (Muscatello *et al*., 2006); however, this cannot be attributed solely to Se, as the effluent is comprised of many compounds, and the exact mechanisms and routes by which Se or other species of concern enter and propagate through the aquatic food chain are not yet fully understood. To study the elevated Se, field chironomids obtained from the affected lake system were compared with laboratory reared *C. dilutus* reared in water spiked with various Se species. This study builds on previous work by Franz *et al*. (2011) and by Wiramanaden *et al*. (2010a and 2010b) in characterizing the Key Lake aquatic ecosystem. In the present study we have combined synchrotron XAS and XRF to study the speciation and localization of Se in chironomids, respectively. Our study provides insights into the localization and route by which Se is transferred through an aquatic ecosystem.

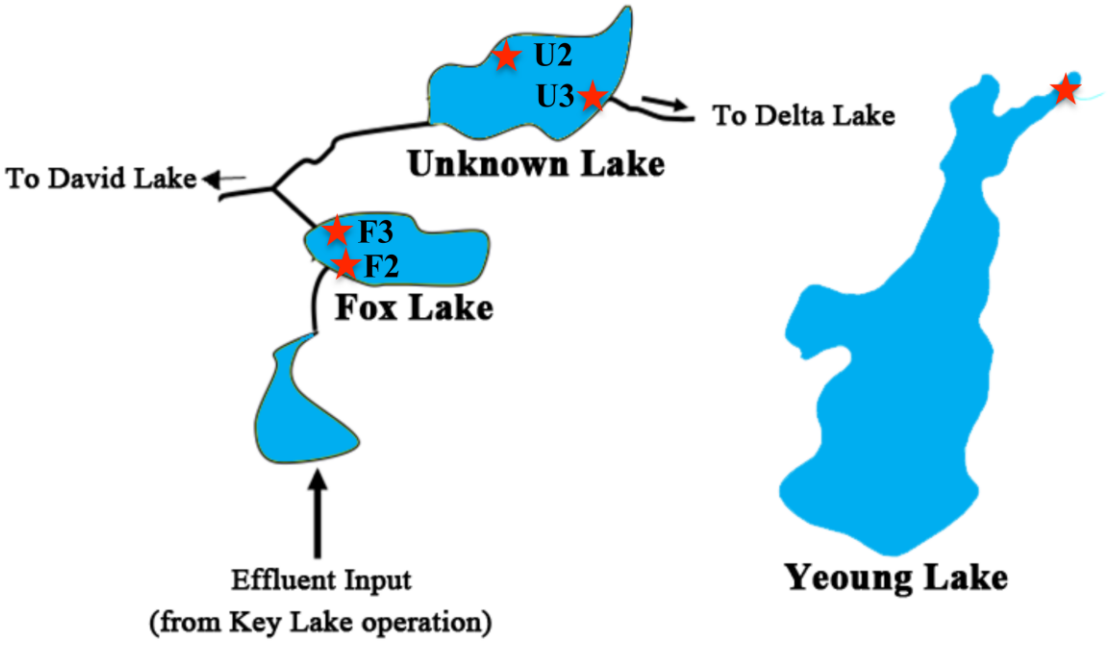


**Fig. 5.1.** A schematic map depicting the locations chosen for sediment and chironomid sampling. Yeoung Lake is located 8.2 km SE of Fox and Unknown Lake and was chosen as the reference lake.

## 5.3. Materials and Methods

### 5.3.1. Field Chironomids

A mixture of various chironomid species and ages was taken from Fox, Unknown, and Yeoung Lakes during the 2009 field season, Jun 11-16$^{th}$. Yeoung is part of a separated lake system located 8.2km SE of Fox and Unknown Lake and was chosen as the reference site. Samples were taken from F2 and F3, representative of the inflow and outflow of Fox Lake, closer to the effluent source; U2 and U3 from Unknown Lake, downstream of Fox Lake (Table 4.1). Sediment grabs, via an Ekman Grab, were sieved through a 500 µm sieve bucket, placed in a cooler with site water, and transported to an onsite environmental shed. Within 24 hours, each cooler was further inspected for the presence of chironomids. Any chironomids found were removed using PTFE coated tweezers (T5665 Sigma Aldrich) and then placed in a petri dish containing 50 µm sieved site water. Chironomids chosen for XRF imaging were 1-2 cm and exhibited the characteristic “bloodworm” redness. Those chosen were preserved at 4°C for later imaging experiments in either a 70% ethanol (EtOH)/Barnstead water solution or a 70% EtOH/50µm filtered site water solution. The remaining chironomids were pooled into 2ml Eppendorf tubes, frozen in liquid nitrogen to preserve Se speciation, and stored at -20ºC for later analysis via bulk XAS and ICP-MS. Late thawing of lakes delayed life cycles of the chironomids; therefore, insufficient chironomids for ICP-MS were collected during our field season. More chironomids were collected by MSc candidate Eric Franz (K. Liber) during the month of July, and combined with chironomids collected in June for ICP-MS analysis; however, insufficient amount Yeoung Lake chironomids prevented analysis via ICP-MS. A beamtime experiment at SSRL was scheduled 10 days after our field season in 2009. Therefore, all subsequent laboratory chironomid exposures were planned to end 10 days prior to a scheduled beamtime, to match the preservation time of the field chironomids.

Several preservatives, as suggested by laboratory members and those of Donald and Paterson (1977) and Morales *et al* (2011), were tested with laboratory *C. dilutus* to determine the ideal preservative. Chironomids were kept in the solution for ten days and then evaluated based on their flexibility, colour, and presence of surface disruptions (Table 5.1).

| Preservative | Observations |
|---|---|
| 10% Neutral Buffered Formalin (NBF) + Barnstead Water | • Still flexible<br>• No longer red/ brownish with some green<br>• A bit more rigid than the past tries<br>• No visible cracks/cuts/leaks/etc… |
| 10% NBF + filtered site water | • Still flexible<br>• More rigid than above<br>• No more red/ lighter brown and almost no green<br>• No visible cracks/cuts/leaks/etc… |
| 10% NBF | • Flexible but rigid near edges<br>• Brownish/green<br>• No visible cracks/cuts/leaks/etc… |
| 5% NBF | • Quite rigid<br>• Similar to 10% NBF – quite opaque<br>• More brownish/some green<br>• No visible cracks/cuts/leaks/etc… |
| 70% Ethanol (EtOH) + Barnstead Water | • Some were flexible<br>• Much more red than the above tries<br>• No visible cracks/cuts/leaks/etc…<br>• Less of a health hazard |
| 70% EtOH + filtered site water | • A bit rigid, but should still be flexible enough<br>• Very weak pink, mostly white<br>• No visible cracks/cuts/leaks/etc… |

**Table 5.1**. Results of various preservative solutions utilized on chironomids.

The results of the laboratory test, as well as previous research, demonstrated that the two “best” preservatives were 70% EtOH + Barnstead water and 70% EtOH + filtered site water to prevent biomass lost (Black and Dodson, 2003; and Gaston *et al*., 1996). Thus from each benthic grab, 2 to 3 chironomids were placed in each preservative.

### 5.3.2. Laboratory chironomids

*Chironomus dilutus* were chosen because it was readily available, from an in house culture (Toxicology Center, University of Sasaktchewan, Saskatoon, Saskatchewan, Canada), and is representative of the local species that serve as a food source for predators, and thus a vector for Se bioaccumulation through a food chain. Their extensive characterization and relatively short life cycle, 23-30 days, make chironomids ideal for exposure studies (Benoit *et al*., 1997; Leung *et al*., 2004; and Choi *et al*., 1999). The laboratory reared *C. dilutus* were raised in one of two water exposures spiked with one of three Se species. One water exposure was performed in dechlorinated water for 10-days, followed by a 10-day depuration period during where the raising of *C. dilutus* was continued in dechlorinated water without any Se additions. Another 10-day uptake exposure was carried out in Barnstead water (Barnstead NANOpure Diamond, 18.2 MΩ-cm) to eliminate any extraneous sources of Se, as the dechlorinated water can contain trace amounts of Se (City of Saskatoon Water Treatment Plant, 2009). In both water treatment scenarios, the water was spiked with prepared sodium selenate ($Na_2SeO_4$), sodium selenite ($Na_2SeO_3$), or seleno-DL-methionine ($C_5H_{11}NO_2Se$) as described below. Selenate and selenite were chosen as they are the predominant forms found in surface waters, and are the most abundant bioavailable forms of Se found in the environment (Besser *et al*., 1993; and Fleet-Stalder *et al*., 2000). Selenomethionine was chosen as it is readily found in nature, from accidental incorporation into proteins to decaying organic matter.

To mimic environmental field conditions, chironomids were reared in the laboratory using a modification of the method of Franz *et al.* (2011). Beakers (300 mL Pyrex) were prepared with 96 ± 10 g of washed silica sand (Granusil silica fillers) and 200 mL of spiked water with constant aeration by bubblers (Optima). The average Se concentrations, determined by ICP-MS, in the water of Fox Lake and Unknown Lake, 10.3 ± 0.4 and 3.9 ± 0.3 µg $L^{-1}$, respectively, were used as the environmentally relevant concentrations to perform laboratory based water exposures. Stock 110 mg $L^{-1}$ solutions of $Na_2SeO_4$ (Aldrich), $Na_2SeO_3$ (Alfa Aesar), and $C_5H_{11}NO_2Se$ (Sigma) were prepared with Barnstead water on day 0. The stock solutions were diluted 1: 10 followed by a 1 : 1000 or 1 : 2750 dilution to represent Fox and Unknown Lake Se water concentrations, respectively, every 3 days for a water change. In addition, water quality tests were performed before and after every water change. Every day, the dissolved oxygen (Orion 3 Star DO Portable, DO Probe 081010MD, Thermo Scientific) content was measured. Chironomid food was prepared by blending 10 g of fish flakes (Sera pond bio flakes) in 100 mL of Barnstead water on day 0. The mixture was aliquoted into 50 mL Falcon tubes, frozen, and then was diluted 1:10 every day to feed 1 mL to each beaker containing 10 chironomids. Each treatment was performed in triplicate to yield sufficient chironomids for ICP-MS, synchrotron XRF and XAS. For both the 10 day exposure and the 10 day exposure followed by a 10 day depuration period, 1 to 2 chironomids were removed at the 10 day and 20 day (if applicable) time points and were preserved in a 70% ethanol solution for synchrotron XRF imaging. The remaining chironomids were separated into two groups, either frozen for speciation analysis by XAS or set aside for total Se content analysis by ICP-MS.

The 10-day uptake in Barnstead water produced the averages of dissolved oxygen (7.5 ± 0.4 mg $mL^{-1}$), conductivity (30 ± 12 µS $cm^{-1}$), pH (7.5 ± 0.1), alkalinity (12.8 ± 4.3 mg $L^{-1}$ of $CaCO_3$), and hardness (78.0 ± 3.7 mg $L^{-1}$ of $CaCO_3$). For a 10-day uptake followed by a 10-day depuration in dechlorinated

water, the following values were obtained for dissolved oxygen (8.32 ± 0.16 mg $mL^{-1}$), conductivity (432 ± 4 µS $cm^{-1}$), pH (8.21 ± 0.01), alkalinity (111 ± 3 mg $L^{-1}$ of $CaCO_3$), and hardness (137 ± 1 mg $L^{-1}$ of $CaCO_3$). Both water treatments had ammonia values that were below the detection limits, < 0.02 mg $L^{-1}$ (Ammonia Nitrogen Test Kit. Low Range Method. La Motte, USA).

### 5.3.3. Total Selenium Analysis Using ICP-MS

All chironomids were dried for several days in a drying oven at 60°C until masses were constant. Dried samples were cold digested using nitric acid (Omnitrace Ultra, EM Science) and hydrogen peroxide (Super Pure; EMD Chemicals). Samples were measured at the Toxicology Center (University of Saskatchewan, Saskatoon, SK) using ICPMS (X Series II Thermo Electron Corporation, Waltham, MA, USA) and analyzed for $^{80}Se$ using collision cell technology as described previously by Wiramanaden *et al.* (2010b). A standard reference material (SRM), Tort-2 (Lobster hepatopancrease, NRC) was used. Triplicates of SRM were within the certified value of 5.63 ± 0.67 mg $kg^{-1}$ (Wiramanaden *et al*., 2010b).

### 5.3.4. Synchrotron X-ray Absorption Spectroscopy (XAS)

X-ray absorption spectroscopy (XAS) analysis can provide information on the oxidation state, nature of the ligands and coordination geometry of a given element in a complex sample. Therefore, XAS is sensitive to the chemical form of a compound since binding energies of core electrons are characteristic for each species. However, XAS cannot distinguish specific molecules but rather the type of local bonding environment around the element; for example, in the case of selenomethionine, XAS will deduce the presence of two local aliphatic groups around Se (R-Se-R) and we can only draw the conclusion of a selenomethionine-like compound rather than specifically selenomethionine, and similar arguments apply to selenocystine (R-Se-Se-R). Though the majority of

endogenous Se is found as selenocysteine incorporated into proteins, the dimerized form, selenocystine, is often used when fitting spectra. This is because the selenol (Se-H) group in the selenocysteine monomeric form is very unstable, and thus is unlikely to be found in organisms. The spectrum of a mixture of more than one chemical form of an element appears as the sum of the spectra of the individual components. Linear combination fitting is used to deduce the relative contributions of standards to the spectrum of the unknown.

Frozen chironomids for XAS analysis were crushed with a liquid nitrogen cooled agate mortar and pestle. The cooling helped to prevent speciation changes and allowed for easier crushing of chironomids into a homogeneous powder. Maintained at liquid nitrogen temperatures, homogenized chironomids were packed tightly into custom printed 2 mm path length cuvettes, sealed with a drop of glycerol, and stored in liquid nitrogen.

XAS data were collected on the structural molecular biology beamlines 7-3 and 9-3 at the Stanford Synchrotron Radiation Lightsource (SSRL) located in Menlo Park, California, USA with a Si(220) double crystal monochromator. A 15 keV cutoff was achieved by adjusting the angle of the upstream Rh-coated vertically collimating mirror; 9-3 additionally has a downstream focusing mirror, also Rh-coated. A 1.0 x 8.0 mm (height x width) beam was defined by upstream slits. Incident and transmitted intensities were recording using $N_2$-filled ion chambers. Samples were measured at 45º to the incident beam and were maintained at 10K using a flowing liquid helium cryostat (Oxford Instruments). Se Kα fluorescence was measured using a 30-element germanium detector (Canberra); arsenic filters and Soller slits were used to enhance the Se fluorescence signal by selectively preventing scatter from entering the detector, thus maintaining the detector count rates in a pseudolinear regime. A downstream elemental Se foil was used for continuous energy calibration

during data acquisition; the first energy inflection of the foil was assumed to be 12658.0 eV. Data analysis, which includes background subtraction, normalization, and data fitting by linear combination fitting was performed using the EXAFSPAK program suite (George and Pickering, 1993), as previously described in 4.3.

### 5.3.5. Synchrotron X-ray Fluorescence (XRF) Imaging

Chironomids were kept in the preservative solution for no more than 25 days at 4ºC prior to XRF imaging measurements, to minimize any possible degradation of the sample. XRF imaging was performed on beamline 10-2 at SSRL. Chironomids were placed between two sheets of polypropylene and mounted at 90º to the incident beam. To prevent dehydration of the sample, a small piece of Kimwipe soaked in preservative was placed between the sheets outside of the field of view. A Si(111) crystal was used to achieve an incident energy of 13.45 keV, just below the bromine edge (Br) to avoid possible excitation of Br Kα fluorescence, as Br is found commonly in plastics and other materials in the beamline environment. X-ray fluorescence was detected using a single element vortex detector, positioned at approximately 45° to the sample. A 50 µm incident beam defocused spot size was achieved downstream of the focal spot of a tapered glass capillary optic. Measurements used a sampling rate of 0.3s per 30 µm increment in continuous scan mode across the chironomid. Data were processed using Sam's microprobe analysis kit (SMAK), written by Sam Webb (Webb, 2010). Data processing included removal both of scatter (Fig. 5.2) and of anomalously high pixels that would cause improper intensity scaling, possibly attributed to occasional dust particles.

The absolute quantification using XRF of metal concentration in a thick and irregularly shaped object is challenging and cannot be done precisely without significant additional measurements of beam pathlengths. The measurements

presented herein are therefore on relative, rather than absolute scales. Chironomids reared at the same time under different treatments were imaged together during the same beamtime with the same conditions, thus the intensity scales should be directly comparable. However, since different beamtime experimental runs are often spaced months apart, minor equipment adjustments do not allow data sets collected from different beamtimes to be directly comparable in terms of intensities. These minor adjustments included varied distances between the sample and the capillary, as the sample mounting media was not rigid, and varied distances and angles between the sample and the detector. Despite these changes, the relative anatomical localization for a given elemental map can be compared across all the treatments.

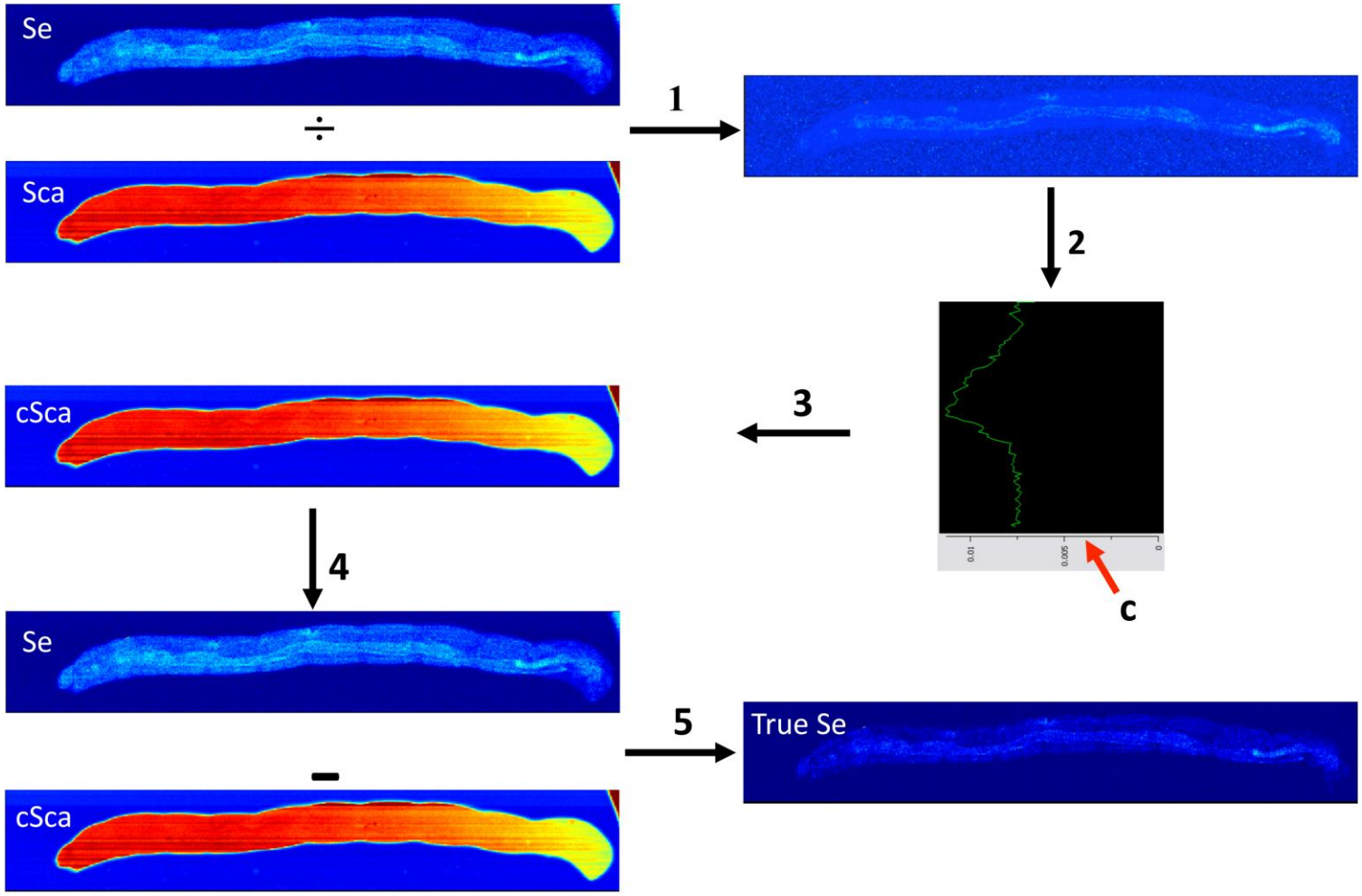


**Fig. 5.2.** Outline of how chironomids imaging results are processed. **Step 1**. The Se channel is divided by the scatter channel (Se/Sca). **Step 2**. Data is averaged along the X-axis to determine a constant value (c, red arrow) for the background. **Step 3**. The scatter channel is multiplied by the constant c (cSca). **Step 4.** The original Se channel has the cSca channel subtracted from it to reveal the true Se image with minimal contribution from the scatter.

## 5.4. Results

### 5.4.1. X-ray Absorption Spectroscopy

XAS may be used to investigate the chemical speciation of trace levels of environmental contaminants in biota essentially without any pretreatment. Currently, the concentration of Se is the most commonly used criteria in assessing environmental risk of different environmental components such as water, sediments, macroinvertebrates, and fish. However, information on the chemical form of Se in the various environmental components is needed to give a more refined indication of the risk (Andrahennadi *et al*., 2007).

XAS Se speciation analysis of chironomid tissue, comparing field chironomids and those reared in the laboratory, was carried out in order to provide a better understanding of the Se species implicated in bioaccumulation in high-level Se aquatic ecosystems (Fig. 5.3). Results of XAS analysis (Fig. 5.4) suggest that the dominant form of Se in chironomids, from both field and laboratory, are organic – selenomethionine-like and selenocystine-like species (Table 5.2). For laboratory reared chironomids, a selenocystine-like species was the dominant form found in both control and selenate exposed chironomids (Table 5.2). In selenite and selenomethionine exposed chironomids, both selenomethionine- and selenocystine-like species were observed; however, the predominant form was a selenomethionine-like species (Table 5.2). In terms of total selenium in the chironomids (Table 5.2), levels were seen to increase in the order of bioavailability (control < selenate < selenite < selenomethionine).

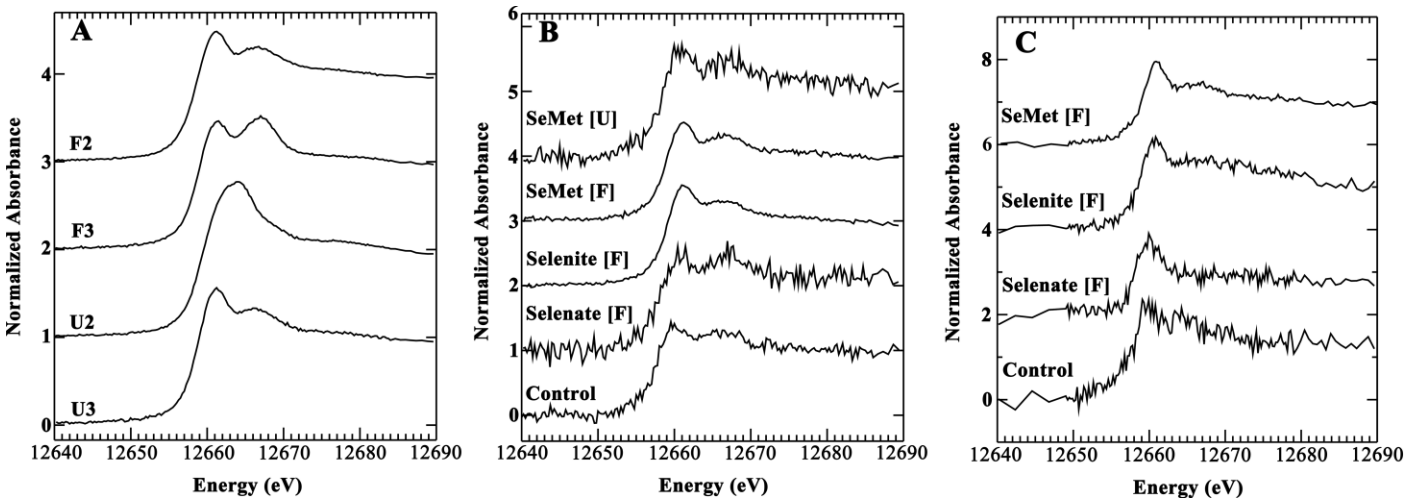


**Fig. 5.3**. Se K-edge XAS of whole chironomids from the field and laboratory. **A**) Field chironomids from Fox Lake (F) and Unknown Lake (U) sites 2 and 3, **B**) chironomids reared in the laboratory with a 10-day uptake in Barnstead water, and **C**) chironomids reared in the laboratory with a 10-day uptake and 10-day depuration in dechlorinated water. [F] and [U] represent the Se concentration in the spiked water, chosen to be equivalent to that of Fox Lake (11 µg $L^{-1}$) or Unknown Lake (4 µg $L^{-1}$), respectively.

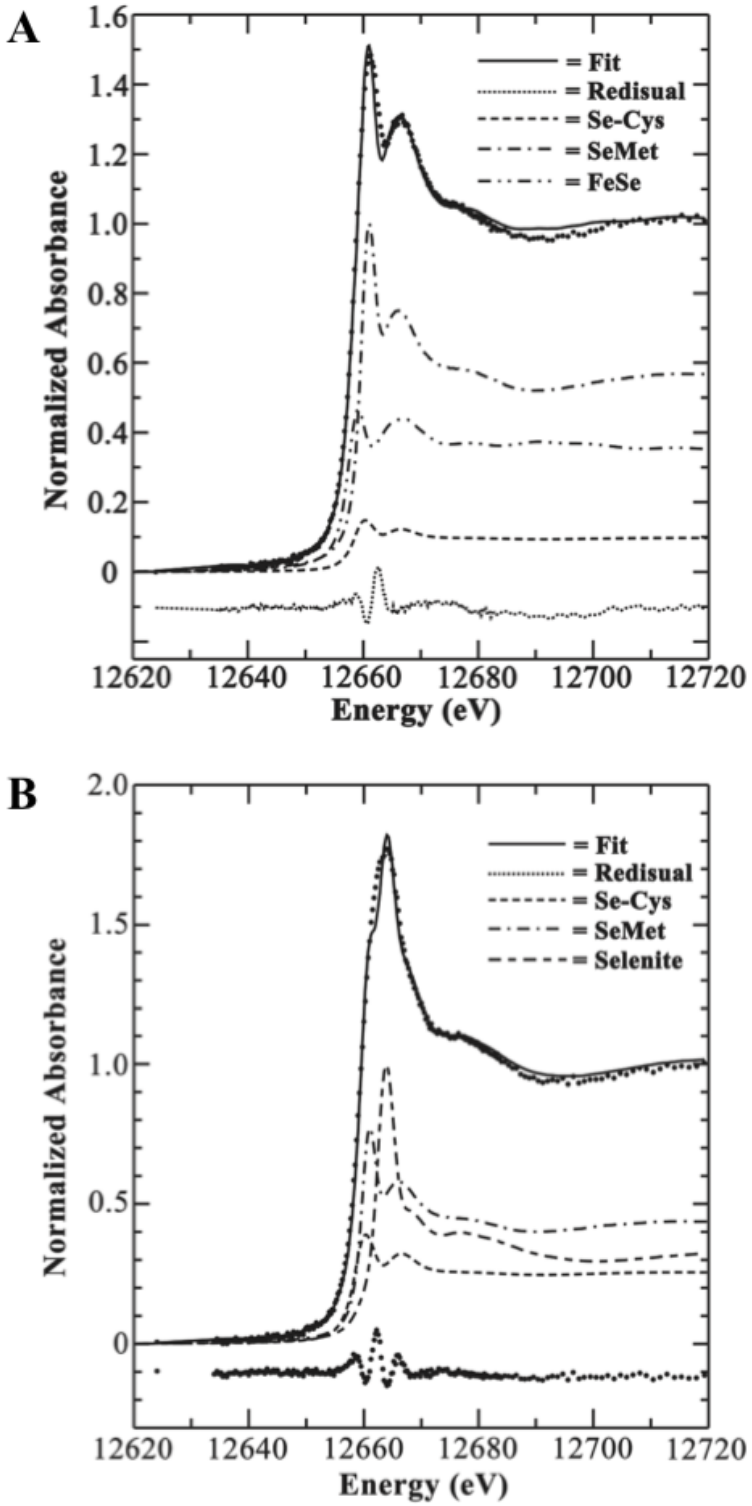


**Fig. 5.4**. Se K near-edge XAS spectra showing results of least squares fitting for field chironomids, **(A)** Fox Lake site 2 and **(B)** Unknown Lake site 2

| Laboratory: | Exposure | Se Species Present | | | | | | |
|---|---|---|---|---|---|---|---|---|
| | | CysSeSeCys | SeMet | Selenite | Selenate | $Me3Sel^{-}$ | FeSe | ICP-MS |
| | | | | | | | | mg $kg^{-1}$ |
| **Barnstead $H_2O$:** | **Control** | 63 (12) | | 5 (3) | | | 32 (13) | 0.60 (0.05) |
| | **Selenate** | 89 (9) | | | 8 (3) | 11 (7) | | 0.74 (0.01) |
| | **Selenite** | 25 (14) | 48 (9) | | 2 (0.1) | 13 (3) | 11 (8) | 2.02 (0.01) |
| | **SeMet (11 µg $L^{-1}$)** | 24 (16) | 48 (11) | | 2 (0.1) | 9 (3) | 17 (10) | 62.7 (0.3) |
| | **SeMet (4 µg $L^{-1}$)** | 77 (16) | 35 (16) | | | | | N/A |
| **Dechlorinated $H_2O$ with depuration:** | **Control[a]** | | | | | | | 1.4 (0.1) |
| | **Selenate[a]** | | | | | | | 0.50 (0.04) |
| | **Selenite** | 59 (14) | 39 (14) | | | | | 3.1 (0.1) |
| | **SeMet (11 µg $L^{-1}$)** | 40 (12) | 70 (12) | | | | | 6.4 (0.2) |
| **Field:** | **Fox Lake Site 2** | 10 (9) | 55 (5) | | | | 36 (6) | 77.8 (0.1) |
| | **Fox Lake Site 3** | 34 (11) | 43 (6) | 8 (1) | 6 (0.6) | | 9 (7) | 80.3 (0.1) |
| | **Unknown Lake Site 2** | 25 (5) | 43 (5) | 33 (1) | | | | 20.9 (0.1) |
| | **Unknown Lake Site 3** | 13 (12) | 63 (6) | | | | 25 (7) | 7.84 (0.1) |

**Table 5.2**. Synchrotron XAS and ICP-MS results of chironomids collected from the field and laboratory. Values for XAS results represent relative percentages with three times the estimated standard deviations in brackets. The bracketed values under ICP-MS represent the error.

[a]: Samples were below detection limits of the beamline, thus spectra were not able to be properly fit.

After a waterborne exposure to a lower concentration (4 µg $L^{-1}$) of selenomethionine, the laboratory reared chironomids were found to have a 2 : 1 ratio of selenocystine- to selenomethionine-like species compared with 0.6 : 1 for the higher concentration of 11 µg $L^{-1}$. Previous studies of Franz *et al*. (2011) and Phibbs *et al*. (2011a and 2011b) made similar observations of a higher R-Se-Se-R to R-Se-R ratio for lower Se exposure concentrations. Additionally, chironomids that have undergone a 10-day depuration period show a larger ratio between selenocystine and selenomethionine-like species compared with their undepurated counterparts. Therefore, when the source of Se is eliminated, the organism appears to excrete or deplete its excess selenomethionine-like component; however, growth dilution of the already present Se cannot be ruled out. In support of this, a decrease in total Se content is observed (Table 5.2) in chironomids sampled after a 10-day depuration compared with those analyzed after a 10-day uptake period. Results of the laboratory reared chironomids in two different water conditions suggest that chironomids after a 10-day uptake and 10-day depuration contained similar species to those observed in chironomids from the Barnstead water exposure after a 10-day uptake. Although total Se levels are very low in the depurated cases, fits from both types of water exposures suggest that both the control and selenate exposures from both water experiments share a selenocystine-like Se species as the dominant species (Table 5.2). Therefore, despite being reared in different types of water exposures, the laboratory-reared chironomids contained similar Se species at the end of the exposures.

In comparison with the results obtained from laboratory-reared chironomids, similar speciation was found in chironomids obtained from the field, although there was a much higher concentration of Se in field chironomids than those reared in the laboratory. Field chironomids have been exposed to a much more complex environment with elevated amounts of Se and throughout their lifecycle; they can also obtain Se from ingestion as well as via waterborne

sources. Each of these might contribute to the significantly higher Se concentration observed compared to laboratory reared chironomids. Despite the differences in concentration, both field and laboratory-reared chironomids displayed a selenomethionine-like species as the dominant form of Se. Among the sampled field chironomids, the biggest difference in speciation was observed in the U2 chironomids (Table 5.2), which showed an increased contribution from metal selenide. As lake beds are quite heterogeneous (Wiramanaden *et al*., 2010a; and Wiramanaden *et al*., 2010b), this increase in metal selenide could be due to an increased amount of this compound in the diet or in the water/sediment system. While care was taken to sample the same types of chironomids from the different sites, it is also possible that different chironomid species might have different uptakes. This speciation distribution difference also appears to provide a different synchrotron XRF imaging result, as discussed below.

Some similarities can be observed in Table 5.2 between field and laboratory chironomids. A 1 : 1.5 (selenocystine : selenomethionine) ratio was observed in the selenite and selenomethionine laboratory exposures as well as F3 and U2 from the field. By contrast, a 1 : 5.2 (selenocystine : selenomethionine) ratio is observed for both F2 and U3. These observations help reinforce the site specificity in an aquatic ecosystem. Wiramanaden *et al* (2010b) performed analysis on the percentage of sand in collected cores revealing that 26% of sediment from Fox 2 was sandy, 95% for Fox 3, 52% for Unknown 2, and 5% for Unknown 3. High sand content generally has less organic material present in the sediment, and possibly therefore less selenomethionine available to chironomids. In support of this, the lower proportions of selenomethionine were observed in chironomids from F3 and U2 (Table 5.2) where the highest sand content is found.

### 5.4.2. X-ray Fluorescence Imaging

The distribution of Se in chironomids was imaged concurrently with the distributions of As, Zn, Cu, Ni, Fe, and Mn. An example of two chironomids with all elements displayed side-by-side is shown in Fig. 5.5. Strong similarities are seen between chironomids taken from the field and those reared in the laboratory. In both cases Se tended to accumulate around the head capsule, salivary gland and around the gut. Selenium in the field chironomid seemed to accumulate more Se into the frontal region, possibly in the head capsule region (Fig. 5.5 and 5.6). As waterborne exposure may not be the primary route of Se bioaccumulation, this may account for the absence in the laboratory-reared chironomids in the XRF results, as the Se concentration present may have been below the detection limit of the beamline. Clearly, the method of Se uptake (food, water, absorption) is an important factor in how Se is biotransformed and transported throughout the organism. There also seems to be a degree of co-localization of Zn with Se, especially around the gut and in the head capsule and salivary gland region (Fig. 5.5), more noticeable in the field chironomid.

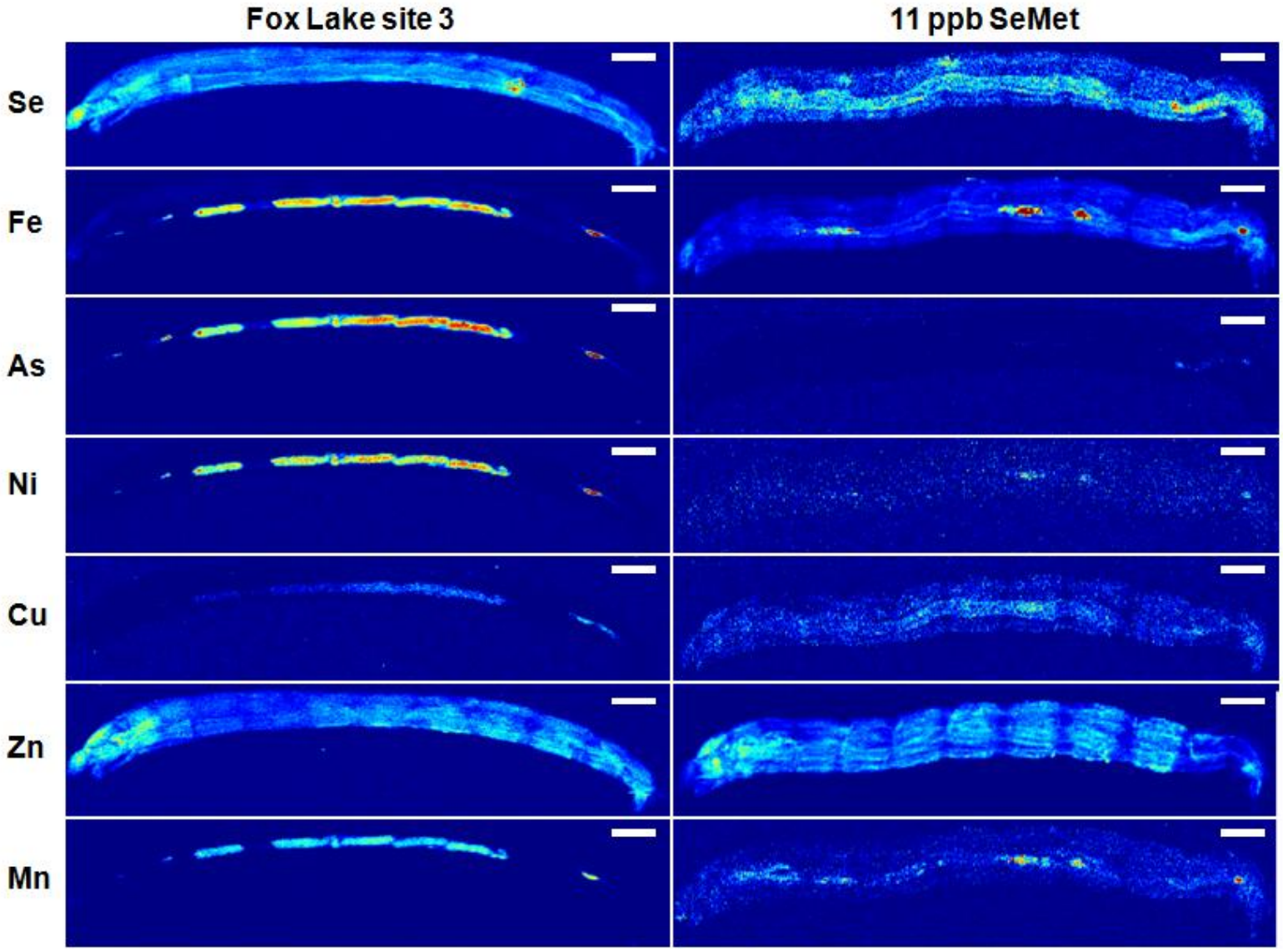


**Fig. 5.5**. Synchrotron XRF imaging results of a Fox Lake site 3 chironomid and a laboratory chironomid reared in 14 µg $L^{-1}$ selenomethionine water spiked exposure. The scale bar represents 1 mm.

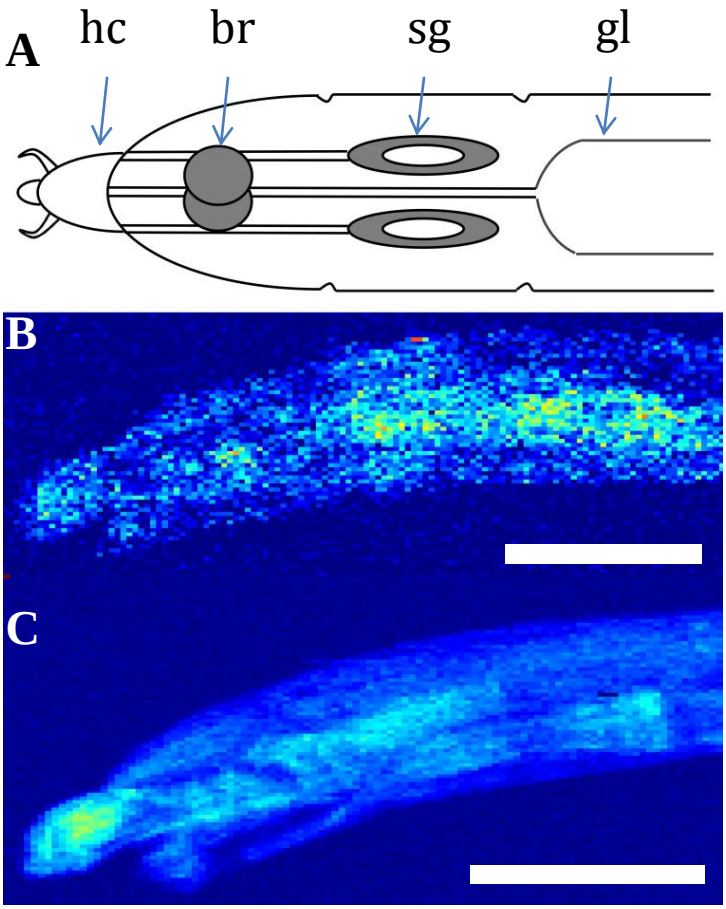


**Fig. 5.6.** **(A)** Model anterior end, in a dorsal view, of a chironomid (modified from Yagi S., 1984) indicating **hc**) head capsule, **br**) brain, **sl**) salivary glands, and **gl**) gut lining. **(B)** 11 µg $L^{-1}$ selenomethionine waterborne exposed laboratory reared chironomids in a sagittal view. **(C)** F3 chironomid, in a sagittal view. The scale bars represent 1 mm.

The remaining elements, As, Ni, Cu, Fe, and Mn seem to be localized similarly in both types of chironomids (Fig. 5.5 and 5.7-9). All were present in the gut, not locally found elsewhere in the chironomid. Field chironomids, and to a less extent laboratory, additionally displayed “pellets” of elements in the gut, presumably taken up through ingestion. As not much is found in any other region, it may suggest that if present in the tissue, it is present in very low concentrations, or that it is not absorbed through the gut lining at all. In the case of As, it was found in the rectum, suggesting that it is on the way to being excreted.

Fig. 5.5 displays the example results of a one field and laboratory reared chironomid. However, similar results for the remaining field chironomids (F2, U2, and U3) and laboratory reared chironomids (control, $Na_2SeO_3$, and $Na_2SeO_4$) were also collected. A chironomid that had gone through a depuration period was imaged to provide more insight into changes of Se localization if the main source of Se, water, is removed. Following a 10-day depuration, the chironomid showed a lack of localization (data not shown), suggesting that present Se is below the detection limit of the beamline. Some Se is expected to remain in tissues, as it is required for the organism’s survival.

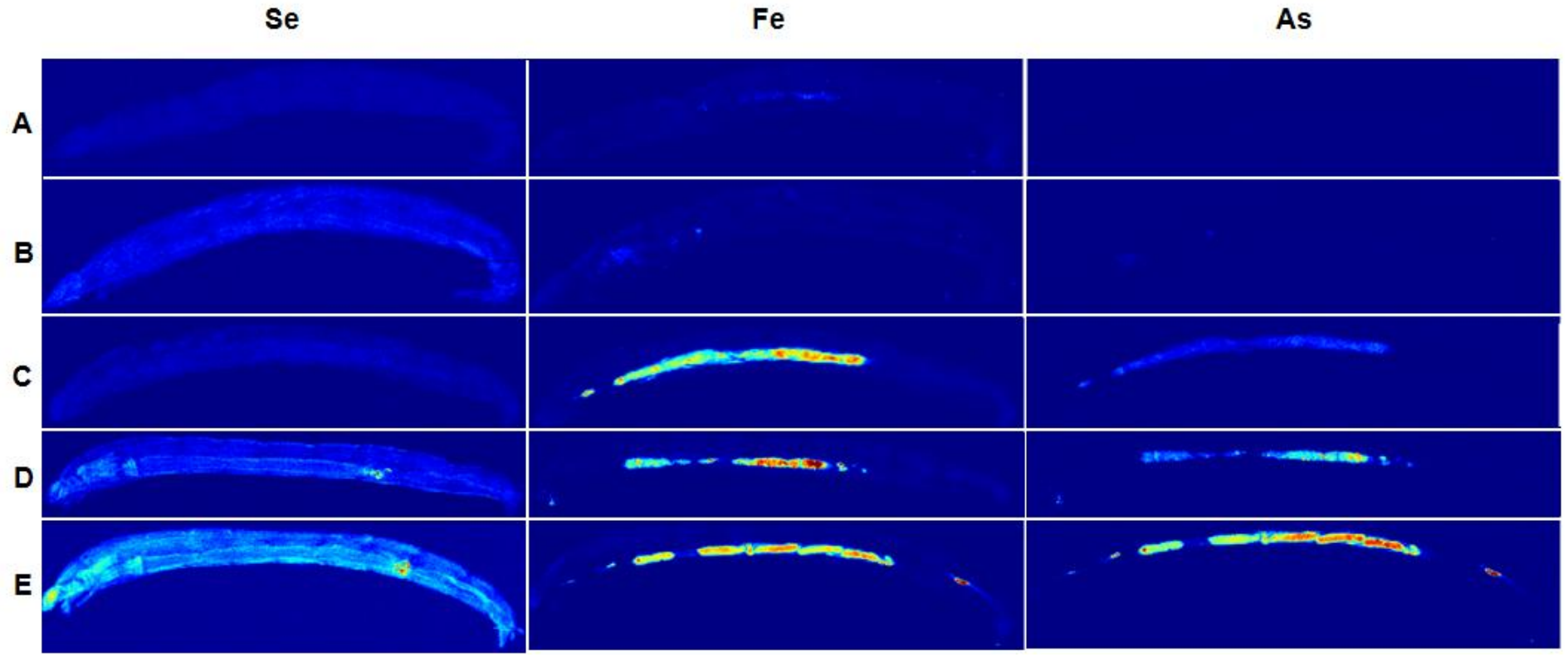


**Fig. 5.7**. XRF imaging results of field chironomids, **(A)** Yeoung Lake, **(B)** Unknown Lake site 2, **(C)** Unknown Lake site 3, **(D)** Fox Lake site 2, and **E**) Fox Lake site 3. Images have been scaled such that chironomids of the same element are comparable.

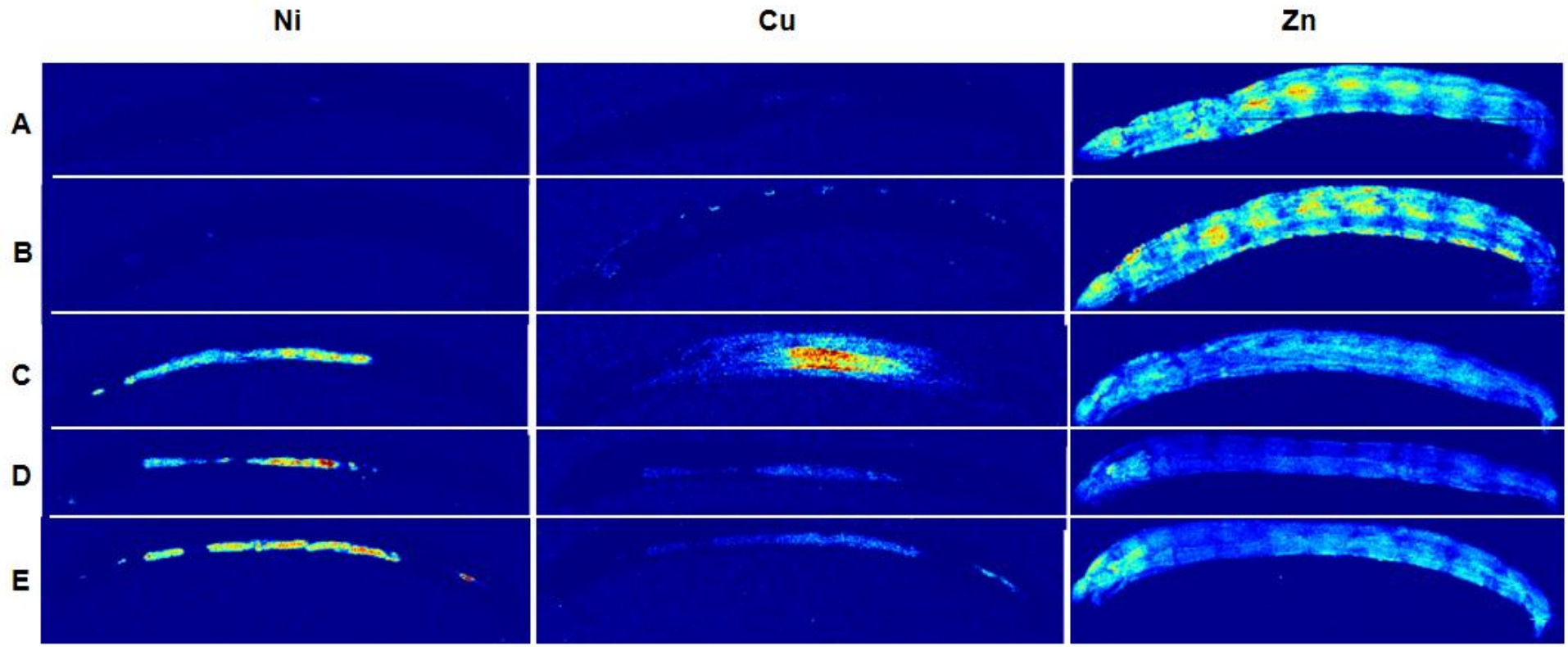


**Fig. 5.8**. XRF imaging results of field chironomids, **(A)** Yeoung Lake, **(B)** Unknown Lake site 2, **(C)** Unknown Lake site 3, **(D)** Fox Lake site 2, and **E**) Fox Lake site 3. Images have been scaled such that chironomids of the same element are comparable.

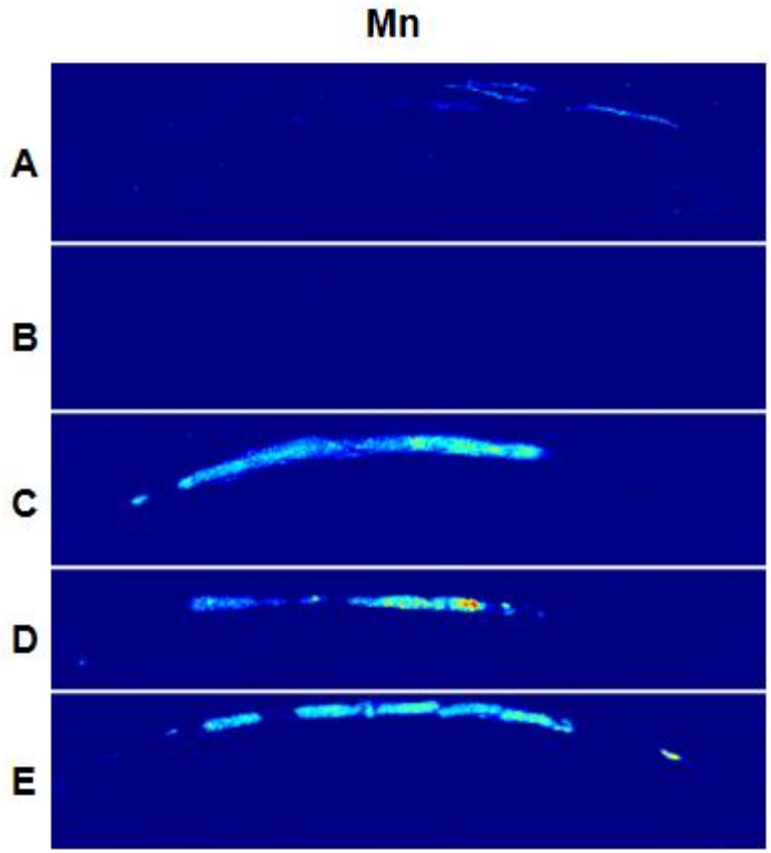


**Fig. 5.9**. XRF imaging results of field chironomids, **(A)** Yeoung Lake, **(B)** Unknown Lake site 2, **(C)** Unknown Lake site 3, **(D)** Fox Lake site 2, and **E**) Fox Lake site 3. Images have been scaled such that chironomids of the same element are comparable.

## 5.5. Discussion

Combining synchrotron XAS and XRF provides insights into the speciation and localization of Se in biological samples. In terms of Se speciation, there were similarities between the Se species present in chironomids analyzed after a 10-day uptake or 10-day depuration period. The majority of Se species present were selenomethionine- and selenocystine- like species. In circumstances of high concentrations of Se in the surrounding environment, the Se taken up by the gut lining, head capsule, and salivary gland is possibly incorporating the Se as selenomethionine into proteins that may possess a high turnover rate or acting as a temporary Se storage/sink. In chironomids reared with a 10-day depuration, the total Se concentration decreases and no specific Se localizations similar to chironomids imaged after a 10-day uptake were observed. This trend was also observed by Franz *et al.* (2011), where after a 3-day depuration the proportion of selenomethionine decreases and selenocystine increases. Therefore, when the source of Se is eliminated, the proteins may return to utilizing S for methionine rather than Se. The Se after a 10-day depuration period may suggest the base level of Se in the chironomid, while un-depurated chironomids (10-day uptake) probably show the excess Se being taken up by the gut lining cells, salivary gland, and head capsule region (Fig. 5.5 and 5.6). The diffusion or decreased concentration of Se in specific tissues may be resolved by imaging with a higher spatial resolution.

While the values of dissolved oxygen and pH are relatively similar between the two different types of water exposure, differences are observed in conductivity, alkalinity, and hardness because of the substantial difference in the amount of ions between Barnstead and dechlorinated water. Even with the lack of ions, chironomids had > 97.4% survival. Deaths were mainly attributed to difficulties experienced in acclimating to a new environment, when the chironomids were transferred from the holding tanks to exposure beakers. Recent studies comparing fresh water and salt water exposures of *Chironomus riparius* and

*Aedes aegypti* have shown that besides varying rates of ion uptake, they are able to adjust to either condition and survive (Nguyen and Donini, 2010; Donini *et al*., 2007; and Jonusaite *et al*., 2011). When the specimens were transferred from salt water to fresh water conditions an increase in the anal papillae was observed, allowing a greater surface for the absorption of scarce ions. A greater concentration of Se was found in chironomids reared in Barnstead water spiked with selenomethionine, than those observed by Franz *et al* (2011). This may be attributed to the increased anal papillae resulting in a greater absorption of selenomethionine. By contrast an increase in total Se concentration after selenite exposure is not observed. It is possible that due to its negative charge, selenite may utilize different ion uptake channels than selenomethionine, which may undergo passive diffusion.

The total concentrations of Se in the chironomid tissue (Table 5.2) show that with increasing distance from the mining effluent discharge, the total Se concentration in the chironomid decreases ([Se]U2 > [Se]U3, Table 5.2), which is also reflected by concentrations found in the surface water, whole sediment, pore water, and chironomids recorded by Wiramanaden *et al.* (Wiramanaden *et al*., 2010b). Speciation results also demonstrated the presence of multiple Se species. Though the study mainly focused on the trend between selenomethionine- and selenocystine-like species, other species are observed including a metal selenide (possibly FeSe), aqueous tri-methyl selenonium ion ($Me_3Se^+$), selenate ($SeO_4^{2-}$), and selenite ($SeO_3^{2-}$). These species are expected, as chironomids can be non-specific feeders, and ingestion of sediment particles and compounds in the floc may lead to these species. Metal selenides are most likely associated with the sediment particles, and $Me_3Se^+$ with urine excretion. Selenite arises from the reduction of selenate, which is the major Se species in the effluent. After the 10-day depuration selenocystine- and selenomethionine-like species are the only species detectable, while at the 10-day uptake time point, FeSe, $SeO_3^{2-}$, and $Me_3Se^+$ are additionally observed.

Therefore, it seems that during the depuration period, because the total Se concentration decreases (Table 5.2), most of the Se is excreted rather than being transformed into another species. This excretion can include urine, fecal matter, or secretion from the salivary glands to form the tubes in which they dwell.

Comparisons between chironomids reared in the laboratory with those in the field provide similar speciation and localization profiles; however, differences are mainly found in the concentrations of total Se present. This is consistent with the main route of Se exposure and accumulation being not through dissolved Se species in water. Further work has been done demonstrating ingestion as the primary route of exposure (Franz *et al.*, 2011). Results from chironomids reared in the laboratory did demonstrate that when exposed to an organic species, selenomethionine, the same Se speciation and localization is observed in chironomids collected from the field (Fig. 5.5 and 5.6). Therefore, the Se accumulation seen in field chironomids may be due at least in part to an organic species of Se and more specifically possibly a selenomethionine-like species. Chironomids do not possess the means to synthesize methionine (Spallholz and Hoffman, 2002); therefore, the methionine/selenomethionine must be obtained from another source that may include the diet or bacterial contributions either in the local environment or present in the gut. The food given to the chironomids, containing wheat and wheat germ, contained low levels of Se, 0.38 ± 0.06 mg $kg^{-1}$ (bio flakes (Sera Pond)). In both field chironomids and selenomethionine and selenite water spiked laboratory chironomids, the percentage of selenomethionine in the fit was always greater than selenocystine. In environments of high Se, accidental incorporation of selenomethionine into proteins will occur; however, the synthesis and incorporation of selenocystine is extremely specific. In the selenate and control exposures, a greater percentage of the fit is attributed to selenocystine than selenomethionine. This does not imply a greater total concentration of

selenocystine but that with a smaller percentage of selenomethionine, the selenocystine component becomes more pronounced.

In XRF imaging on *C. dilutus* samples, Se was found to be accumulating in the head, salivary gland, and gut region. Research on the Drosophila suggests that its genome may encode a possible three selenoproteins: selenophosphate synthetase 2 (SPS2), G-rich, and BthD (Martin-Romero *et al*., 2001). SPS 2 is thought to accumulate in the brain during growth, while BthD is shown to accumulate in the salivary glands and may help with oxidative stress, vitality, and viability (Martin-Romero et al., 2001; and Hirosawa-Takamori *et al*., 2004). The present research will help further emphasize and verify the localizations of Se that may be attributed to selenoprotein analogs of those found in Drosophila.

Thus, the combination of synchrotron XAS and XRF can provide new insight into the speciation and localization of Se within chironomids. Monitoring and analyzing chironomids on a daily basis could provide a better understanding on the biotransfer and biotransformation of Se, as one could examine the uptake and loss of specific Se species as well as where and if localizations of Se may change. What should be also noted is even though the chironomids are exposed to concentrations of only 11 µg $L^{-1}$, Fox Lake, 4 µg $L^{-1}$, Unknown Lake, they have the ability to bioaccumulate Se to concentrations exceeding 7.5 mg $kg^{-1}$ and up to 80 mg $kg^{-1}$, or bioaccumulation factors ranging from 2000 – 7300 ([Se] in the chironomids divided by [Se] in the water). Therefore, the similarities observed in the distribution and speciation between field and laboratory chironomids suggest that a selenomethionine-like species is readily taken up and bioaccumulated.

# CHAPTER 6

# SUMMARY

# Chapter 6 - Summary

## 6.1. Overall Summary

This thesis is one component of a larger collaborative research program which aimed at a holistic approach to the study of the Key Lake aquatic ecosystem. Individual projects encompassed studies of the water, sediment, benthic invertebrate community, and small fish inhabiting this lake system. Experimental designs ranges from purely field-based observations through to controlled laboratory simulations. While work performed by Franz *et al.* (2011), Phibbs *et al.* (2011a and 2011b), and Wiramanaden *et al.* (2010a and 2010b), are mentioned throughout this thesis, the scope of this whole project does have a further reach. Work performed by Driessnack *et al.,* (2011) examined the effects on health and reproduction of fathead minnows (*Pimephales promelas*) when exposed to diluted effluent. An increase in egg production was observed when fathead minnows were exposed to the 25% effluent; however, the eggs also were hatching early. This sped up hatching process may contribute to the observed increased larval deformities and decreased larval survivability observed in this high treatment 5-days post hatch by preventing the proper and full maturation of the fish.

In conjunction with studying the health and reproduction of fathead minnows, Goertzen *et al.,* (2011) studied the effects of the effluent on their swimming performance and energy homeostasis. They reported that no change in energy homeostasis was observed between fish in 5% diluted effluent and those in dechlorinated water; however, a change in the critical swim speed, $U_{crit}$, was noticed (Goertzen *et al.,* 2011). This value, $U_{crit}$, represents the endurance and maximal swim speed of the fish (Brett, 1964). Though the exact mechanism for the decrease in $U_{crit}$ is not known, it is believed that effluent exposure may alter biochemical or metabolic cycles (Goertzen *et al.,* 2011).

The research presented in this thesis focused on the sediments and benthic invertebrates from the Key Lake aquatic ecosystem. These samples were chosen as they may function as points of entrance for foreign matter in the aquatic ecosystem present at the Key Lake site. The results of studies of sediment and chironomids help give a better understanding of the methods by which Se may be entering the aquatic ecosystem. Chironomids, or benthic invertebrates, were chosen because of their ubiquitous nature, the fact that they inhabit the sediment, and their previous use in toxicology studies (Maier and Knight, 1993; Benoit *et al.,* 1996; Wise *et al.,* 2001; Krantzberg and Stokes, 1989; Krantzberg and Stokes, 1990; and Hare *et al.,* 1991). Therefore, understanding the routes of exposure by Se may provide insight into its mobilization throughout a food web.

From the successful testing of the sediment sample holder (Chapter 3) analyzing small segments of a whole core at high resolution is achievable. Prior work on sediment cores (Wiramanaden *et al.*, 2010a) was done by extracting 1 cm sections, grinding a homogeneous sample, and analyzing via bulk XAS. The new holder allowed intact 1 x 1 x 0.5 cm (length x height x width) sediment samples to be analyzed. Combined with beamline motion controls, 100 and 250 µm step profiles were obtained from the sediment sample. Compared to previous research (Wiramanaden *et al*., 2010a; Tetsu *et al*., 1991; and Tetsu *et al*., 2008) a more detailed picture of the Se speciation changes and additional elements can be analyzed as a function of depth. Obtaining depth profiles to this resolution is important in understanding, amongst other things, what (micro) organisms may be able to access the Se. One can imagine that the microbial community can drastically vary as a function of depth, from more aerobic species to anaerobic ones, as less oxygen becomes available the further the depth increases (Machel and Foght, 2000; and Hansen and Blackburn, 1991).

It might be expected that oxidized species would dominate over reduced species at the surface of sediments, whereas as the depth increases reduced species predominate, and these effects are observed in the analyzed sediment depth profiles. The sediment-water interface was not a sharp transition, as first believed. This sharp interface, of no Se to some Se, was expected due to the transition between a liquid (water) and solid (sediment) phase. Instead, what is observed is a more gradual change in Se. This gradual change is hypothesized to be due to flocculation, a murky layer between the "clear" water and dense sediment in which suspended particles are found. One of the benefits of analyzing the sediment cores via bulk XAS is the collection of other elements that may be of interest. After analyzing a sediment sample for the presence of Se, the filters were replaced, and the same sample was measured again identically (though, with a smaller energy range) to examine other elements that may be present. Therefore, elemental maps of Fe, As, Ni, Cu, Zn, and Mn can be plotted on top of Se to demonstrate their change in concentrations as a function of depth. The sediment depth profiling not only revealed the change in Se species, but by expanding the analysis to 3 cm of depth, trends in Se and other elemental accumulation are observed as a function of depth (Fig. 4.6). Due to time constraints, only relative concentrations, instead of full spectra, of the secondary elements could be taken, but in principle whole XAS spectra could be collected, given significantly more beamtime. Though Fig. 4.6 does demonstrate that Fe is the dominant metal species present regardless of depth, up to 3 cm, the relative proportions of one secondary element to another as a function of depth may provide insight into the mineral composition.

The work on chironomids helped expand the picture of Se's movement from sediment into benthic invertebrates of Key Lake. Though chironomids from the field can be easily collected and then analyzed by bulk XAS or XRF, there are a multitude of factors affecting the uptake of Se by chironomids from the field. To help minimize outside factors, *C. dilutus* were reared in the laboratory in

Barnstead water. The work done here and by Franz *et al.* (2011) with chironomids in controlled laboratory environments, help explain the forms and routes by which Se may enter chironomids. Though some differences are observed in the bulk XAS speciation data between Franz's and our data, we attribute it largely to the water in which the chironomids were reared. Franz *et al.* utilized dechlorinated water, while my experiments involved Barnstead water in order to remove the effects of additional foreign matter. Overall, our data largely complements one another. Both of our experiments suggest that water is not the major route of exposure to Se; however, water may still play a small role in Se bioaccumulation. Concentrations of 7 – 80 mg $kg^{-1}$ of Se were found in field chironomids, while 0.6 – 63 mg $kg^{-1}$ were found in chironomids reared in the laboratory in Barnstead water. By coupling ICP-MS with the results of synchrotron techniques, our results suggest that waterborne exposure may only contribute a very small amount of the present Se in the chironomids found in the field. Combined with XRF, a versatile synchrotron based imaging technique, observing the localization of the Se accumulation within chironomids is achievable. Results suggest that selenomethionine from the water is taken up and accumulated primarily in the gut or gut lining. Cells of the intestinal gut lining, responsible for absorbing nutrients from food, in the presence of Se may be responsible for its absorption, biotransformation, and short-term storage, Se absorbed may be taken up and biotransformed in the cells lining the gut. Imaging results of selenate-exposed chironomids resembled those of the control, which is expected due to the low bioavailability of selenate. Aqueous selenite exposure resulted in a similar distribution to that of selenomethionine, however, the overall concentration was much lower. Exact concentrations of Se are difficult to obtain from chironomids because of the varying thickness throughout the chironomids. Comparing the images of the laboratory reared chironomids and field chironomids gives a remarkable result, in that similar localization is observed. This was a very exciting achievement, that despite all the factors affecting Se uptake in the field, we were able to duplicate some similar results in the laboratory. The field chironomids also accumulated Se in

the gut or gut lining. By comparing the bulk XAS from both sets of chironomids, selenomethionine is present in both chironomids, suggesting that selenomethionine may be an important endpoint species, regardless of the Se species exposed to the chironomids. Lack of Se in images from laboratory selenate and control reared chironomids suggest that Se levels were below the detection limit of the current set up; however, bulk XAS suggest that there are trace amounts of Se present in both treatments of chironomids (Fig. 5.2).

Chironomids from the field as well as those reared in the laboratory in water exposures spiked with bioavailable species (ie. selenite and selenomethionine) bioaccumulated and localized Se in similar areas. The 3 main areas of localization were the head capsule, salivary glands, and gut. In relation to *Drosophila melanogaster* selenoproteins, three areas of accumulation are expected. The genome of *D. melanogaster* has been shown to encode several selenoproteins, and recent work has been centered on 3 of these selenoproteins: selenophosphate synthetase 2 (SPS 2), BthD, and G-rich (Martin-Romero et al., 2001; Hirosawa-Takamori *et al*., 2004; and Kwon *et al*., 2003). In Drosophila, SPS 2 only accumulates in the brain during larval stages; however, in the laboratory, the early larval stages of chironomids are experienced in holding tanks that do not contain large amounts of Se. Therefore, in the latter part of the chironomids larval stage, when it is being exposed to Se, there may be not enough time for the SPS 2 protein to accumulate in the head capsule. In Drosophila, SPS 2 was found to be required for the formation of imaginal discs. Imaginal discs are important in the formation of limbs, and during Drosophila metamorphosis, pupal and adult appendages form from the imaginal discs. When the SPS protein was knocked out, the Drosophila were not able to live past 8 days. SPS 2 is also known to be responsible and essential for the transformation of serine tRNA's (Ser) into selenocysteine tRNA's (Sec) (Itoh *et al*., 2009). A quick look into the wormbase, a complete genomic sequence of *C. elegans*, has shown that

Chironomidae do posses a genome encoding for selenophosphate synthetase (WormBase, 2011). The localization of Se is only clearly observed in the head capsules of chironomids collected from the field. We believe that the absence of Se in the head capsules of chironomids reared in the laboratory is due to time and concentration. As SPS 2 is responsible for the production of Sec and the brain will be fully formed early in the larval stages, it might suggest that there are proteins in the brain that contain Sec. This is further enforced by the localization of Se in the head capsule of chironomids collected in the field, and the absence of this localization in chironomids reared in the laboratory. The selenoprotein BthD will accumulate in the salivary glands and may be required for survival. Work is being done to analyze the tubules created by chironomids, by Gallegos *et al*. (personal communication), initial results have demonstrated the presence of Se. Therefore, it is likely that *C. dilutus* contains a selenoprotein analog of BthD.

The Chironomidae community generally dwells within the first 2 cm of sediment; however, in rare cases, they have been found to be dwelling at much further depths (> 2 m) (Cannings and Scudder, 1978). Therefore, analyzing these depths of sediments at high resolution will provide us with the speciation and localization of Se that may be accessible by the benthic invertebrate community. The species of Se present is important, as this will determine its ability to be bioaccumulated. The more biologically available the species, the more it will be taken up and the greater possibility that Se is biomagnified through the food chain. Thus, by determining the Se species present in the sediment, utilizing the biologically available species for laboratory exposures, we can determine and verify whether the species found in the field is being taken up and where it might be localizing within the organism. Therefore, the presence of the organic selenomethionine- like species and elemental Se may be the species responsible for the Se bioaccumulation found in the Key Lake aquatic ecosystem. This hypothesis is further reinforced by the synchrotron

XRF results of chironomids. In laboratory chironomids spiked with selenomethionine, similar localization and speciation compared to those collected from the field were observed.

## 6.2. Future Work

A holistic approach was undertaken to study the aquatic ecosystem present at the Key Lake site. In conjunction with 3 principal investigators from the Toxicology Centre (University of Saskatchewan), the food web was only studied up to the level of fish. Studies on Se's effects on breeding birds downstream of the U mill have been performed (Weech *et al*., 2011). However, surrounding vegetation and other higher level organisms need to be examined for the effects of Se bioaccumulation. By applying the same synchrotron and laboratory based techniques, one could easily analyze samples of vegetation and wildlife and help expand the current picture of Se throughout the food web.

### 6.2.1. Sediments

Samples of several centimeters of section were created every time a sediment core was sectioned for “pseudo-bulk imaging”. Analyzing these additional cores will provide a better understanding of the trend of Se as a function of depth. At the moment, Fox Lake has been studied at a high resolution (100 and 250 µm) for a total of 3 cm. The first cm of Unknown Lake has been studied at this high resolution and depths 2 - 4.5 cm were analyzed in 0.5 cm sections. Observing the trends of Se and other elements at lower depths in Unknown Lake at the high resolution will provide a better comparison with Fox Lake.

Using the previously analyzed sediment cores, digesting for multi-elemental ICP-MS analysis can be used to calibrate the observed fluorescence intensities in terms of a mg $kg^{-1}$ scale as a function of depth. Since Se may not be the sole

cause of decreased wildlife in the Key Lake aquatic ecosystem, research is required on other elements and compounds that may be present. Our data on the other elements present demonstrate a large peak of As that may be accumulating at the redox boundary. Arsenic, similarly to Fe and Mn can become mobile under reducing conditions; therefore, it will always been present at the redox boundary and constantly in the presence of dwelling benthic invertebrate communities.

Some modifications may need to be made to sample preparation. As detectors on beamlines may contain dead channels, eliminating as many possible sources of scatter in the sample would help greatly with the data collected. As this cannot always be avoided in the sample, sectioning thinner sections would provide less substance for the beam to pass through, and therefore less chance of hitting a scattering object.

The sample holder itself functioned as expected. Modifications may need to be made to the printed pillar. At 45° incident to the beam not every position on the observable sample area will provide the same intensity. The printed pillar was observed to reduce some of the incoming beam into $I_1$. Therefore, another material for the printed pillar may need to be utilized, or ensuring that if samples are to be analyzed via transmittance, that the sample holder is positioned at 90° to the incident beam.

### 6.2.2. Chironomids

Since most of the conclusions for the localization of Se have been correlated with selenoproteins found in Drosophila, performing and obtaining a complete genomic sequence of *C. dilutus* will prove invaluable. Using BLAST (Altschul *et al*., 1990), or homebrew software, to compare genomic sequences between *C.*

*dilutus* and *D. meloganster* will see if some sequences will enlighten the presence of selenoprotein analogs present in the *C. dilutus*. Genomic matching could also be performed to observe whether chironomids have similar Se processing pathways as Drosophila.

The initial experiments done using chironomid imaging have provided a new way to view chironomids and Se localization. We used a standard sagittal orientation of the chironomids for ease of mounting; however, alternate orientations will be very important in separating localizations that will otherwise superimpose in this orientation, such as the eyes and brain. Therefore, work is ongoing to examine Se localization in a dorsal orientation rather than our typical sagittal orientation.

## 6.3. References


Altschul, S.F., Gish, W., Miller, W., Myers, E.W., and Lipman D.J. Basic local alignment search tool. *J. Mol. Biol*. 1990, v. 215, pp 403-410

Andrahennadi, R., Wayland, M., and Pickering. I. J. Speciation of selenium in stream insects using X-ray absorption spectroscopy. *Environ. Sci. Technol*. 2007, v. 42, pp 7683-7687.

Arnér, E. S. J., and Holmgren, A. Physiological functions of thioredoxin and thioredoxin reductase. *Eur. J. Biochem*. 2000, v. 267, pp 6102-6109.

Beke, G. J., and Hironaka, R. Toxicity to Beef Cattle of Sulfur in Saline Well Water-A Case Study. *Sci. Total. Environ*. 1991, v. 101, pp 281 – 290.

Benoit, D. A., Sibley, P. K., Jeunemann, J. L., and Ankley, G. T. *Chironomus tentans* Life-Cycle Test: Design and Evaluation for Use in Assessing Toxicity of Contaminated Sediments. *Environ. Toxicol. Chem*. 1997, v. 16, pp 1165-1176.

Bercovici, D., Schubert, G., and Glatzmaier, G.A. Three - Dimensional Spherical Models of Convection in the Earth's Mantle. *Science*. 1989. v. 244, pp 950-955

Berzelius, J. J. Letre de M. Berzelius a M. Berthollet sur deux métaux nouveaux. *Annals de chimie et de physique*. 1818, v. 7, pp 199-206.

Besser, J. M., Canfield, T. J., and La Point, T. W. Bioaccumulation of organic and inorganic selenium in a laboratory food chain. *Environ. Toxicol. Chem*. 1993, v. 12, pp 57-72

Black, A.R., and Dodson, S.I. Ethanol: a better preservation technique for *Daphnia*. *Limnology and Oceanography: Methods*. 2003, v.1, pp 45-50

Boyle, J. Redox mobilization and the heavy metal record in lake sediments: a modeling approach. *Journal of Paleolimnology*, v. 26, pp 423-431.

Brett, J. R. The respiratory metabolism and swimming performance of young Sockeye salmon. *J. Fish. Res. Bd. Can*. 1964, v. 21, pp 1183-1226.

Cameco. Key Lake Extension Project: Project Description. Safety, Health, Environment & Quality. Retrieved March, 2010 from http://www.cameco.com/common/pdf/responsibility/regulatory/key_lake/Cameco_Key_Lake_Extension_Project.pdf.

Cameco. McArthur River. September 3, 2011 <http://www.cameco.com/mining/mcarthur_ river/>

Canadian Light Source, (2009), How does the CLS Synchrotron work?. <http://www.lightsource.ca/education/pdf/materials/1.2_How_does_the_CLS_Synchrotron_work.pdf>

Cannings, R. A., and Scudder, G. G. E. The littoral Chironomidae (Diptera) of saline lakes in central British Columbia. *Canadian Journal of Zoology*. 1978, v. 56, pp 1144-1155.

Chau, Y. K., Wong, P. T. S., Silverberg, B. A., Luxon, P. L., and Bengert, G. A. Methylation of Selenium in the Aquatic Environment. *Science*. 1976, v. 192, pp 1130 – 1131.

Chen, Y.-W., Truong, H.-Y.T., and Belzile, N. Abiotic formation of elemental selenium and role of iron oxide surfaces. *Chemosphere*, 2008, v. 74, pp 1079-1084.

Choi. J, Roche, H., and Caquet, T. Characterization of superoxide dismutase activity in *Chironomus riparius* Mg. (Diptera, Chironomidae) larvae – a potential biomarker. *Comparative Biochemistry and Physiology Part C: Pharmacology, Toxicology and Endocrinology*. 1999. v. 124, pp 73-81.

City of Saskatoon Water Treatment Plant. Drinking Water Quality and Compliance. 2009. pp 1 – 7

Clark, D. R. Selenium Accumulation in Mammals Exposed to Contaminated California Irrigation Drainwater. *The Science of the Total Environment*, 1987, v.66, pp 147-168

Clark, D. R., Ogasawara, P. A., Smith, G. J., and Ohlendorf, H. M. Selenium Accumulation by Raccoons Exposed to Irrigation Drainwater in Kesterson National Wildlife Refuge, California, 1986. *Arch. Environ. Contam. Toxicol.* 1989, v. 18, pp 787 – 794.

Combs, G. F., Food system-based approaches to improving micronutrient nutrition: the case for selenium. *Biofactors*. 2000, v. 12, pp 39-43.

Committee on Accessory Elements. Board on Mineral and Energy Resources. Commission on Natural Resources. National Research Council. Redistribution of Accessory Elements in Mining and Mineral Processing. Part II: Uranium, Phosphate, and Alumina. Washington, D.C. National Academy of Sciences, 1979.

Cornwell, J. C. Diagenetic Trace-Metal profiles in Arctic Lake Sediments. *Environ. Sci. Technol*. v. 20, pp 299-302.

Cramer, S. P., Tench, O., Yocum, M. and George, G. N. A 13-element Ge detector for fluorescence EXAFS. *Nucl. Instrum. Methods. Phys. Res. A*. 1988, v. 266, pp 586–591.

Cummins, L. M., and Kimura, E. T. Safety evaluation of selenium sulfide antidandruff shampoos. *Toxicol. Appl. Pharmacol*. 1971, v. 20, pp 89-90.

Donald, G.L., and Paterson, C.G. Effect of preservation on wet weight biomass of chironomid larvae. *Hydrobiologia*. 1977, v. 53, pp 75-80.

Donini, A., Gaidhu, M. P., Strasberg, D. R., and O'donnell, M. J. Changing salinity induces alterations in hemolymph ion concentrations and $Na^+$ and $Cl^-$ transport kinetics of the anal papillae in the larval mosquito, *Aedes aegypti*. *J. Exp. Biol*. 2007, v. 210, pp 983 – 992.

Driessnack, M. K., Dubé, M. G., Rozon-Ramillo, L. D., Jones, P. D., Wiramanaden, C. I. E., and Pickering, I. J. The use of field-based mesocosm systems to assess the effects of uranium milling effluent on fathead minnow (Pimephales promelas) reproduction. *Ecotoxicology*. 2011, v. 20, pp 1209-1224.

Elrashidi, M. A., Adriano, D. C., Workman, S. M., and Lindsay, W. L. Chemical Equilibria of Selenium in Soils: Theoretical Development. *Soil Sci*. 1987, v. 144, pp 141-152

Ezquerra, T. A., García-Gutiérrez, MC., Nogales, A., and Gómez, M. Applications of Synchrotron Light to Scattering and Diffraction in Materials and Life Sciences. Heidelberg, Berlin, Springer, 2009.

Fleet-Stalder, V. V., Chasteen, T. G., Pickering, I. J., George, G. N., and Prince, R. C. Fate of Selenate and Selenite Metabolized by *Rhodobacter sphaeroides*. *Appl. Environ. Microbiol*. 2000, v. 66, pp 4849-4853 Frakenberger, W. T., and Arshad, M. Bioremediation of selenium-contaminated sediments and water. *Biofactors*. 2001, v. 14, pp 241 – 254.

Franz, E.D., Wiramanaden, C.I.E., Janz, D.M., Pickering, I.J., and Liber, K. Selenium bioaccumulation and speciation in Chironomus dilutus exposed to water-borne selenate, selenite, or seleno-DL-methionine. *Environ. Toxicol. Chem*. In Press, Corrected Proof

Gao, X., Zhang, J., and Zhang, L. Acute toxicity and bioavailability of nano red elemental selenium. *Journal of Hygiene Research*. 2000, v. 29, pp 57-58.

Garbisu, C., Ishii, T., Leighton, T., and Buchanan, B. B. Bacterial reduction of selenite to elemental selenium. *Chemical Geology*. 1996, v. 132, pp 199 – 204.

Gaston, G.R., Bartlett, J.H.W., and McAllister, A.P. Biomass Variations of Estuarine Macrobenthos Preserved in Ethanol and Formalin. *Estuaries*. 1996, v.19, pp- 674-679

Gautreau, R., and Savin , W. Modern Physics: Second Edition. USA, The McGraw-Hill Companies, Inc, 1999.

Geering, H. R., Cary, E. E., Jones, L. H. P., and Allaway, W. H. Solubility and Redox Criteria for the Possible Forms of Selenium in Soils. *Soil Sci. Soc. Am. Proc*. 1968, v. 32, pp 35-40

George, G. N., and Pickering, I. J. X-ray Absorption Spectroscopy in Biology and Chemistry. *Brilliant Light in Life and Material Sciences*. Springer. 2007, pp 97-119.

George, G.N., and Pickering, I.J. EXAFSPAK: A Suite of Computer Programs for Analysis of X-ray Absorption Spectra. Stanford Synchrotron Radiation Laboratory. 1993.

Giessel-Nielsen, G. Influence of pH and Texture of the Soil on Plant Uptake of Added Selenium. J. Agr. Food. Chem. 1971, v. 19, pp 1165 – 1167.

Goertzen, M. M., Driessnack, M. K., Janz, D. M., and Weber, L. P. Swimming performance and energy homeostasis in juvenile laboratory raised fathead minnow (*Pimephales promelas*) exposed to uranium mill effluent. *Comparative Biochemistry and Physiology, Part C.* 2011, v. 154, pp 420-426.

Gupta, C. K., and Singh, H. Uranium Resource Processing: Secondary Resources. Germany, Springer, 2003.

Hansen, L. S., and Blackburn, T. H. Aerobic and anaerobic mineralization of organic material in marine sediment microcosm. *Mar. Ecol. Prog. Ser*. 1991, v. 75, pp 283-291.

Hare, L., Tessier, A., and Campbell, P. G. C. Trace Element Distributions in Aquatic Insects: Variations among Genera, Elements, and Lakes. *Can. J. Fish. Aquat. Sci.* 1991, v. 48, pp 1481-1491.

Hartikainen, H. Biogeochemistry of selenium and its impact on food chain quality and human health. *Journal of Trace Elements in Medicine and Biology*. 2005, v. 18, pp 309 – 318.

Herndon, J. M. Substructure of the inner core of the Earth. *Proc. Natl. Acad. Sci*. 1996, v. 93: 646-648

Hirosawa-Takamori, M., Chung, H-R., and Jäckle, H. Conserved selenoprotein synthesis is not critical for oxidative stress defence and the lifespan of Drosophila. *EMBO reports*, 2004, v.5, pp 317-322

Hodson, P. V., and Hilton, J. W. The nutritional requirements and toxicity to fish of dietary and water-borne selenium. *Ecol. Bull*. 1983, v. 35, pp 335-340.

Howard, J. H., Geochemistry of selenium: formation of ferroselite and selenium behavior in the vicinity of oxidized sulfide and uranium deposits. *Geochemica et Cosmochimica Acta.* 1977, v. 41, pp 1665 – 1678.

Hulbert, S. L., and Williams, G. P. Synchrotron Radiation Sources. *Experimental Methods in the Physical Sciences*, 1998, v. 31, pp 1-25

Hymer, C. B., and Caruso, J. A. Selenium speciation analysis using inductively coupled plasma – mass spectrometry. *Journal of Chromatography A*. 2006, v. 1114, pp 1-20

Institute of Medicine, Food and Nutrition Board. Dietary Reference Intakes: Vitamin C, Vitamin E, Selenium, and Carotenoids. Washington, DC. National Academy Press, 2000.

International Atomic Energy (IAE). In Situ Leaching of Uranium: Technical, Environmental and Economic Aspects. IAEA-TECDOC-492, 1989.

Itoh, Y., Sekine, S., Matsumoto, E., Akasaka, R., Takemoto, C., Shirouzu, M., and Yokoyama, S. Structure of Selenophosphate Synthetase Essential for Selenium Incorporation into Proteins and RNAs. *J. Mol. Biol.* 2009, v. 385, pp 1456-1469.

Jonusaite, S., Kelly, S.P., and Donini, A. The physiological response of larval *Chironomus riparius* (Meigen) to abrupt brackish water exposure. *J. Comp. Physiol. B*. 2011, v. 181, pp 343 – 352.

Krantzberg, G., and Stokes, P. M. Metal Concentrations and Tissues Distribution in Larvae of *Chironomus* with Reference to X-ray Microprobe Analysis. *Arch. Environ. Contam. Toxicol* 1990, v. 19, pp 84.93.

Krantzberg, G., and Stokes, P. M. Metal Regulation, Tolerance, and Body Burdens in the Larvae of the Genus *Chironomus*. *Can. J. Fish. Aquat. Sci*. 1989, v. 46, pp 389-398.

Kudo, A. Volume 1: Plutonium in the environment. Proceedings of the Second International Symposium. The Netherlands, Elsevier Science Ltd, 2000.

Kwon, S. Y., Badenhorst, P., Martin-Romero, F. J., Carlson, B. A., Paterson, B. M., Gladyshev, V. N., Lee, B. J., and Hatfield, D. L. The Drosophila Selenoprotein BthD Is Required for Survival and Has a Role in Salivary Gland Development. *Molecular and Cellular Biology*. 2003, v. 23, pp 8495-8504.

Lamoureux, S. F. Embedding unfrozen lake sediments for thin section preparation. *J. Paleolimnol*. 1994, v. 10, pp 141-146.

Lemly, A. D. Assessing the Toxic Threat of Selenium to Fish and Aquatic Birds. *Environmental Monitoring and Assessment*. 1996, v. 43, pp 19-35.

Lemly, A. D. Guidelines for evaluating selenium data from aquatic monitoring and assessment studies. *Environ. Monit. Assess*. 1993, v. 28, pp 83-100.

Lemly, A. D. Selenium Transport and Bioaccumulation in Aquatic Ecosystems: A Proposal for Water Quality Criteria Based on Hydrological Units. *Ecotoxicology and Environmental Safety*. 1999, v. 42, pp 150 - 156.

Lemly, A. D. Symptoms and implications of selenium toxicity in fish: the Belews lake case example. *Aquat. Toxicol*. 2002, v. 57, pp 39-49.

Leung, Y.K., Wong, K.F., Lee, H.K., and Ho, J.W. Cloning and characterization of chironomidae ferrochelatase: Copper activation of the purified ferrochelatase. *Mol. Cell. Biochem*. 2004. v. 262, pp 225-231.

Li, G. S., Wang, F., Kang, D., and Li, C. Keshan disease: An edemic cardiomyopathy in China. *Human Pathology*. 1985, v. 16, pp 602-609.

Li, Y.-F, and Macdonald, R. W. Sources and pathways of selected organochlorine pesticides to the Arctic and their impacts to the existence of these pesticides in the Arctic environment: A review. *Science of the Total Environment*. 2005, v. 342, pp 87-106.

Losi, M. E., and Frankenberger, W. T. Bioremediation of Selenium in Soil and Water. *Soil Science*. 1997, v. 162, pp 692 – 702.

Lytle, F. W., Sayers, D. E., and Stern, E. A. Extended x-ray-absorption fine-structure technique. II. Experimental practice and selected results. *Phys. Rev. B.* 1975, v.11, pp 4825–4835.

Machel, H. G., and Foght, J. "Products and Depth Limits of Microbial Activity in Petroliferous Subsurface Settings". Microbial Sediments. Eds. Riding, R. E., and Awramik, S. M. Germany. Springer. 2000, pp 105-120.

Maier, K. J., and Knight, A. W. Comparative Acute Toxicity and Bioconcentration of Selenium by the Midge *Chironomus decorus* Exposed to Selenate, Selenite, and Seleno-DL-methionine. *Arch. Environ. Contam. Toxicol.* 1993, v. 25, pp 365-370.

Mandelkow, E., and Bazin, D. Synchrotron radiation in chemistry and biology I. Springer. 1988 ISBN 9783540183853

Martin-Romero, F. J., Kryukov, G. V., Lobanov, A. V., Carlson, B. A., Lee, B. J., Gladyshev, V. N., and Hatfield, D. L. Selenium Metabolism in Drosophila: selenoproteins, selenoprotein mRNA expression, fertility, and mortality. *J. Biol. Chem*. 2001, v. 276, pp 29798-29804.

Martin-Romero, F. J., Kryukov, G. V., Lobanov, A. V., Carlson, B. A., Lee, B. J., Gladyshev, V. N., and Hatfield, D. L. Selenium Metabolism in Drosophila. *J. Bio. Chem*. 2001, v. 276, pp 29798-29804.

Martin, A. J., Simpson, S., Fawcett, S., Wiramanaden, C. I. E., Pickering, I. J., Belzile, N., Chen, Y. W., London, J., and Wallschläger, D. Biogeochemical Mechanisms of SElenium Exchange between Water and Sediments in Two Contrasting Lentic Environments. *Environ. Sci. Technol.* 2011, v.45, pp 2605-2612.

Masscheleyn, P. H., Delaune, R. D., and Patrick, W. H. Transformation of Selenium As Affected by Sediment Oxidation-Reduction Potential and pH. Environ. Sci. Technol. 1990, v. 24, pp 91 – 96.

May, T. W., Fairchild, J. F., Petty, J. D., Walther, M. J., Lucero, J., Delvaux, M., Manring, J., and Armbruster, M. An evaluation of selenium concentrations in water, sediment, invertebrates, and fish from the Solomon River Basin. *Environ. Monit. Assess*. 2008, v. 137, pp 213-232.

McCarty, S., Chasteen, T., Marshall, M., Fall, R., and Bachofen, R. Phototrophic bacteria produce volatile, methylated sulfur and selenium compounds. *FEMS Microbiology Letters*. 1993, v. 112, pp 93 – 98.

McMaster, W. H., Kerr Del Grande, N., Mallet, J. H. and Hubbell, J. H. Compilation of X-ray Cross Sections. Lawrence Livermore National Laboratory Report. Lawrence Livermore National Laboratory, Livermore,CA, USA. 1969.

Morales, M., Plannelló, R., Martínez-Paz, P., Herrero, O., Cortés, E., Martínez-Guitarte, J. L., and Morcillo, G. Characterization of Hsp70 gene in *Chironomus riparius*: Expression in response to endocrine disrupting pollutants as a marker of ecotoxicological stress. *Comparative Biochemistry and Physiology, Part C*. 2011. v. 153, pp 150-158.

Moreno-Reyes, R. "Iodine, Selenium Deficiency and Kashin-Beck Disease." Comprehensive Handbook of Iodine: Nutritional, Biochemical, Pathological and

Therapeutic Aspects. Ed. Preedy, V. R., Burrow, G. N., and Watson, R. R. USA. Academic Press. 2009. pp. 685.

Muscatello, J. R., Bennet, P. M., Himbeault, K. T., Belknap, A. M., and Janz, D. M. Larval Deformities Associated with Selenium Accumulation in Northern Pike (*Esoxlucius*) Exposure to Metal Mining Effluent. *Environ. Sci. Technol*., 2006a, v.40 (20), pp 6506-6512

Mustacich, D., and Powis, G. Thioredoxin reductase. *Biochem. J.* 2000, v. 346, pp 1-8

Myneni, S. C. B., Tokunaga, T. K., and Brown, G. E. Abiotic Se Redox Chemistry in the PResence of Fe (II, III)-oxides. *Science*. 1997, v. 278, pp 1106-1109.

Nguyen, H., and Donini, A. Larvae of the midge *Chironomus riparius* possess two distinct mechanisms for ionoregulation in response to ion-poor conditions. *Am. J. Physiol. Regul. Integr. Comp. Physiol.* 2010, v. 299, pp 762 – 773.

Ohlendorf, H. M. and Hothem, R. L. Selenium Contamination of the Grasslands, A Major California Waterfowl Area. *The Science of the Total Environment*, 1987, v.66, pp 169-183

Ohlendorf, H. M., Hoffman, D. J., Saiki, M. K., and Aldrich, T. W. Embryonic mortality and abormalities of aquatic birds: Apparent impacts of selenium from irrigation drainwater. *Science of the Total Environment.* 1986, v. 52, pp 49 – 63.

Oremland, R. S., Hollibaugh, J. T., Maest, A. S., Presser, T. S., Miller, L. G., and Culberston, C. W. Selenate Reduction to Elemental Selenium by Anaerobic Bacteria in Sediments and Culture: Biogeochemical significance of a Novel, Sulfate-Independent Respiration. *Appl. Environ. Microbiol*. 1989, v. 55, pp 2333-2343.

Parizek, J., Kalouskova, J., Babicky, A., Benes, J., and Pavlik, L. "Interaction of selenium with mercury, cadmium and other toxic metals". Trace Elements Metabolism in Animals. Eds. Hoekstra, W. G., Suttie, J. W., Ganther, H. E., and Mertz, W. Baltimore. University Park Press. 1974.

Phibbs, J., Franz, E., Hauck, D., Gallego, M., Tse, J.J., Pickering, I.J., Liber, K., and Janz, D.M. Evaluating the trophic transfer of selenium in aquatic ecosystems using caged fish, X-ray absorption spectroscopy and stable isotope analysis. *Ecotoxicology and Environmental Safety.* 2011a July. In Press

Phibbs, J., Wiramanaden, C. I. E., Hauck, D., Pickering, I. J., Liber, K., and Janz, D. Selenium uptake and speciation in wild and caged fish downstream of a metal mining and milling discharge. *Ecotoxicology Environmental Safety.* 2011b March, v. 74, pp 1139-1150.

Pickering, I. J., Prince, R. C., Salt, D. E., and George, G. N. Quantitative, chemically specific imaging of selenium transformation in plants. *Proc Natl Acad Sci*. 2000, v. 97, pp 10717-10722.

Pickering, I. J., Wright, C., Bubner, B., Ellis, D., Persans, M. W., Yu, E. Y., George, G. N., Prince, R. C., and Salt, D. E. Chemical Form and Distribution of Selenium and Sulfur in the Selenium Hyperaccumulator *Astragalus bisculcatus*. *Plant Physiology*. 2003, v. 131, pp 1460 – 1467.

Pisa, R., and Polo, M. *Livres des merveilles du monde*. Venice. 1300

Presser, T. S., and Barnes, I. Selenium concentrations in waters ributary to and in the vicinity of Kesterson National Wildlife Refuge, Fresno and Merced counties, California. US Geological Survey Water Resources Investigation Report 84-4122. 1984, pp 1- 26.

Presser, T. S., and Ohlendorf, H. M. Biogeochemical cycling of selenium in the San Joaquin Valley, California, USA. *Environmental Management*. 2005, v. 11, pp 805 – 821.

Pushie, M. J., McDonald, A., Millhauser, G. L., & George, G. N. (2011). In preparation.

Reilly, C. Selenium in Food and Health. Padstow, Cornwall: Blackie Academic & Professional, 1996.

Rosenfield, I., and Beath, O. A., Selenium: geobotany, biochemistry, toxicity and nutrition. Academic Press, New York. 1964.

Rotruck, J.T., Pope, A. L., Ganther, H. E., Swanson, A. B., Hafeman, D. G., and Hoekstra, W. G. Selenium: Biochemical Role as a Component of Glutathione Peroxidase. *Science*. 1972, v. 179: 588-590

Saisho, H., and Gohshi, Y. Applications of Synchrotron Radiation to Materials Analysis. Amsterdam, The Netherlands, Elsevier Science Ltd, 1996.

Samant, M. G., Borges, G. L., Gordon, J. G. II, Melroy, O. R. and Blum, L. In situ surface extended x-ray absoption fine structure spectroscopy of a lead monolayer at a silver (111) electrode/electrolyte interface. *J. Am. Chem. Soc*. 1987, v. 109, pp 5970–5974.

Saskatchewan Environment. Surface Water Quality Objectives Interim Edition. EPB 356. 2006.

Schultz, R., and Hermanutz, R. Transfer of Toxic Concentrations of Selenium from Parent to Progeny in the Fathead Minnow (*Pimephales promelas*). *Bull. Environ. Contam. Toxicol.* 1990, v.45, pp. 568-573.

Selenium-Tellurium Development Association (STDA). Sources of Selenium and Tellurium. November 29, 2010 < http://www.stda.org/se-te.htm>

Shamberger, R. J., Selenium in the Environment. *The Science of the Total Environment*. 1981, v. 17, pp 59 – 74.

Soller, W. A new precision X-ray spectrometer. *Phys. Rev*. 1924, v. 24, pp 158–167.

Sors, T. G., Ellis, D. R., and Salt, D. E. Selenium uptake, translocation, assimilation, and metabolic fate in plants. *Photosynthesis Research*. 2005, v. 86, pp 373 – 389.

Spallholz, J. E., and Hoffman, D. J. Selenium toxicity: cause and effects in aquatic birds. *Aquatic Toxicology*. 2002, v. 57, pp 27-37.

Stadtman, T. Biosynthesis and Function of Selenocysteine-containing Enzymes. *The Journal of Biological Chemistry*. 1991, v. 266, pp 16257-16260

Stadtman, T. Selenium Biochemistry. *Annu. Rev. Biochem*. 1990, v. 59, pp. 111-27.

Stewart, S. Public Health Statement: Selenium - Production, Import/Export, Use, and Disposal. Agency for Toxic Substances and Disease Registry, 2004.

Terry, N., Zayed, A. M., de Souza, M. P., and Tarun, A. S. Selenium in Higher Plants. *Annu. Rev. Plant. Physiol. Plant Mol. Biol*. 2000, v. 51, pp 401 – 432.

Trelease, S. F., Di Somma, A. A., and Jacobs, A. L. Seleno-Amino Acid Found in *Astragalus bisulcatus*. *Science.* 1960, v. 132, pp 618.

Tetsu, T. K., Brown, G. E., Pickering, I. J., Sutton, S. R., and Bajt, S. Selenium Redox Reactions and Transport between Ponded Waters and Sediments. *Environ. Sci. Technol*. 2008, v. 31, pp 1419-1425.

Tetsu, T. K., Lipton, D. S., Benson, S. M., Yee, A. W., Oldfather, J. M., Duckart, E. C., Johannis, P. W., and Halvorsen, K. E. Soil Selenium Fractionation, Depth Profiles and Time Trends in a Vegetated Site at Kesterson Reservoir. *Water, Air, and Soil Pollution*. 1991, v. 57, pp 31-41.

Thomassen, Y., Nieboer, E., Romanova, N., Nikanov, A., Hetland, S., VanSpronsen, E. P., Odland, J. Ø., and Chashchin, V. Multi-component assessment of worker exposures in a copper refinery Part 1. Environmental monitoring. *J. Environ. Monit*. 2004, v. 6, pp 985-991.

Tse, J. J., Wiramanaden, C. I. E.,& Pickering, I. J. (2011). In preparation.

Tsezos, M. and Noh, S.H. Extraction of Uranium from Sea Water Using Biological Origin Adsorbents. *The Canadian Journal of Chemical Engineering*. 1984. v. 62: 559-561

Vickerman, D. B., Trumble, J. T., George, G. N., Pickering, I. J., and Nichol, H. Selenium Biotransformations in an Insect Ecosystem: Effects of Insects on Phytoremediation. *Environ. Sci. Technol*. 2004, v. 38, pp 3581 – 3586.

Wapnir, R. Protein Nutrition and Mineral Absorption. Boca Raton, Florida. CRC Press. Inc. 1990.

Webb, S.M. SMAK: Sam's Microprobe Analysis Kit. <http://home.comcast.net/~sam_webb/smak.html>, 2010.

Weech, S. A., Scheuhammer, A. M., and Wayland, M. E. Selenium accumulation and reproduction in birds breeding downstream of a uranium mill in northern Saskatchewan, Canada. *Ecotoxicology*. 2011, DOI: 10.1007/s10646-011-0788-9.

Weres, O., Jaouni, A.-R., and Tsao, L. The distribution, speciation and geochemical cycling of selenium in a sedimentary environment, Kesterson Reservoir, California, USA. *Applied Geochemistry*. 1989, v. 4, pp 543 – 563.

Willmott, P. An Introduction to Synchrotron Radiation: Techniques and Applications. Singapore, Wiley, 2011.

Winick, H. Synchrotron Radiation Sources: A Primer. Singapore, World Scientific Publishing Co. Pte. Ltd, 1994.

Wiramanaden, C. I. E., Forster, E. K., and Liber, K. Selenium distribution in a lake system receiving effluent from a metal mining and milling operation in Northern Saskatchewan, Canada. *Environmental Toxicology and Chemistry*. 2010b March, v. 29, pp 606-616

Wiramanaden, C. I. E., Liber, K., & Pickering, I. J. Selenium Speciation in Whole Sediment using X-ray Absorption Spectroscopy and Micro X-ray Fluorescence Imaging. *Environ. Sci. Technol*. 2010a July, v. 44, pp 5389-5394.

Wise, R. R., Pierstorff, C. A., Nelson, S. L., Bursek, R. M., Plude, J. L., McNello, M., and Hein, J. Morphological Deformities in *Chironomus* (Chironomidae: Diptera) Larvae as Indicators of Pollution in Lake Winnebago, Wisconsin. *J. Great Lakes Res*. 2001, v. 27, pp 503-509.

World Nuclear Association (WNA). Uranium in Canada. May 2011. <http://world-nuclear.org/info/inf49.html>

WormBase. "Gene Summary for seld-1". WormBase. September 4, 2011. < http://www.wormbase.org/db/gene/gene?name=WBGene00012867;class=Gene>

Yagi, S. Effects of ligation on ethanol-induced Balbiani ring puffing in salivary glands of *Chironomus*. *Chromosoma*. 1984, v. 89, pp 274-279

Yuan, T., Weljie, A. M., and Vogel. H.J. Tryptophan Fluorescence Quenching by Methionine and Selenomethionine Residues of Calmodulin: Orientation of Peptide and Protein Binding. *Biochemistry*. 1998, v. 37, pp 3187-3195

Zayed, A., Lytle, C. M., and Terry, N. Accumulation and volatilization of different chemical species of selenium by plants. *Planta*. 1998, v. 206, pp 284-292.

Zhang, J. -S., Gao, X. -Y., Zhang, L. -D., and Bao, Y. -P. Biological effects of a nano red elemental selenium. *BioFactors*. 2001, v. 15, pp 27-38.

Zimmerman, M. B., and Kohrle, J. The impact of iron and selenium deficiencies on iodine and thyroid metabolism: biochemistry and relevance to public health. *Thyroid*. 2002, v. 12, pp 867-878.